ISTANBUL TECHNICAL UNIVERSITY ★ GRADUATE SCHOOL OF SCIENCE ENGINEERING AND TECHNOLOGY

DESIGN OF BIOCOMPATIBLE HYDROGELS WITH REGIONS OF DIFFERENT CHEMICAL AND MECHANICAL PROPERTIES

Ph.D. THESIS

Aslıhan ARĞUN

Department of Chemistry

Chemistry Programme

NOVEMBER 2018

ISTANBUL TECHNICAL UNIVERSITY ★ GRADUATE SCHOOL OF SCIENCE ENGINEERING AND TECHNOLOGY

DESIGN OF BIOCOMPATIBLE HYDROGELS WITH REGIONS OF DIFFERENT CHEMICAL AND MECHANICAL PROPERTIES

Ph.D. THESIS

Aslıhan ARĞUN
(509122012)

Department of Chemistry

Chemistry Programme

Thesis Advisor: Prof. Dr. Oğuz OKAY

NOVEMBER 2018

İSTANBUL TEKNİK ÜNİVERSİTESİ ★ FEN BİLİMLERİ ENSTİTÜSÜ

FARKLI KİMYASAL VE MEKANİK ÖZELLİKTE BÖLGELER İÇEREN BİYOUYUMLU HİDROJEL TASARIMLARI

DOKTORA TEZİ

Aslıhan ARĞUN
(509122012)

Kimya Anabilim Dalı

Kimya Programı

Tez Danışmanı: Prof. Dr. Oğuz OKAY

KASIM 2018

Aslıhan ARĞUN, a Ph.D. student of ITU Graduate School of Science Engineering and Technology student ID 509122012, successfully defended the thesis entitled "DESIGN OF BIOCOMPATIBLE HYDROGELS WITH REGIONS OF DIFFERENT CHEMICAL AND MECHANICAL PROPERTIES", which she prepared after fulfilling the requirements specified in the associated legislations, before the jury whose signatures are below.

Thesis Advisor :	**Prof. Dr. Oğuz OKAY** İstanbul Technical University	.....
Jury Members :	**Prof. Dr. Nermin ORAKDÖĞEN** Istanbul Technical University	.....
	Prof. Dr. Gülten GÜRDAĞ Istanbul University	.....
	Prof. Dr. Mine YURTSEVER Istanbul Technical University	.....
	Assoc. Prof. Dr. Deniz C. TUNCABOYLU Bezmialem Vakif University	.....

Date of Submission : 22 October 2018
Date of Defense : 14 November 2018

To my family,

FOREWORD

Low back pain is a common health issue around the world. We do not need any citation to prove it. It is possible to find many walking references around to be convinced. One, having a spinal disc herniation, is me, indeed. However, this was not the why that I conducted this study. Because, when I was diagnosed with herniation, I have been already started to this study. I opted in favor of turning it into an opportunity. I made use of each orthopedist's appointment opportunity to learn more about intervertebral disc (IVD). Moreover, I was the one who even cannot touch any raw meat. But, I visited many butcher shops to find a real IVD. What I really want to explain is the lesson I took from my PhD.

I deeply learned that a PhD study is not an only heavy laboratory work or sitting at a computer for hours. A PhD is an uphill struggle including fighting with many complex problems. Of course, my back pain, making itself evident during the days and nights long works, my issue, about not to touch any raw meat, or any of others were not the fight. Since a scientific research is a costly attempt, today it is barely possible to do a research without a support. Therefore, one of these real fights was that if the research is materially supported. Finding a material support is a long way which have been traveled over by a supervisor as a lifelong labor. For a PhD candidate, this stands for getting a slice of the experience cake from the supervisor's valuable lifelong labor. Moreover, not only the material support, but also the patience, tolerance and countless others are the part of this cake. One of the rare examples of the best experience cake is my supervisor's and he always generously let us to take slices. Through my researches, I greedily benefitted from his experiences. Thus, first and foremost I want to thank my supervisor Prof. Dr. Oğuz OKAY. It was always an honor and a source of pride for me to be a student of him. I appreciate that he never let me alone when I fallen through the floor and he always supported me, even under hard conditions, to achieve my dream. Besides my conscious knowledge, I am sure that I gained many by unconsciously. The enthusiasm he has for researches was motivational for me. He fitted me to the challenging academic life with a solid science ethic discernment rather than just being an academic survivor and as a role model, he encouraged me about struggle along even under poor conditions. All explained above were written to present my gratitude but still not enough to explain. Therefore, I want sincerely thank to him for every single told or still untold things.

I would like to present my special thanks to Prof. Dr. Gülten GÜRDAĞ and Prof. Dr. Nermin ORAKDÖĞEN for their tolerance, kindness and support through my thesis work. I am grateful that they allocated their valuable time for me. I also would like to specially thank to esteemed Prof. Dr. Mine YURTSEVER and Assoc. Prof. Dr. Deniz CEYLAN TUNCABOYLU for the inpirational comments and their precious attandance to my thesis defence. It was my honor to present my work to them.

Walking along this PhD road was not a single journey of my own. It would never come true without taking the heart of family, friends and colleagues. I always proud that I have my family. I specially thank to my mother Ümmühan ARĞUN and my father

Turhan ARĞUN that they always supported me to reach my dreams. I always feel their priceless existence just next to me. I believe that they are the only example against thermodynamic in the world with their ability to create infinite happiness and peace out of nothing. Words always fail to explain my thankfulness and love about them. Having a sister, but specifically as mine, F. Neslihan ARĞUN, would be my greatest chance I have that she always somehow renders me blissfulness. She will always be my idol as she ever have been with her mysterious sourced power. I also would like to present my sincere thanks to my stand-in sister, Aylin GELGEÇ, who always supported me by spinning a happier life around us with her kind heart. And, I must say that, as a powerful woman model, and as just my warmhearted aunt, Şadiye ARĞUN is my driving force to stay tough in my life. I will always be grateful to have her.

As well as my family, my friends are also my source of power to step forward. They never gave up to tolerate me while I was stealing the time, with work based excuses, from the times we would be together with friends. They never let me felt alone. Thanks from heart to my dear friends, whom I met them during my academic life: MSc. Pınar KARACAN, MSc. Gizem AKAY, Dr. İpek ÖSKEN, Dr. Volkan CAN, Assoc. Prof. Dr. Suzan ABDURRAHMANOĞLU, Asst. Prof. Dr. Ümit GÜLYÜZ, MSc. Gözde AKTAŞ EKEN. I always felt me the luckiest people in the world with their valuable existance in my life. More than their academic titles, they are just as my family in Istanbul. And I also thank to my friends who are physically far away but always felt me as we're closer: İlkay DÖNMEZ ÇAL, Dr. Münteha Nur SONUÇ KARABOĞA.

I would like to say that it was my pleasure to conduct my researches in Polymer Gels Research Lab. Through the period, I took part of our research lab, between 2010 to 2018, I gain opportunity to meet with many great people. I owe my several nice memories to them. Besides, I also have to say that, I am glad to have my joyful time with my colleagues Dr. Çiğdem BİLİCİ, MSc. Tuğba ÇELİKER, MSc. Burak TAVŞANLI, MSc. Berkant YETİŞKİN, MSc. Esra SU and Sevil MÜSLÜMOVA.

Special thanks to MSc. Ilgın IŞILTAN for her guide during the cell studies of my thesis. Besides all, she stand by me for all struggles in my personal life too with her pleasant friendship. I must also thank to Prof. Dr. Arzu KARABAY KORKMAZ that she let me benefit from her research laboratory.

Thank you all great people in my life who make the world a better place with their kind-heart.

Thank you for the material support of "The Scientific and Technological Research Council of Turkey (TUBITAK)" and Istanbul Technical University (ITU).

October 2018

Aslıhan ARĞUN

TABLE OF CONTENTS

Page

FOREWORD ..... **ix**
TABLE OF CONTENTS ..... **xi**
ABBREVIATIONS ..... **xiii**
SYMBOLS ..... **xv**
LIST OF TABLES ..... **xvii**
LIST OF FIGURES ..... **xix**
SUMMARY ..... **xxv**
ÖZET ..... **xxix**
1. INTRODUCTION **1**
1.1 Silk-Fibroin Cryogels 2
1.1.1 Application of silk-fibroin 3
1.1.2 Scaffolding in tissue engineering 7
1.1.2.1 Decellularized ECM from allogenic or xenogenic tissues 9
1.1.2.2 Cell sheets with self secrated ECM 9
1.1.2.3 Cell encapsulation by self-assambled hydrogel matrix 10
1.1.2.4 Pre-made porous scaffolds for cell seeding 10
1.1.3 SN, DN and TN silk-fibroin cryogels as a cell scaffold 11
1.2 Hybrid Hydrogels 16
1.2.1 Hydrogels 17
1.2.1.1 Hydrogels according to the cross-link type 17
1.2.1.2 Hydrophobically modified hydrogels 20
1.2.1.3 Self-healing ability 23
1.2.1.4 Shape-memory behavior 27
1.2.2 Multi-segmented hybrid hydrogels 31
2. EXPERIMENTAL PART **35**
2.1 Silk Fibroin Cryogels 35
2.1.1 Materials 35
2.1.1.1 Materials and devices required for cell culturing 35
2.1.1.2 Materials for cell viability assay 36
2.1.1.3 Materials for Laser Scanning Confocal Microscopy (LSCM) 36
2.1.2 Preperation of silk–fibroin cryogels 36
2.1.3 Sterilization of cryogels 37
2.1.4 Cell culturing 37
2.2 Hybrid Hydrogels 37
2.2.1 Materials 37
2.2.2 Preperation of hybrid hydrogels 38
2.2.2.1 Two-segmented hybrid hydrogels 39
2.2.2.2 Three-segmented hybrid hydrogels 45
3. CHARACTERIZATION METHODS OF GELS **49**
3.1 Characterization of Silk Fibroin Cryogels 49
3.1.1 Determination of proper cell/well amount for MTT asssay 49
3.1.2 Biocompatibility – MTT cell viability test 50

3.1.3 Scanning laser confocal microscopy (LCSM) 52
3.2 Characterization of Hybrid Hydrogels 53
3.2.1 Pycnometer measurements 53
3.2.2 Swelling measurements 53
3.2.3 Uniaxial elongation and compression tests 54
3.2.4 Self - healing tests 55
3.2.5 Uniaxial cyclic elongation tests 55
3.2.6 Rheological measurements 56
3.2.7 Differential scanning calorimetry (DSC) measurements 57
3.2.8 Shape memory tests 57
4. RESULTS AND DISCUSSION 59
4.1 Silk-Fibroin Cryogels 59
4.1.1 Determination of cell/well amount 60
4.1.2 Cell viability results by use of MTT assay 61
4.1.3 Imaging by Laser Scanning Confocal Microscopy (LSCM) 64
4.2 Hybrid Hydrogels 68
4.2.1 Two-segmented hybrid hydrogels 68
4.2.1.1 Stratification Study 70
4.2.1.2 Differential Scanning Calorimetry (DSC) 72
4.2.1.3 Shape memory 75
4.2.1.4 Uniaxial compression and elongation 76
4.2.1.5 Self healing 81
4.2.1.6 Rheology 84
4.2.1.7 Cyclic elongation 87
4.2.2 Three-segmented hybrid hydrogels 90
4.2.2.1 Stratification Study 90
4.2.2.2 Differential scanning calorimetry (DSC) 92
4.2.2.3 Uniaxial elongation 94
4.2.2.4 Shape memory 96
5. CONCLUSIONS 101
REFERENCES 105
CURRICULUM VITAE 119

ABBREVIATIONS

SN : Singe Network
DN : Double Network
TN : Triple Network
MTT : (3-(4,5-Dimethylthiazol-2-yl)-2,5-Diphenyltetrazolium Bromide)
LCSM : Laser Scanning Confocal Microscopy
ECM : Extra Cellular Matrix
NHDF : Normal Human Dermal Fibroblast
FGM : Fibroblast Growth Medium
FBM : Fibroblast Basal Medium
hFGF : Human Fibroblast Growth Factor
HEPES : 4-(2-Hydroxyethyl)piperazine-1-ethanesulfonic acid, *N*-(2-Hydroxyethyl)piperazine-*N′*-(2-ethanesulfonic acid)
EDTA : Ethylenediaminetetraacetic acid
DMSO : Dimethyl Sulfoxide
DAPI : 4',6-Diamidino-2-Phenylindole, Dihydrochloride
BSA : Bovine Serum Albumin
PBS : Phosphate Buffered Saline
IVD : Intervertebral Disc
VF : Volume Fraction
C_{SF} : Silk-Fibroin Concentration
3D : Three Dimensional
2D : Two Dimensional
ISO : International Standard Organisation
UV : Ultra Violet
CDC : Constituional Dynamic Chemistry
DMA : *N*,*N*- Dimethyl Acrylamide
AAc : Acrylic Acid
C18A : Octadecyl Acrylate
C17.3M : Stearyl Methacrylate
C12M : Lauryl Methacrylate

IRGACURE : 2-Hydroxy-4′-(2-hydroxyethoxy)-2-methylpropiophenone

RS : Reaction Solution

H2 : Two-Segmented Hybrid Hydrogel

H3 : Three-Segmented Hybrid Hydrogel

C1 : First Component of any Hybrid Hydrogel

C2 : Second Component of any Hybrid Hydrogel

C3 : Third Component of any Three-Segmented Hybrid Hdrogel

M1 or M2 : Mixture Hdrogel (Interfaces of Two-Segmented Hybrid Hdrogel)

MPa : Mega-Pascal

kJ : Kilo-Joule

C_0 : Initial, Total Monomer Concentration

DSC : Differential Scanning Calorimetry

SYMBOLS

E	: Young's Modulus
σ_{nom}	: Nominal Stress
σ_{true}	: True Stress
ε	: Strain
λ	: Deformation Ratio
T_m	: Melting Temperature
T_{trans}	: Transition Temperature
T_g	: Glass Transition Temperature
G'	: Storage Modulus
G''	: Loss Modulus
γ_o	: Deformation Amplitude
ω	: Frequency
η	: Viscosity
ΔH_m	: Enthalpy change during melting
χ_{HM}	: Mole fraction of the hydrophobic monomer in the comonomer feed
f_{cry}	: Degree of crystallinity

LIST OF TABLES

Page

Table 2.1 : Table of all synthesized hydrogels in different compositions. **45**
Table 2.2 : Table of molar ratios and densities (at 25 °C) of monomer mixtures which create the components of three segmented hybrids. **46**
Table 4.1 : Compositions of hybrid segments. **69**
Table 4.2 : Densities of reaction solutions belonging to hybrid segments. **71**
Table 4.3 : Thermal mechanical properties of hybrid segments and mixture gels. **74**
Table 4.4 : Tensile and compressive mechanical properties of gels. **84**
Table 4.5 : Compositions (mol %) and densities (g/mL) of reaction solutions with T_m (°C) values of their gel states. **91**
Table 4.6 : Composition, water content and thermal properties of gels **93**
Table 4.7 : Compositions and tensile mechanical properties of gels. **95**

LIST OF FIGURES

Page

Figure 1.1 : Representative demonstrations of (a) an intervertebral disk (IVD) in a spine (Reprinted from *Intervertebral Disc: What is it? What does it do? And how to keep it healthy*, Greg Schroeder, 2016. Retrieved October 1, 2017, from http://www.wieberphysicaltherapy.com/intervertebral-disc-keep-healthy/. Copyright 2016 by Greg Schroeder. Reprinted with permission.) [11] and (b) its anisotropic architecture (Reprinted from "Mechanical design criteria for intervertebral disc tissue engineering.", by Nerurkar, N. L., et al., 2010, *Journal of Biomechanics*, 43 (6), 1017–1030. Copyright 2018 by Elsevier Ltd. Reprinted with permission.) [12]. **5**

Figure 1.2 : Schematic diagram of different scaffolding approaches. Adapted from "Scaffolding in tissue engineering: general approaches and tissue-specific considerations", by Chan, B. P. and Leong, K.W., 2008, *Eur Spine J,* 17: (Suppl 4), S467–S479. Copyright 2008 by Springer-Verlag. Reprinted with permission [32]. **9**

Figure 1.3 : Schematic illustration of the fibroin cryogel formation with single-, double-and triple-network structures Reprinted from "Cryogelation within cryogels: Silk fibroin scaffolds with single-, double- and triple-network structures.", by Yetiskin, B., Akinci, C. and Okay, O., 2017, *Polymer*, 128, 47–56. Copyright 2017 by Elsevier Ltd. Reprinted with permission [7]. **14**

Figure 1.4 : Schematic illustration demonstrates: (A) the localization of applied energy in a conventional chemically-crosslinked hydrogels which results in a crack generation and (B) the dissipation of the applied energy in a physically-crosslinked hydrogel (e.g. hydrophobically modified hydrogel). Reprinted from "Design of high-toughness polyacrylamide hydrogels by hydrophobic modification.", by Abdurrahmanoglu, S., Can, V. and Okay, O., 2009, *Polymer*, 50, 5449–5455. Copyright 2009 by Elsevier Ltd. Reprinted with permission [101]..... **18**

Figure 1.5 : Various strategies used to synthesize physical (upper) and chemical (down) self-healing gels based on CDC. Reprinted from "Self-healing gels based on constitutional dynamic chemistry and their potential applications.", by Wei, Z. et al., 2014, *Chem. Soc. Rev.*, 43 (23), 8114–8131. Copyright 2014 by Royal Society of Chemistry. Reprinted with permission [140]. **24**

Figure 1.6 : (a, b) Autonomous self-healing of HM PAAm hydrogels formed using 2 mol% of C17.3M hydrophobe in 7 % SDS + 0.5 M NaCl solution; (a) C_0 : 5 %. Reprinted from "Tough and self-healing hydrogels formed via hydrophobic interactions.", by Tuncaboylu, D.,C. et al., 2011, *Macromolecules*, 44, 4997-5005. Copyright 2011 by American Chemical Society. Reprinted with permission [106]. and (b) 10 %. Reprinted from "Dynamics and large strain behavior of self-healing hydrogels with and

without surfactants.", by Tuncaboylu, D.,C. et al., 2012, *Macromolecules*, 45 (4), 1991-2000. Copyright 2012 by American Chemical Society. Reprinted with permission [129]. In (a), one of the hydrogel samples is colored for clarity. **25**
Figure 1.7 : Reversible leaf-shutting mechanism of Venus fytrap. Reprinted from "How the Venus flytrap snaps.", by Forterre, Y., et al. 2005, *Nature*, 433 (7024), 421-425. Copyright 2005 by Springer Nature. Reprinted with permission [160]. **27**
Figure 1.8 : Schematic illustrations of (a) Dual-shape memory effect; and (b) Triple-shape memory effect. Reprinted from "Recent progress in shape memory polymer: New behavior, enabling materials, and mechanistic understanding.", by Zhao, Q., et al. 2015, *Progress in Polymer Science*, 49 (50), 79-120. Copyright 2015 by Elsevier Ltd. Reprinted with permission [162]. **28**
Figure 1.9 : (1) An optical image of hybrid gel. Interface regions is smooth and hence not visible. (2) Optical images showing mechanical differences between the zones of hybrid gel. The gel/gel interface is highly robust. Reprinted from "A New Approach for Creating Polymer Hydrogels with Regions of Distinct Chemical, Mechanical, and Optical Properties.", by Banik, S. J., et al. 2012, *Macromolecules*, 45 (14), 5712−5717. Copyright 2012 by American Chemical Society. Reprinted with permission [182]. **32**
Figure 1.10 : (a) Ten-layer gel prepared by connecting gel slices together (b) Multi-layer gels obtained by connecting as a soft glue. (c) "ATRP" embedded letter made of and surrounding matrix. Reprinted from "Combining ATRP and FRP Gels: Soft Gluing of Polymeric Materials for the Fabrication of Stackable Gels.", by Beziau, A., et al. 2017, *Polymers*, 9 (6), 186-196. Copyright 2017 by MDPI AG, Basel, Switzerland. Reprinted with permission [186]. **33**
Figure 2.1 : Hydrophilic monomers, used in synthesis of hybrid hydrogels. (a) *N*,*N*-dimethylacrylamide (DMA), (b) Acrylic acid (AAc). **38**
Figure 2.2 : Hydrophobic monomers used in the synthesis of hybrid hydrogels. **38**
Figure 2.3 : Radicalic photoinitiator IRGACURE 2959. ..... **38**
Figure 2.4 : Optical images of an example interbedded and flat shaped H2. ..... **39**
Figure 2.5 : Optical images of H2-1 and H2-2 hydrogels. **40**
Figure 2.6 : Illustration of interbedded hybrid hydrogel template and expected shape of final interbedded hybrid hydrogel. **40**
Figure 2.7 : Illustration of interbedded hybrid hydrogel preparation in 6 steps. **41**
Figure 2.8 : Template and the preparation steps of flat-shaped hybrid hydrogels. **42**
Figure 2.9 : Schematic illustration of three-segmented hybrid hydrogel synthesis through the stratification of monomer mixtures. **46**
Figure 2.10 : Schematic illustration of three- and two-segmented hybrid hydrogels. **47**
Figure 3.1 : Representative illustration of MTT assay setup for single network (SN) cryogels for 3^{rd}, 7^{th} and 10^{th} day. Red "X" symbols: loaded wells. **51**
Figure 3.2 : Representative illustration of a running MTT assay at its 3^{th} day. Red "X" symbols: loaded wells. **52**
Figure 4.1 : Viable cell percentages are plotted against the cell amounts (in 200 μL of full growth medium) per well of a 96 well plate. Termination times of MTT assays are denoted by red, green and blue symbols for 3^{rd}, 7^{th} and

10^{th} days, respectively. Results of most proper cell amounts are indicated by yellow hoops for each cryogels of single network (SN) sample series. (a) SN-4, (b) SN-7, (c) SN-12.5, (d) SN-22. ..... **61**
Figure 4.2 : Change in cell viability results are plotted against the pore size and porositiy values of (a) Single network (SN) cryogels, (b) SN-4.2, double network (DN) cryogels and triple network (TN) cryogel. Total silk-fibroin concentrations (C_{SF}) of DNs and TN are stated on graph for the consideration purposes. (For example, TN-4/7/20 has total C_{SF} of (4+7+20=33) 33). Control groups denoted as "0". Porosity of "0" assumed as 100% and the pore size taken as 85200μm (well diameter). **62**
Figure 4.3 : Change in cell viability (%) rates are ploteted against the pore size (μm) and porosity (%) values of SN, DN and TN cryogels. Graph exhibits all the results shown in Figure 2.14 "a" and "b" together. Viability results are given in the order of increasing total silk-fibroin concentration (C_{SF}). **64**
Figure 4.4 : Confocal laser micrographs of Normal Human Dermal Fibroblast (NHDF) cells cultured on SN-4.2 which were stained with Rhodamine–phalloidin for detecting actin filaments (red) and DAPI for nuclei (blue). Micrograms were obtained from the 7^{th} day culture..... **66**
Figure 4.5 : Confocal laser micrographs of Normal Human Dermal Fibroblast (NHDF) cells cultured on TN-4/7/20 which were stained with Rhodamine–phalloidin for detecting actin filaments (red) and DAPI for nuclei (blue). Micrograms were obtained from the 7^{th} day culture. **66**
Figure 4.6 : Optical images of feasible and unfeasible hybrid gels in interbedded and flat shapes. **69**
Figure 4.7 : Optical images of hybrid gels in interbedded and flat shapes. **69**
Figure 4.8 : Illustration of stratification study performed for H2-1 samples' reaction solutions (RS). (RS 1: monomer mixture of C1, RS 2: monomer mixture of C2-1)..... **70**
Figure 4.9 : Illustration of stratification study performed for solution-dyed reaction solutions. **72**
Figure 4.10 : Sampling method on an optical image of Hybrid 1 (H2-1) gel as an example for DSC measurements of hybrid gel samples. **73**
Figure 4.11 : DSC results of Hybrid 1 (H2-1) gel. DSC results obtained from (a) H2-1 gel sample, (b) Individual C1, C2-1 and Mixture 1 (denoted as M1) gel (C1+C2-1) samples. **73**
Figure 4.12 : DSC results of Hybrid 2 (H2-2) gel. DSC results obtained from (a) H2-2 gel sample, (b) Individual C1, C2-1 and Mixture 2 (denoted as M2) gel (C1+C2-2) samples. **74**
Figure 4.13 : Images demonstrating pseudo triple-shape-memory behavior of H2-1 hydrogels. Permanent shape (a), temporary shapes 1 and 2 (b, c), and successive shape recoveries at 42 and 70 °C (d, e). **76**
Figure 4.14 : Uniaxal test results and optical images of H2-1 and H2-2 at room temperature. White arrows on optical images indicate the interface region. (a) Stress (σ_{nom})-strain (ε %) curves of H2-1, C1, C2-1 and M1 (b) Stress (σ_{nom})-strain (ε %) curves of H2-2, C1, C2-2 and M2. ..... **77**
Figure 4.15 : Tensile mechanical properties of hybrids, H2-1 and H2-2, and their components, C1, C2-1 and C2-2, mixtures mimicking the interface regions, M1 and M2 are given. Graphs on left side demonstrates the results of H2-1 and related gels' results, while the graps on right side

show H2-2 and related results. (a, b) Young's modulus (E), (c, d) strain % (ε %) (e, f) nominal stress (σ_{nom})..... **79**
Figure 4.16 : (a) An example of compressive correction method applied on C2-2 sample. Dashed line shows the true stress (σ_{true})-deformation ratio (λ) curve. λ_f denotes deformation ratio at break and $\varepsilon = 1 - \lambda$. σ_{true} can be read on right axis, while the σ_{nom} is on the left side. (b) Compressive σ_{nom} − strain % (ε %) curves of H2-2 and its components (C1 and C2-2) at 24 ± 1 °C. **80**
Figure 4.17 : Compressive σ_{nom} (MPa) − strain % (ε %) curves of H2-1 and its components (C1 and C2-1) at (a) room temperature (24 ± 1 °C) and (b) body temperature (37 ± 1 °C). **81**
Figure 4.18 : Stress (MPa)−strain (%) curves of virgin (solid curves) and healed (a) H2-1 and (b) H2-2 gel samples (dashed curves) obtained from tensile tests. **82**
Figure 4.19 : (a) Images of a H2-1 gel specimen before and after cutting and after repairing. (b) Images of a H2-2 gel specimen after repairing. Yellow arrows indicate the cut regions while red arrow is the interface region. **82**
Figure 4.20 : Stress (MPa) –strain (%) curves of virgin (solid curves) and healed (a) H2-1 gel samples (at room and body temprerature) and (b) H2-2 gel sample (at room tempretature) (dashed curves) obtained from compression tests. **83**
Figure 4.21 : (a) Storage modulus G' (MPa) of H2-1 (upper panel) and H2-2 (bottom panel) and their gel components during heating from 5 to 80 °C at a rate of 5 °C min^{-1}. ω = 6.3 rad s^{-1} and γ_0 = 0.1%. (b, c) Frequency dependences of G' (filled symbols) and the loss modulus G''(MPa) (open symbols) of H2-1 (b) and H2-2 hybrids (c) and their components. Temperature = 37 °C (b) and 25 °C (c). γ_0 = 0.1%..... **85**
Figure 4.22 : Frequency dependences of G' (MPa) (filled symbols) and G'' (MPa) (open symbols) of C1, C2-1, and H2-1 hydrogels at (a) 25 °C and (b) 37 °C. γ_0 = 0.1%. **86**
Figure 4.23 : Viscosity (η/Pa.s) changes of C1, C2-1, C2-2 segments of H2-1 and H2-2 during the course of polymerization s plotte againt reaction time. Results were collected at 25 °C. **87**
Figure 4.24 : Stress (MPa)−strain (%) (a−c) 3 sets of successive 20 tensile cycles separated by the thermal treatment for a H2-1 gel specimen. ε_{max} = 30%. (d) Stress−strain curve of H2-1 after subjecting 60 tensile cycles is shown by dashed line. For comparison, stress−strain curve of a H2-1 gel sample is also shown by the solid curve. **88**
Figure 4.25 : Uniaxial cyclic elongation test of H2-2 gel at room temperature. (a) 20 successive cycles at strain ratio of 300%, (b) 20 more successive cycles in same strain ratio, after a waiting time of 1h in a water bath at 25 °C. **89**
Figure 4.26 : DSC scans conducted on the individual components of (a) H3-1 and (b) H3-2 hybrids..... **92**
Figure 4.27 : Tensile stress (σ_{nom})(MPa) -strain (%) (ε %) curves of three segmented hybrids (H3-1 and H3-2, solid lines). To compare the three segmented hybrid samples, their own individual components' (dashed lines) elongation results were also added to the graphs. (a) H3-1 and its components C1, C2-1 and C2-1 (b) H3-2 and its components C1, C2-2 and C3-2..... **94**

Figure 4.28 : Elongation test results comparison of H3-1 and H3-2 with two segmented hybrids and individual gel segments by their (a) Young's modulus E (MPa), (b) percent of strain ε_f % and (c) fracture stress $\sigma_{nom(f)}$ (MPa). **96**
Figure 4.29 : Images demonstrating pseudo-triple shape memory behavior of H3-1 hybrid hydrogel. Permanent shape (1), temporary shape (2), shape recoveries of C1 and C3-1 segments at 40 °C (3), and following shape recovery of C2-1 segment to reach total shape recovery at 60 °C (4). ... **97**
Figure 4.30 : Images demonstrating pseudo multiple-shape-memory behavior of H3-2 hybrid hydrogel. Permanent shape (1), temporary shape (2), successive shape recoveries of C1 (3), C2-2 (4) and C3-2 (5) segments at 40, 50 and 60 °C, respectively. **98**

DESIGN OF BIOCOMPATIBLE HYDROGELS WITH REGIONS OF DIFFERENT CHEMICAL AND MECHANICAL PROPERTIES

SUMMARY

A polymer gel is simply a soft and wet material. There are two critical points to form a polymer gel. These are: a crosslinked, elastic three dimentional (3D) polymer network architecture and a fluid, filling the interstitial spaces of network, in which the polymer network can swell without dissolving. Their elastic crosslinked network brings them a soft texture, while the entrapped fluid renders this materials wet. Although polymer gels have wet and soft look, they are capable of bearing large deformations. Therefore, polymer gels are mostly used materials with their wide-ranging and tunable properties in such areas like bone-tissue engineering, biomedical applications, etc.

Within this thesis, two different kinds of gels were investigated from two different aspects. First, single network (SN), double network (DN) and triple network (TN) cryogels were investigated in the manner of biocompatibility. Then, in the second part, multi-segmented hybrid hydrogels were discussed within the framework of their synthesis, creation aspects and mechanical properties.

Silk, as a biological material, covers a history more than 5000 years. This protein polymer in the form of fibers spun by silkworms has served as a bridge between cultures. Today, silk is mainly utilized in textile industry, for its unique properties such as strength, low heat conductivity, luster and moisture absorbance capacity. Another interesting applications of silk include: the interior decoration of houses, parachute clothing, bicycle tires, bed filling, etc. Moreover, most importantly, silk is used in biomedical fields such as tissue engineering and regenerative medicine with their various physical characteristics, biocompatibility and ability to support the attachment, proliferation and differentiation of many types of cells.

Within the scope of this thesis, biocompatibity of *Bombyx mori* based silk-fibroin protein was investigated as a pre-made scaffold through the specific form of porous gels, SN-, DN- and TN- silk-fibroin cryogels. Investigations were carried out on readily-prepared scaffold samples which of their mechanical and morphological properties were already identified by our research group. Pre-identified feature-dependent changes in cell viability was tested quantitatively by MTT assay and qualitative observations were conducted through layer-by-layer images (3D images, composite images collected from different depths of scaffold) from Laser Confocal Scanning Microscopy (LCSM). For all cell-culturing purposes, Normal Human Dermal Fibroblast (NHDF) cell line was used.

Among the scaffolds, there were two kinds of materials available to clarify the relationships between cell viability and pore size, surface area and wall thickness. SN cryogels synthesized by increasing fibroin concentrations represents decreasing pore size and porosity while wall thickness is increasing. The other set of cryogels, named

as DN and TN through this thesis, formed by double-networking concept represent increasing fibroin concentrations by the penetration of new networks into the SN. However, DN and TN cryogels exhibit no increase in wall thickness with the help of formed pores inside the bigger pores of single network pores, called as second generation pores. Moreover, decreasing in pore size occasioned by second generation pores and increasing fibroin concentration cases were run with increasing surface area.

Besides all, both of two cryogel types have an advantage for biomedical applications as they have interconnected pores. MTT assay results represented that cryogels with the porosity (%) ratios between 90 and 75% reveal better cell viability (%) ratios which are in correlation with literature. Additionally, it was revealed that the cell viability results are independent from silk-fibroin concetrations (C_{SF}) of cryogels. Pore size ranges of scaffolds in dermal fibroblast culturing were reported between 5-15μm. Within the range of scaffolds, SN-4 codded cryogel has the bigger pore sizes as 33μm which decrease to 3.4μm for DN-4/29. For both case, MTT say results show good level of cell viability (far more higher than 50 % for 3rd, 7th and 10th days which are the evidence for the absence of acute toxicity). LCSM images received from the SN-4 (33 μm) and TN4/7/20 (4.3μm) cryogels supported the viability results. This good viability results of TN-4/7/20 is attributed to the extraordinary pore architecture generated by second generation pores.

As a summary of these results, it was revealed that the DN and TN cryogels can increase the cell viability and be protected from any loss on mechanical properties as well. For this reason, these "second generation pores" make DN and TN cryogels a good candidate for load-bearing pre-made scaffolding approaches.

Within the second part of this thesis, multi-segmented hybrid hydrogels with two or three individual segments, which of each have chemically and physcially different properties were investigated from the stand point of designing and mechanical characterization.

As a general meaning, "hybrid" term corresponds to a thing which combines two different elements to obtain a new, mixed character. Within hydrogel studies, hybrid is a common use to describe the material via their structural components' character in a chemical or physical manner. Within a chemical manner, a hybrid hydrogel may be a combination of a synthetic and a natural, organic and inorganic sources. On the other hand, in terms of physical manner, a hybrid hydrogel may be a combination of different components having different physical properties together, such as isotropy and anisotropy, amorphus and semicrystalline structure, rigidity and flexibility, etc. to create a new material with a new desired character.

Biological tissues are mainly anisotropic, non-homogenous and multi-phasic natural constructs in an intermeshed architecture of hard and soft components with an extremely tough interface. Such important examples are bone, cartilage, ligament, tendon and intervertebral disc (IVD). Hydrogels are important materials with their similarity to biological tissues as they are matrices with ability to entrap the water or aqueous solutions. However, even their common brittle character was overcome by many techniques improved for decades, these high strength hydrogels reported so far were mostly isotropic.

Here, for the first time, preparation step of monomer mixtures for the one-step synthesis of hybrid hydrogels was achieved by stratification method to form an anisotropic multi-segmented hybrid hydrogel. By taking advantage of stratification, it was exhibited that, this method is available for a wide range of monomers. Therefore,

with several combination possibilities of different segments (with required physical and chemical properties), a multi-segmented hybrid gel formation serves as a puzzle-like method to use in various desired applications. Additionally, based on the biocompatibity of the polymers utilized in this study, hybrid hydrogels are potentially biocompatible.

Within this study, two- and three- segmented hybrid hydrogels were synthesized by using UV-initiated bulk copolymerization technique as polymerized density-stratified monomer solutions of hydrophobic (at least one or more) and hydrophilic monomer mixtures. Hydrophilic monemers were N-dimethyl acrylamide (DMA) or acrylic acid (AAc); hydrophobic monomers were octadecyl acrylate (C18A), stearyl methacrylate (C17.3M) or lauryl methacrylate (C12M). Hydrophobic monomers carrying alkyl side chains of different lengths lead to the formation of supramolecular, semi-crystalline hybrid hydrogels. Through this concept, it was possible to adjust the mechanical and thermal properties of segments and interfaces by varying the combinations of monomers. By this means, anisotropic biological tissue inspired hybrid hydrogels were demonstrated, as intermeshed hard and soft components through a strong interface(s), which never rupture at interface region(s).

According to the investigations, two-segmented hybrids exhibit a high modulus (0.46−74 MPa) and tensile strength (0.19−3.9 MPa) and sustain 24−30 MPa stresses at 78−83% compressions which are comparable to the natural IVD. Moreover, it was seen that it is possible to expose these gels to cyclic deformation without any irreversible deformation by the help of their semi-crystalline or supramolecular structure. In case of three-segmented hybrids, obtained results show also a high modulus (89-118 MPa) and tensile strength (3.6−4.6 MPa) with tensile strain of 50−75%.

Multi-segmented hybrids have the ability to self-heal upon heating above melting temperatures (T_m) once one or both of their gel components are damaged. It was also tested by separate examinations that the interface regions, also, have self-healing ability. Besides the self-healing ability, they exhibit a pseudo triple- or multiple- shape memory effect as well, arising from the different T_m belonging to the gel components of hybrids. For instance, two-segmented hybrid H2-2 (two-segmented hybrid) have only one semi-crystalline segment because the other segment shows an amorphous character. Thus, the H2-2 exhibit only dual shape memory. However, H2-1 (two-segmented hybrid) possesses two semi-crystalline segments which reflect to the whole body of two-segmented hybrid as a pseudo-triple- shape memory effect. Moreover, in case of three- segmented hybrids, H3-1 hydrogel comprises of three semi-crystalline segments which of their two have close Tm values than that of the remaining segment. Thus, two different T_m are obtained resulted in a pseudo-triple- shape memory. Another hybrid example, three-segmented H3-2 hydrogel, was observed as it has three semi-crystalline segments, hence three T_m which of these are in far different temperatures. Stemming from these three different T_m, H3-2 is able to exhibit pseudo-multiple- shape memory effect.

The synthetic strategy presented here thus enables combination of multiple gel components in a single, intermeshed material, leading to the preparation of multiple-shape memory hydrogels with multi-responsivity. Moreover, it is also possible to decide the place of stretchable and rigid parts in a multi component hybrid structure, according to the requisite, by using the monomers in different densities and chemical properties.

FARKLI KİMYASAL VE MEKANİK ÖZELLİKTE BÖLGELER İÇEREN BİYOUYUMLU HİDROJEL TASARIMLARI

ÖZET

Jeller canlılarda sıkça rastlanan, kolay ve etkin şekilde iyon ve molekül taşıyabilmeyi sağlayan yapılardır. Bir polimer jel, basitçe ıslak ve yumuşak malzeme olarak tanımlanır. Polimer jelleri tanımlayan iki kritik bileşen vardır. Bunlar, sahip oldukları çapraz bağ yapısının bir arada tuttuğu üç boyutlu, elastik, polimer ağyapı ve içerisinde çözünmediği ancak şişebildiği, ağyapısını ayakta tutan ve çökmesini engelleyen sıvıdır. Polimer jellerin elastik, çapraz bağlı ağyapısı malzemeye yumuşak olma özelliğini verirken, içinde hapsolan sıvı sayesinde jeller ıslak malzemeler olarak anılırlar. Her nekadar bu malzemeler ıslak ve yumuşak tabiata sahip görünseler de, endüstride kullanılan cam, metal, seramik gibi malzemelere kıyasla oldukça yüksek deformasyonlara dayanabilirler. Çok çeşitli yapısal mimarilerde ve kimyasal içerik çeşitliliğinde sentezlenebilen bu malzemelerin pek çok alanda yaygın olarak kullanılmalarının yanı sıra, biyomedikal uygulamalar ve kemik-doku mühendisliği gibi alanlarda da oldukça dikkat çekici uygulamalara dahil olmakta ve süren çalışmalar ile geliştirilmektedir.

Bu tez çalışması dahilinde, iki farklı jel malzeme farklı yönleri ile incelenmiştir. Bunlardan ilki olan tek ağyapılı (SN), çift ağyapılı (DN) ve üç ağyapılı (TN) kriyojeller, biyo-uyumlulukları bakımından incelenmiştir. İkinci çalışma ise; sentez aşamasının, tasarımının ve termal, mekanik özelliklerinin incelendiği çok parçalı hibrit hidrojelleri içermektedir.

İpek, kökleri 5000 yıldan fazla bir geçmişe dayanan biyolojik malzemedir. İpek böceği kozalarından iplikçikler şeklinde elde edilen ipek proteini, geçmişte kraliyet ailelerinin giyiminde de tercih edilmeleri ile seçkin bir ham madde olarak kültürler arasında bir köprü vazifesi görmüştür. Günümüzde de çekme dayanımı, düşük ısı iletkenliği, parıltısı ve nem emme kapasitesi ile yaygın olarak tekstil endüstrisine hizmet etmektedir. İpeğin diğer ilgi çekici uygulama alanları ise şöyle sıralanabilir: ev içi dekorasyon, paraşüt kumaşı, bisiklet tekerleği, yatak dolgusu, vb. Ayrıca ipek, çeşitli fiziksel özellikleri, biyo-uyumluluğu ve pek çek hücre türünün tutunması, gelişimi ve yayılışını desteklemesi sayesinde doku mühendisliği ve rejeneratif tıp gibi biyomedikal sahalarda kullanılan en önemli malzemelerdendir.

Bu tez çalışmasının ilk bölümü kapsamında, *Bombyx mori* türü ipek böceğinden elde edilen ipek-fibroin proteini kullanılarak sentezlenen SN, DN ve TN ipek-fibroin kriyojellerinin biyo-uyumlulukları ön-yapım hücre iskelesi olarak incelenmiştir. Araştırmada kullanılan kriyojeller, araştırma grubumuz tarafından önceden mekanik ve morfolojik özellikleri belirlenmiş malzemelerdir. Önceden belirlenmiş mekanik ve morfolojik karakterleri göz önüne alınan bu kriyojellerin kantitatif sonuçları MTT hücre canlılığı tespit testi ile elde edilmiştir. Kriyojellere ait kalitatif izlenimler ise Lazer Taramalı Konfokal Mikroskopi (LCSM) tekniği ile edinilmiştir. Hücre iskelelerindeki hücre canlılığını kanıtlayan bu teknikle elde edilen görüntüler hücre

iskelesinin çeşitli derinliklerinden alınıp üst üste istiflenmesi ile elde edilmiş, kompozit görüntülerdir. Bütün hücre kültürü içeren çalışmalarda normal insan deri fibroblast (NHDF) hücre hattı kullanılmıştır.

Çalışmada kullanılan hücre iskeleleri arasında hücre canlılığı- ile gözenek boyutu, yüzey alanı, çeper kalınlığı ilişkisini gözlemleyebileceğimiz iki tür malzeme bulunmaktadır. Farklı ipek-fibroin derişimlerinde sentezlenen SN kriyojelleri serisinde, artan ipek-fibroin derişimine bağlı olarak düşen gözenek boyutu ve gözeneklilik, çeper kalınlığında ise artış gözlemlenmiştir. Diğer kriyojel serisi ise, ipek-fibroin derişimi artışı ilk ağyapı olan SN'e yeni ağyapıların gömülmesi ile elde edilen DN ve TN kriyojel serisidir. Bu seriye dahil kriyojel örneklerinde gözlemlenen en önemli özellik, çeper kalınlığının artmamasıdır. Bu özellik SN kriyojelin sahip olduğu büyük gözenekler içerisinde, yeni ağyapıların eklenmesiyle meydana gelen, "ikinci nesil gözenekler" olarak adlandırılan, yeni küçük gözeneklerin oluşmasındandır. Ayrıca, çeper kalınlığı artmaksızın oluşan bu ikinci nesil gözenekler sayesinde hücre tutunması için yüzey alanı oldukça artmaktadır. Hem SN kriyojellerin, hem de ikinci nesil gözeneklere sahip DN ve TN kriyojellerin ortak ve önemli özelliği ise, biyomedikal uygulamalarda büyük önem taşıyacak olan içten birbiri ile bağlantılı gözenek yapısına sahip olmalarıdır.

MTT hücre canlılığı tespit testi sonuçları %90 ve %75 gözeneklilik oranına sahip kriyojellerde hücre canlılığının daha iyi olduğunu göstermiştir. Bu sonu. literatür ile uyumludur. Ayrıca sonuçlar hücre canlılığı oranlarının kriyojellerin sahip olduğu ipek-fibroin derişiminden bağımsız olduğunu göstermiştir.

Normal insan deri fibroblast hücresinin büyütülmesi için gerekli hücre iskelesinin gözenek boyutu literatürde 5-15μm olarak belirtilmesine rağmen, Bu çalışmada incelenen SN-4 (33μm) ve DN-4/29 (3,4μm) kodlu kriyojellerde, 3., 7. ve 10. günlerde, %50'nin oldukça üzerinde iyi hücre canlılığı gözlemlenmiştir. Değerlerin %50'nin üzerinde olması kriyojellerin akut toksititeye sebep olmadığının kanıtıdır. Lazer Taramalı Konfokal Mikroskopi yöntemi ile SN-4 (33μm) ve TN-4/7/20 (4,3μm) kriyojelleri için alınan kompozit görüntüler ile de kantitatif hücre canlılığı testi sonuçları doğrulanmıştır. TN-4/7/20 kodlu kriyojelde gözlemlenen iyi seviyedeki hücre canlılığının bu malzemenin iç yapısında oluşan ikinci nesil gözenekler ile sağlandığı tespit edilmiştir. Görüntülerde hücre çekirdeği ve aktin filamentleri sırasıyla mavi ve kırmızı renklerde net olarak gözlemlenmiştir. Bu gözlem de sağlıklı bir sonuç alındığını kanıtlamıştır.

SN, DN ve TN ipek- fibroin kriyojelleri ile yapılan çalışma sonucunda bütün malzemelerin iyi derecede hücre canlılığı gösterdiği, ancak DN ve TN kriyojellerin yapılarındaki ikinci nesil gözenekler yardımı ile küçük gözenek boyutlarına rağmen beklenenin ötesinde iyi hücre canlılığı oranları gösterdiği belirlenmiştir. Bu sebeple, SN kriyojellerin yanı sıra özellikle DN ve TN kriyojellerin ikinci nesil gözenekleri ve üstün mekanik dayanım özellikleri yardımı ile yük dayanımı gerektiren ön-yapım hücre iskelesi uygulamalarında kullanılabilecek uygun malzeme adayları olduğu görülmüştür.

Bu tez çalışmasının ikinci kısmında ise çok segmentli hibrit hidrojeller incelenmiştir. Çalışma dahilinde sentezlenip incelenen çok segmentli hibrit hidrojeller, iki ya da üç adet kendi içerisinde farklı fiziksel ve kimyasal özelliklere sahip segmentlerin bir arada olduğu tek bir hibrit hidrojel yapısıdır ve bu hidrojeller, mekanik karakterizasyona tabi tutulmuştur.

Genel anlamı ile “hibrit” tabiri iki farklı elamanı yeni bir karakter elde etmek için yapısında birleştiren, yapısında bulunan elementlerin karışık bir karakterini sergileyen her hangi bir şeydir. Hidrojel çalışmalarında genel kullanımına göre ise fiziksel ya da kimyasal iki bileşeni bünyesinde toplayarak, içeriğindeki bileşenlerden farklı bir karakter sergileyen malzemedir. Kimyasal anlamda doğal ve sentetik, kimyasal ve fiziksel gibi farklı özelliklerin hibriti oluşturabilir. Fiziksel anlamda ise, malzemeden beklenen performansın sergilenebilmesi için, izotropi ve anizotropi, amorfluk ve yarı-kristalin yapı gibi özelliklerin bir araya getirilmesinden doğan yeni bir hidrojel karakteri olabilir.

Biyolojik dokular genellikle anizotropik, homojen olmayan, çok fazlı, yumuşak ve sert dokuların oldukça tok bir arayüz ile birbirine kenetlendiği yapılardır. Bazı önemli örnekleri, intervertebral disk (IVD), kemik, ligament ve tendon olarak sıralanabilir. Hidrojeller de, yapılarında su ya da vücut sıvısı gibi sulu-çözeltileri hapsedebilme özellikleri ile biyoloji dokulara oldukça benzer özellikler gösteren malzemelerdir. Son zamanlarda, kimyasal çapraz bağlı geleneksel hidrojellerin sahip olduğu kırılgan yapı dezavantajı, yapılan pek çok çalışma ile aşılmaya çalışılmış ve oldukça iyi örnekleri rapor edilmiştir. Ancak bu hidrojel çalışmalarının çoğu izotropik karakterli malzemeleri sunmuştur.

Bu çalışmada ilk defa, anizotropik çok segmentli hidrojeller, segmentleri oluşturan monomer çözeltilerinin yoğunluk farkı katmanlaştırması/stratifikasyonu yöntemi ile bir araya getirilmiş ve tek basamaklı, UV-tetikleyicili kütle polimerizasyonu metodu ile sentezlenmiştir. Yoğunluk farkı ile katmanlaştırma yöntemi yardımı ile çok segmentli hibrit hidrojel yaklaşımı çok çeşitli monomerler için uygulanabilir, uygun bir yöntem olarak sunulbilmektedir. Bu yöntem ile yap-boz parçaları birleştirir gibi, kimyasal ya da fiziksel olarak istenen özellikteki bileşenler bir araya getirilebilir ve anizotropik çok segmentli hibrit hidrojeller elde edilebilir. Ayrıca, bu çalışmada kullanılan polimerlerin biyouyumlu oldukları bilindiği için, malzemenin olası biyo-uyumlu malzemeler olduğu söylenebilmektedir.

Çalışma dahilinde sentezlenen çok segmentli hibrit hidrojellerin segmentleri, bir hidrofilik ve bir ya da iki hidrofobik monomer içermektedir. Kullanılan hidrofilik monomerler N-dimetil akrilamid (DMA) veya akrilik asit (AAc)’dir. Hidrofobik monomerler ise oktadesil akrilat (C18A), stearil metakrilat (C17.3M) ve lauril metakrilat (C12M)’dır. Farklı uzunlukta alkil yan zincirlerine sahip hidrofobik monomerler sayesinde hidrojellerde supramoleküler ve yarı-kristalin yapı sağlanmıştır. Yapıdaki hidrofilik ve hidrofobik monomerlerin değiştirilmesi ya da derişimlerinin değiştirilmesi yoluyla, hidrojellerin termal ve mekanik özellikleri istenilen şekilde ayarlanabilmektedir.

İncelemeler sonucunda elde edilen sonuçlara göre, iki segmentli hibrit hidrojeller, yüksek modül (0,46-74 MPa) ve çekme dayanımı (0,19-3,9 MPa) göstermektedir. Basma dayanımı testlerinde ise 24-30 MPa yüke %78-83 gerinim ile dayanım gösterdikleri belirlenmiştir. Üç segmentli hibrit hidrojellerinde yüksek modül (89-118 MPa) ve %50-75 gerinim oranı aralığında 3,6-4,6 MPa çekme dayanımı sergilediği bulunmuştur. Bu özelliklerin IVD’nin mekanik dayanım özelliklerini karşılayabilecek sınırlarda olduğu belirlenmiştir.

Çok segmentli hidrojellerin bir ya da iki segment zarar gördüğünde, hidrojellerin kendilerini erime sıcaklığı (Te) üzerinde bir sıcaklıkta onarabildiği görülmüştür. Hidrojellerin arayüzünü taklit etmesi için ayrıca sentezlenen hidrojeller üzerinde yapılan çalışmaya göre, arayüzler de kendilerini onarma özelliğine sahiptirler.

Kendini onarma özelliği yanında, çok segmentli hibrit hidrojeller psödö/sözde üçlü- ve çoklu- şekil hafıza özelliği sergilemektedirler. Şekil hafıza yeteneği de bu hibritlerin segmentlerinde var olan yarı-kristalin yapıdan kaynaklanmaktadır. Örneğin, iki segmentli H2-2 olarak kodlanmış hidrojel örneği: bir segmenti amorf, diğer segmenti yarı-kristalin bölge içeren bir hidrojeldir. Yarı-kristalin yapıdaki segment kendi özelinde ikili-şekil hafıza özelliği göstermektedir. Amorf kısım bir T_e sıcaklığı göstermediği için şekil hafıza özelliği göstermemektedir (ancak supramoleküler yapısı dahilindeki hidrofobik etkileşimler sayesinde kendini onarma özelliği göstermektedir). Dolayısı ile H2-2 hidrojeli ikili şekil hafıza özelliği göstermektedir. Ancak örneğin, H2-2 hidrojeli her iki segmenti yarı-kristalin yapıda olduğu için ancak geçici şekiller bölgesel olarak segmentlerde sergilenip, malzeme bütününde yaygın olmadığı için psödö/sözde üçlü-şekil hafıza özelliği göstermektedir. Benzer şekilde üç segmentli H3-2 hidrojeli yapısındaki her üç yarı-kristalin bölgeye sahip segment yardımı ile psödö/sözde çoklu-şekil hafıza özelliği sergilemektedir. H3-1 hidrojeli örneğinde ise, her üç segment yarı-kristalin bölgeye sahiptir. Ancak iki uç segmentin T_e sıcaklığı birbirine çok yakın, orta segmentin Te sıcaklığı diğerlerinde belirgin şekilde farklı olduğu için bu hidrojel örneği psödö/sözde üçlü- şekil hafıza özelliği göstermektedir.

Bu çalışmada sergilenen sentetik yöntem ile beklentilere uygun çok segmentli hibrit hidrojellerin kendini onarma ve çoklu-şekil hafıza gibi üstün özelliklerle sentezlenebildiği gösterilmiştir. Yöntem segmentlerin gerekli mekanik ve termal özelliklerde ayarlanabileceği ve istenen dizilimle bir araya getirilebileceğini göstermiştir. Çalışmada hazırlanan hidrojeller yüksek yük dayanımı gerektiren biyomedikal uygulamalar için uygun birer adaydır.

Çalışmadan edinilen genel çıkarım ise, jel sentezinde kimyasal kompozisyon kadar, malzeme mimarisini değiştiren sentez tasarımlarının da büyük önem taşıdığıdır. Aynı kimyasal kompozisyon ve derişimlerdeki malzemelerin sentezde kullanılacak yeni bir tasarımla yepyeni ve daha gelişmiş özellikler sergileyebileceği bu çalışma dahilinde gösterilmiştir.

1. INTRODUCTION

A polymer gel, in the simplest term, is defined as soft and wet material. Their elastic cross-linked network brings them a soft texture, while the fluid, filling the interstitial spaces of network and in which the polymer network can swell without dissolving, renders this materials wet. Although polymer gels have wet and soft look, they are capable of bearing large deformations which are in contrast with most of the industrial materials such as ceramics, plastics or metals [1].

Gels are common structures found in living organisms which can sustain its solidity and allow the transportations of ions and molecules easily and efectively in the organisms. Therefore, polymer gels are mostly used materials with their wide-ranging and tunable properties in such areas like bone-tissue engineering, biomedical applications, etc. [1-5].

Various types of polymer gel classifications would be possible. Some of their well-known examples given below are made according to:

- the origin of polymer, *natural or synthetic gel*;
- source of liquid captured in the structure, *hydrogel or organogel*;
- nature of cross-link (the intermolecular bonds in the polymer gel junctions) they have, *chemical or physical*;
- the processes applied for the gel formation, *chemotropic gels, ionotropic gels, chelatotropic gels, solvotropic gels, thermotropic gels, psychrotropic gels, croyotropic gels*, or etc. [2,6].

Within the scope of this thesis, two different gel kinds were investigated which of them can be identified through the several classification routes mentioned above. Specific names of these polymer gels are:

- Single network (SN), double network (DN), triple network (TN) cryogels
- Multi-segmented hybrid hydrogels with multiple-shape memory and self healing abilities.

SN, DN and TN silk-fibroin cryogels are comprising of chemical and physical cross-links. According to the the processes applied for the gel formation and the origin of polymer, they can be called as cryotropic, natural gels. In the multi-segmented hybrid hydrogel case, naming can be made according to the nature of cross-link, origin of polymer and the source of the liquid captured in the structre. Thus, they can be called as physically cross-linked, synthetic hydrogels.

1.1 Silk-Fibroin Cryogels

This thesis is divided into two sections. Within the first part of the thesis, biocompatibility results of single network (SN), double network (DN) and triple network (TN) silk-fibroin cryogels will be presented. Through this first part, cryogels were examined as a cell scaffold. Synthesis of these cryogels and their morphological and mechanical characterization were already studied by our research group [7].

Silk has a unique coverage in history. As a biological material with provenience more than 5000 years ago, this protein polymer in the form of fibers spun by silkworms has served as a bridge between cultures, as a natural curiosity, as a scientific wonder and as an economic engine for developing countries over the millennia. The unique properties of silk in terms of mechanics, feel and luster have propelled this longstanding utility of silk, with high volumes of raw silk fiber generated annually throughout the world today [8].

As natural silk source, hundreds of various silkworm species are exist throughout the world. Among them, the Bombycoidea family comprises of eight families which of two, Bombycidae and Saturniidae, has commercial importance. Silks from the source of Bombycoidea family silkworms are categorized as “mulberry” while the Saturniidae family silkworm sourced silks are under the “non-mulberry” category. Commercially available mulberry silk is produced only from *Bombyx mori* species which are entirely domesticated and not occur naturally, thus, they need human care to grow [8].

Silkworms secrate two main protein, fibroin (around 72-81 % of cocoon) and sericin (around 19-28 % of cocoon), to form silk. Fibroin is secrated from the larvae during its spinning as two twin strands which are simultaneously glued to each other and covered with the sericin. This fiber, sericin covered twin fibroin strands, becomes

strong and hard with air exposure. As a hydrophobic glycoprotein, fibroin is water-insoluble protein and contains large amount of hydrogen bonds. Their highly oriented crystalline anti-parallel β-sheet structure forms semi-crystallinity by less oriented β-sheet spacers. Highly oriented β-sheets serves as a source of tougness and strength to silk fibers, while the less oriented sapacers provide flexibility and elasticity [8].

Today, silk is mainly utilized in textile industry, for its unique properties such as strength, low heat conductivity, luster and moisture absorbance capacity, as well as the interior decoration of houses, parachute clothing, bicycle tires, bed filling, etc. Moreover, most importantly, silk is used in biomedical fields such as tissue engineering and regenerative medicine [8].

Here in this study, biocompatibity of silk-fibroin protein was investigated through the specific form of porous gels, SN-, DN- and TN- silk-fibroin cryogels, for their potential use in biomedical applications such as bone-tissue engineering [8].

1.1.1 Application of silk-fibroin

Silk structure and morphology can be engineered by varying the physical, chemical and biological parameters to create desired features in material for target tissue. Silk is recognized by US Food and Drug Administiration for the medical or biomedical purposes. Their structure is suitable for high temperature sterilization, without any degredation or change in composition, as well as the chemical treatment, UV and gamma radiation exposure and 70% ethanol treatment. This studies were conducted between the years 2003-2005 [8]. However, in 2015, Kaplan and coworkers reported that low average molecular weight and low concentration silk-fibroin solutions can be sterilized by autoclaving or filtration without any significant loose of protein, but by autoclaving they obtained with a reduce in molucular weight distribution of these solutions. It was also reported by this study that, the degredation of silk-fibroin sponges cast from this autoclaved solution provide noticeably higher stiffness compared to the sponges cast from unsterilized or filtered solution. In contrast with the increasing degredation rate of sponges by means of gamma irradiation, sterilization of sponges by autoclaving in post-casting state were exhibited decrease in degredation with increased scaffold stifness. Ethylene oxide treatment significantly decreased cell proliferation rate on the silk-fibroin scaffolds but it is possible to be aware of this situation by phosfate buffer solution (PBS) leaching of ethylene oxide treated sponges

prior to cell seeding [9]. Here in this study, two step sterilization was made. First silk-fibroin scaffolds were sterilized by immersing them in to a 70% ethanol. Then, scaffolds were processed through PBS leaching prior to the second sterilization step of UV-irradiation sterilization.

Important silk-fibroin based matrices for use in biomedical applications include: 2D films and patterned nanostructures, 3D sponges/foams, hydrogels, nonwoven mats, fibers, spheres and capsules. The methods of production of the matrices are various [8]. Within this study, 3D sponge like scaffolds, synthesized by a special gelation procedure of cryogelation with a supporting double-networking concept, was used.

According to the description introduced by National Institutes of Health (USA):

"Tissue engineering/regenerative medicine is an emerging multidisciplinary field involving biology, medicine, and engineering that is likely to revolutionize the ways we improve the health and quality of life for millions of people worldwide by restoring, maintaining, or enhancing tissue and organ function".

Tissue engineering is a promising alternative for surgical methods like amputation or organ transplantation. In regenerating a neo-tissue, scaffolds provide a matrix for supporting the cells to grow. Among the natural polymers, silk has emerged as one of the foremost biomaterials to be used in tissue engineering. The potential use of silk based scaffolds for tissue engineering in the past few decades were broadly reported under three main heading as hard tissue (bone, cartilage, fibro-carilage-meniscus, intervertebral disc (IVD), hyaline cartilage-trachea, joint surface), soft tissue (ligaments and tendons, vascular tissue, nervous tissue), organ (skin, liver, eye, breast, cardiac, bladder, ear) [8].

Due to the intense mechanical strength and extensibility, silk scaffolds could be an convenient choice in repearing load-bearing tissues such as osteochondral tissue, ligament, muscle, or IVD [8].

An IVD is a complex multilamellar interbody join that transmits load and preserves stability and strength through the entire range of spinal motion (flexion, axial compression, torsional twisting, and lateral bending). Each disc is a biconvex structure consisting of three different region in the aspects of deveplopmental, histological and morphological architecture. This seperate regions are the nucleus pulposus (NP) which is central semifluid, gelatinous mass as a load dissipative core mechanism; annulus

fibrosus (AF) composing of ligamentous peripheral tissue which withstands under many load cycles of spinal motion by taking the advantage of their anisotropic, angular-lamellar orientd structure; and two cartilaginous end plates that attach the disc to the vertebral body [10]. Figure 1.1 demonstrates the architecture of an IVD.

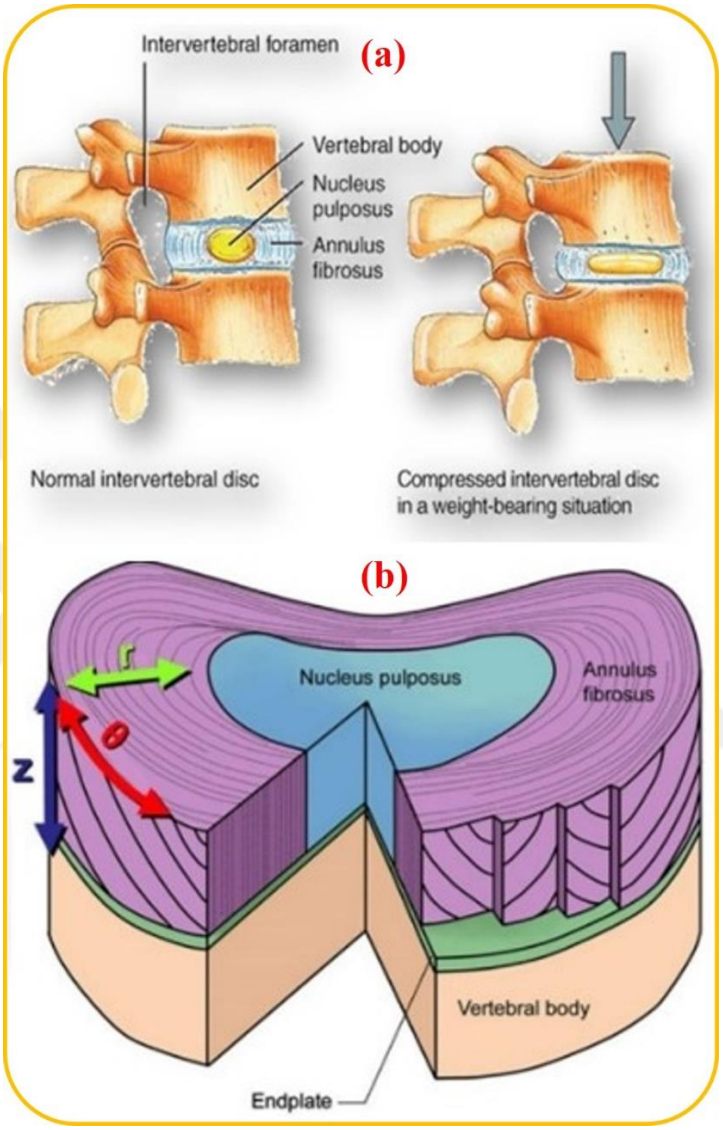

Figure 1.1 : Representative demonstrations of (a) an intervertebral disk (IVD) in a spine (Reprinted from *Intervertebral Disc: What is it? What does it do? And how to keep it healthy*, Greg Schroeder, 2016. Retrieved October 1, 2017, from http://www.wieberphysicaltherapy.com/intervertebral-disc-keep-healthy/. Copyright 2016 by Greg Schroeder. Reprinted with permission.) [11] and (b) its anisotropic architecture (Reprinted from "Mechanical design criteria for intervertebral disc tissue engineering.", by Nerurkar, N. L., et al., 2010, *Journal of Biomechanics*, 43 (6), 1017–1030. Copyright 2018 by Elsevier Ltd. Reprinted with permission.) [12].

Within the existing scaffolding approaches for IVD tissue engineering, using pre-made scaffolds (cell seeding after scaffold contruction approach), as in this thesis study, is most common. Several scaffolding studies were carried ot by dominating the materials

(collagen [13], atellocollagen [14,15], alginate [16,17], gelatin [18], chitosan [19], collagen/ glycosaminoglycan [20], collagen/hyaluronan [21] and poly- L-lactic acid [22]) by natural sources. On the other hand, a wide range of scaffolding investigation were conducted (silk [23], polycaprolactone [24] and its derivatives [18], polyglycolic acid/ polylactic acid [17] and bioglass [25] with a few natural biomaterials such as collagen/hyaluronan [21]) by dominating the materials from synthetic sources. Within this study, silk-fibroin natural material was used to construct a pre-made scaffolds by the additon of synthetic cross-links to support the juctions already exist in fibroin protein as β-sheet architectures.

Chang et al. prepared porogen leached scaffold from *Bombyx mori* silk in 2007. With this study, AF cells (isolated from bovine caudal spines) seeded scaffolds, having randomly oriented pores in 150–250 μm sizes, were investigated They also modified silk scaffold with RGD peptidesequences which did not significantly enhanced cell attachment, collagen accumulation, or extra cellular matrix formation compared to only silk scaffold. They observed that, tey can obtain uniformly distributed tissue growth in the scaffold. But they also reported that, randomly oriented pores could not generate cellular orientation as required in AF tissue [8,26].

In 2010, Chang et al. investigated same scaffoling approach in a dynamic culture. Large pore sized (200, 600, and 1000 μm pore size) silk scaffolds have been used in combination with bovine AF cells. Investigation revealed that 600 μm was the most suitable pore size for uniform tissue formation and highest production of collagen type I [27]. Although this so-called proper scaffold was maintained a good cell enviroment, mechanical withstand capability was low because of the hich pore sizes, which is the main requisity for the load-bearing tissues.

See et al. conducted a study, with knitted silk fabrics wrapped around silicone NP-substitute. Rabbit bone marrow-derived mesenchymal stem (BMSC) cultured over poly(N-isopropyl acrylamide) (PNIPAAm) to obtain cell sheet. Then this cell sheet was allowed to adhere to the knitted scaffold. A multi-layered lamellar architecture was acquired. At the beginning, BMSC cell sheets pre-dominantly synthesized collagen type I. However, after 4 weeks culture on the silk assembly, collagen type II deposition increased drastically. Cellular orientation and mechanical properties were not studied [28].

Park et. carried out a scaffold by lyophilization of silk-fibroin and sodium alginate solution mixture. Sodium alginate was subsequently removed from scaffold, as they used as a template for lamellar pore geometry. To use in a comparison manner, carbodiimide/*N*-hydroxysuccinimide doped silk gel freezedried with water annealing generated randomly. Porcine AF cells were cultured over these scaffolds. As they observed, only silk lyophilized solutions resulted in 10–20 μm pores, addition of alginate was increased the pore sizes to 150–250 μm. Lamellar pores were not circannual orientated, sothe scaffold could not simulated the orientation of AF cells. Tensile strength and elongation test made were showed scaffold has similar properties with the native tissue, with inferior properties for lamellar scaffolds [29,30].

Bhattacharjee et al. invstigated a chondroitin sulfate crosslinked scaffold which was precisely oriented silk fibers wrapped around silk gel. They cultured human nasal chondrocytes on the scaffold. Fibrous scaffold (as a multilayered fibrous structure, where silk filaments are wrapped at different angles in successive layers) simulated multilamellar structural hierarchy of the AF. As they observed, scaffolds supported cell attachment and orientation similar to the fiber orientation and ECM produced by the cells also followed the orientation of the cell alignment. Compressive strength of the scaffold was similar to the native goat AF tissue [31].

Park et al. conducted a study with a scaffold for whole disk purpose. For culturing, human articular condrocytes (for NP part) and porcine condrocyte (for AF part) as used. For NP, cell viability was found 90%. Homogeneous distribution of cells over lamellar scaffold was obtained but cells could not penetrate into inner layers of the porous inner. Precise cellular and fiber orientation could not not achieved and mechanical sufficiency was not studied [29].

Here, within this study a pre-made silk- fibroin scaffolds with a complex interconnected pore architecture and outstanding mechanical withstand capacity was investigated by means of biocompatibility through the use of hurman normal dermal fibroblast cell line cultures.

1.1.2 Scaffolding in tissue engineering

Except the blood cells, usually normal cells in human tissues are tend to reside in solid matrix as anchored called extracellular matrix (ECM). Several types of ECM are exist

in human tissues which of them generally have multiple components and tissue-specific composition. The functions of ECM in native tissues are:

- providing structural support for cells to attach, grow and migrate,
- contibuting to the mechanical properties of tissues
- providing bioactive signals for cells to respond their microenvironment
- acting as the reservoirs of growth factors and increase their actions
- providing a proper flexible physical environment to allow remodeling during the dynamic processes of tissues like wound healing [8].

In a tissue engineering process, scaffolds take the place of ECM analogously by means of supporting cells to have the environment they used to have in the existence of ECM [32].

Since its emergence in the middle of 1980s, tissue engineering has retain its crucial role in restoring and replacing the biological substitutes or in regenerating the defective tissues [32-34]. A tissue engineering process has three main components as scaffold, cells and growth-stimulating signals. An ideal scaffold, typically made of polymeric biomaterials, should provide the structural support as a framework for initial cell attachment and subsequent tissue development [32,33]. Scaffold microstructures (porosity, pore size, pore shape, interconnectivity, specific surface area) [25] and mechanical properties [36-38] have also significant effect on cell behaviors such as adhesion, growth and differentiation and to affect the bioactivity of scaffolds used for in vivo regeneration applications of various tissues, such as cartilage, skin and peripheral nerves [38]. Well known scaffolding approaches for tissue engineering can be collected under four major titles. These are:

1) Decellularized extra cellular matrix (ECM) from allogenic (tissues from same species but having different gene constitutions) or xenogenic tissues (tissues from different species) for cell seeding,
2) Cell sheets with self-secreted ECM,
3) Cell encapsulation in self-assembled hydrogel matrix
4) Pre-made porous scaffolds for cell seeding [32].

A schematic summary of these titles can be seen in Figure 1.2.

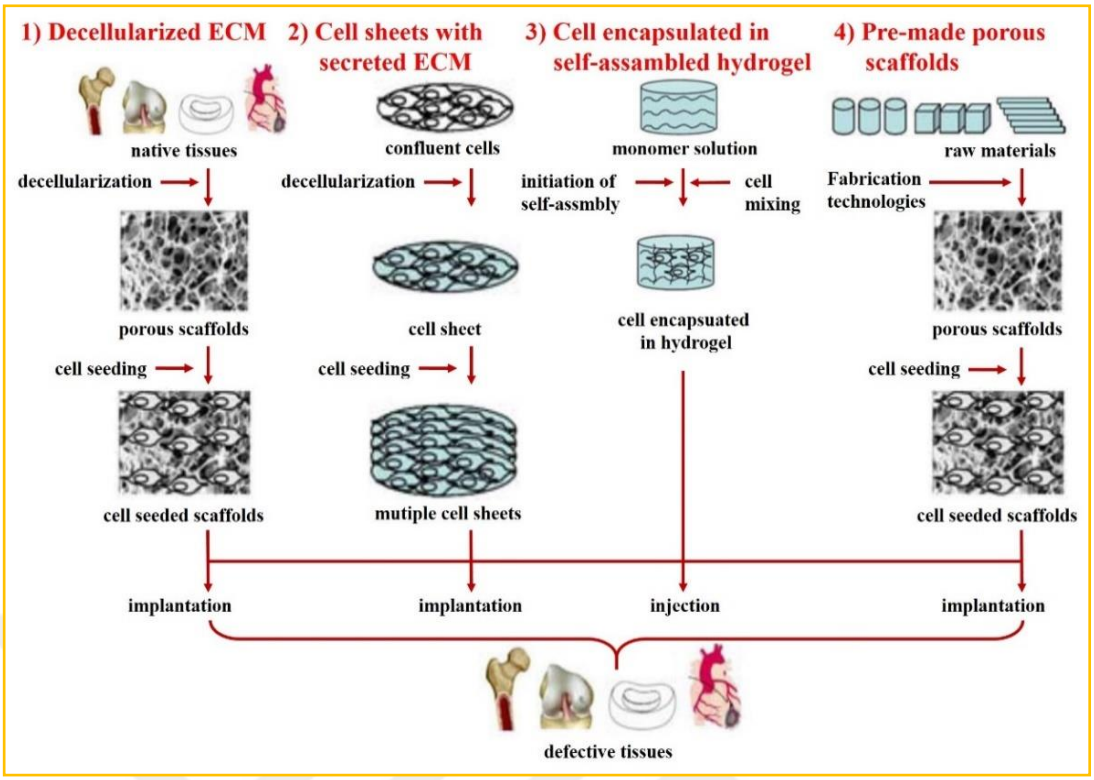

Figure 1.2 : Schematic diagram of different scaffolding approaches. Adapted from "Scaffolding in tissue engineering: general approaches and tissue-specific considerations", by Chan, B. P. and Leong, K.W., 2008, *Eur Spine J*, 17: (Suppl 4), S467–S479. Copyright 2008 by Springer-Verlag. Reprinted with permission [32].

1.1.2.1 Decellularized ECM from allogenic or xenogenic tissues

Scaffolds obtained by using this method are the most nature-simulating scaffolds, which have been used for many tissues including heart valves [39], vessels [40], nerves [41], tendon and ligament [42]. This scaffolding approach removes the sources for immunogenicity upon implantation but preserves the ECM components, which render these scaffolds immunologically well-tolerated. Besides the excellent biocompatibility of the natural ECM, decellularized matrix preserves growth factors which is in favor of further facilitating of the cell growth and remodeling [43]. Nevertheless, this method may also lead to inhomogeneous distribution of cells or immune reactions after the implantation because of the possible deficient removal of cellular components [32,44].

1.1.2.2 Cell sheets with self secrated ECM

By using this method, cells secrete their own ECM upon confluence and are harvested without the use of enzymatic methods. By means of repeating the process, laminating of multiple single cell layers to form thicker matrix is possible. Cell sheet engineering approach is excellent for epithelium, endothelium and cell-dense tissues [45,46]

However, issues with rich ECM for load bearing purposes are unlikely to be acquired by this approach [32, 46].

1.1.2.3 Cell encapsulation by self-assambled hydrogel matrix

Encapsulation is, simply, the entrapping of living cells within a semi-permable membrane or a homogenous solid mass. [47-49]. Hyrogels having covalent or ionic cross-links are mostly used biomaterials for the encapsulation. Several types of natural and synthetic hydrogels can be used with an only limitation of availibity of hydrogel formation in the existance of living cells. Nevertheless, hydrogel materials suitable for this approach usually have poor mechanical properties, resulting in limited or no use of this approach in load bearing functions [32].

1.1.2.4 Pre-made porous scaffolds for cell seeding

Seeding therapeutic cells in pre-made porous scaffolds process is the most commonly used and well-established scaffolding approach thenceforward the early times of tissue engineering [50,51]. According to the sources of biomaterials used for fabricating the porous scaffolds can be divide into two types as natural and synthetic biomaterials. Natural sources, like silk-fibroin protein, usually have superb biocompatibility so that cells can attach and grow with excellent cell viability. However, the physical and mechanical instability of naturally derived scaffolds cause their limited or no use in load-bearing applications. Another issue is the potential immunogenicity may rise from the antigenic state of host against the source of biomaterial. Synthetic biomaterials can be generally categorized into inorganic (bioglasses, etc.) and organic (synthetic polymers, etc.). Generally synthetic biomaterials are thought as materials with better controlled physical and mechanical properties which makes them suitable for both soft and hard tissues. Nevertheless, synthetic biomaterials usually have biocompatibility issues [32].

This scaffolding approach has a number of advantages some of which are including:

- having wide range of biomaterial choice (from ceramics to hydrogels),
- having relatively precise designs on architecture and microstructure of the scaffolds which favours especially in their use in load-bearing applications [32].

Nevertheless, this approach also has certain disadvantages as the post-fabrication cell-seeding to porous scaffolds is time-consuming and inefficient because of the limited penetration ability of cells into the scaffolds. For this reason, agitation, perfusion and enlarged pore size are needed to enhance cell seeding efficiency which them may cause lower cell viability and high costs [32].

In this study, "pre-made porous scaffolds for cell seeding" approach was used. Pre-made scaffolds were silk-fibroin single network (SN), double network (DN) and triple network (TN) cryogels. They are naturaly derived biomaterials as they were synthesized by using silk-fibroin protein. Since the source, silk cocoons, are widely utilized as raw-material in industry and has a sustainable fabrication, this material is highly cost-effective. In contrast with their equivalents using the silk-fibroin, cryogels investigated within this study have extraordinary mechanical properties as well as their well-known biocompatibility state [7,53-57]. These cryogel materials, having chemical crosslinks besides the physical crosslink points based on the formation of β-sheets, are recently synthesized by our research group [7], according to a toughening method called as double-networking concept. This concept was used for the first time in silk-fibroin cryogels [7]. Cryogels, synthesized by use of this concept, gained futher improvement in mechanical endurance. Moreover, as a main outcome of use of this concept, porosity was increased by the formation of second-generation pores which directly affects the cell viability. By considering all advantages mentioned above, silk-fibroin SN, DN, TN cryogels have a great potential in bone-tissue engineering applications.

1.1.3 SN, DN and TN silk-fibroin cryogels as a cell scaffold

Silk-fibroin, derived from *Bombyx mori,* is a fibrous protein exhibiting extraordinary material properties such as good biocompatibility, biodegradability, high strength and toughness, and ease of processability. Silk fibroin has been used for cell culture, wound dressing, drug delivery, enzyme immobilization and as a scaffold for bone tissue engineering [7,53-58].

Gelation of aqueous fibroin solutions mainly proceeds via self-assembly of fibroin molecules induced by hydrophobic associations to form intermolecular β-sheet crystallites acting as physical cross-link zones [68,69]. In many application areas such as in bone tissue engineering, silk fibroin gels are required to possess a high

mechanical strength and a 3D interconnected pore structure to provide a favorable microenvironment for cell attachment, infiltration, proliferation, and differentiation [56]. Several techniques have been developed to produce porous fibroin-scaffolds such as freeze−thawing, porogen leaching, gas foaming, electrospinning, and freeze-drying [57-67]. An alternative simple route to produce 3D highly porous fibroin networks is the low-temperature gelation technique, known as cryotropic gelation or cryogelation [7,53].

By cryogelation technique, polymerization and/or cross-linking reactions are conducted in apparently frozen reaction solutions. During the freezing of an aqueous polymer solution containing a chemical cross-linker, the polymer chains and the cross-linker molecules are expelled from the ice concentrate within the liquid channels between the ice crystals, so that the cross-linking reactions only proceed in these unfrozen domains. After cross-linking and after thawing of ice, a macroporous material is produced whose microstructure is a negative replica of the ice formed. In contrast to the mechanically weak macroporous gels prepared by a phase separation technique, cryogels are very tough and withstand very large strains without permanent deformation or fracture [7,53].

Silk fibroin scaffolds developed by the techniques other than cryogelation, which were mentioned above, exhibit Young's moduli between 10 kPa and 3 MPa. According to the cryogelation technique, introduced by our research group [53], macroporous silk fibroin scaffolds exhibit a very high Young's modulus (50 MPa). Although macroporous scaffolds in aqueous environments are usually brittle and rupture at a few tens percent of deformation, those derived from cryogels can completely be squeezed without any crack development [53]. Therefore, as shown recently, silk fibroin cryogels are most promising candidates as a scaffold for bone regeneration [7,53].

Recently, an outstanding advancement was reported by our research group in improving the mechanical and structural properties of the silk-fibroin cryogels by using double-networking concept [7], which of this concept’s pioneering studies were conducted as a hydrogel [70,71].

Double network (DN) hydrogels described by Gong and co-workers consist of interpenetrating brittle and ductile polymer networks containing 60−90% water [72]. For instance, DN hydrogels made from poly(2-acrylamido-2-methylpropanesulfonic

acid) (PAMPS) polyelectrolyte and linear polyacrylamide (PAAm) exhibit exceptional compressive strengths of about 20 MPa and fracture energies in the hundreds of J m^{-2} [72]. Under large strain, the highly cross-linked, brittle first network (PAMPS) breaks up to form many cracks while the second ductile network (PAAm) keeps the gel sample together [72-75]. DN hydrogels are prepared by swelling a highly cross-linked polyelectrolyte first network hydrogel in a solution of a second monomer and then polymerizing the second monomer to form a loosely crosslinked (or linear) second network. Although both networks are sequentially polymerized, some cross-linking between the two networks is possible due to the incomplete polymerization of the first network [76]. Based on the pioneering work of Gong and co-workers [72], several kinds of DN hydrogels were reported in the literature [77-82], including the inverse DN hydrogels in that a loosely cross-linked polyelectrolyte network is prepared within the highly cross-linked nonionic network [83,84].

Recently, Okay and co-workers achieved to obtain nonionic PAAm and PDMA hydrogels with extraordinary mechanical properties by the triple network (TN) approach (containing 89−92% water and exhibiting high compressive fracture stresses up to 19 MPa and compressive moduli up to 1.9 MPa) [85].

Utilization of double–networking concept in cryogelation technique was recently by reported by Zhao et al. Reported DN cryogel was synthetic according to its source and exhibit pH- and temperature sensitiveness [86]. However, their mechanical strength is much lower than that of fibroin cryogels. To produce double network (DN) and triple network (TN) silk fibroin cryogels of high mechanical strength, entreated within this thesis by means of biocompatibility investigation, the initial single network (SN) fibroin cryogel scaffolds were first immersed in aqueous fibroin solutions containing chemical crosslinker and then cryogelation reactions were conducted to produce fibroin cryogels with a DN structure. By repeating this step, TN cryogels were generated. Thus, SN and DN fibroin scaffolds were used as precursors for the DN and TN cryogels, respectively [7]. Figure 1.3 shows the schematic illustration of SN, DN and TN silk-fibroin cryogel formation. In this cryogels, fibroin network components interpenetrate and interconnect to each other resulting in the formation of waterinsoluble SN, DN, and TN cryogels.

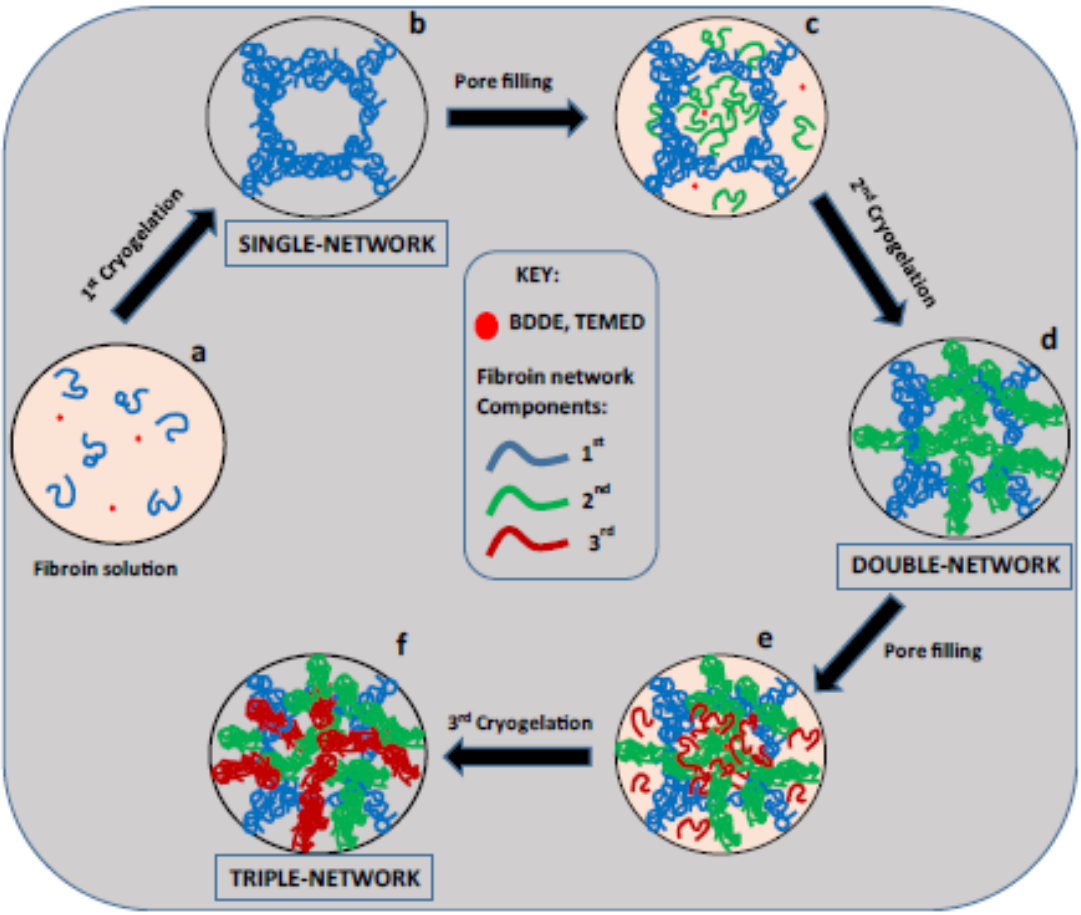

Figure 1.3 : Schematic illustration of the fibroin cryogel formation with single-, double-and triple-network structures Reprinted from "Cryogelation within cryogels: Silk fibroin scaffolds with single-, double- and triple-network structures.", by Yetiskin, B., Akinci, C. and Okay, O., 2017, *Polymer*, 128, 47–56. Copyright 2017 by Elsevier Ltd. Reprinted with permission [7].

The main underlying idea in the multiple network silk-fibroin cryogel formation is to produce cryogels having two generations of pores by carrying out the cryogelation reactions within the pores of a precursor cryogel, as schematically illustrated in Figure 1.3 [7]. Scaffolds having both large and small pores receive significant interest in tissue engineering due to the fact that the large pores of tens of micrometers in diameter are suitable for cell migration while smaller pores with a few micrometers are highly effective for nutrients and oxygen delivery [87-90].

It was reported that increasing cell viability is mainly occurs due to enhanced nutrient supply and more efficient metabolic waste removal from the interior regions of scaffold constructs. Due to the formation of smaller pores, as second generation pores, in SN cryogels by obtaining a DN, specific surface area increases. Thus, a more

favourable environment can be acquired in which cells could remain viable and proliferate to a greater extent [91-94].

In order to obtain a scaffold for tissue engineering, material clustering, pore size, surface area, wall thickness and homogeneity etc. have critical importance [38]. For the study which will be exhibited through the first part of the thesis, we have two kinds of materials to clarify the relationships between cell viability and pore size, surface area and wall thickness. SN crogels synthesized by increasing fibroin concentrations represents decreasing pore size and porosity while wall thickness is increasing. The other set of cryogels, named as DN and TN cryogels represent increasing fibroin concentrations by the penetration of new networks inside the single network. However, DN and TN cryogels exhibit no increase in wall thickness with the help of formed pores inside the bigger pores of single network pores which are called as second generation pores. Moreover, decreasing in pore size occasioned by second generation pores and incresing fibroin concentration cases were run with increasing surface area. Besides all, both of two cryogel type have an advantege for biomedical applications as they have interconnected pores. It was reported in the literature that, pores of adequate size allow cells to migrate or adhere to the surface of a material, but interconnecting pores are necessary to permit cell growth into the scaffold interior [38].

Reported studies mention that, there are limits of acceptable scaffold architecture (volume fraction (VF:surface area/volume ratio), pore size) that influence in vitro cellular responses. Additionally, pore size and VF have combined effect on cellular adhesion, viability, ingrowth, distribution, and the formation of an ECM by specific cell types. A high VF combined with a proper pore size is required for *in vitro* cell attachment, proliferation, and subsequent matrix deposition. It was also reported that the optimum VF for engineering homogeneous tissues may be greater than 90% or between 75% and 90% [95].

It was reported that the diameter of cells at issue in a tissue engineering study determines the minimum pore size required in a scaffold structure, which varies from one cell type to another. Therefore, pore size should be carefully controlled depending on the planned application. Studies made about the effect of scaffold pore size on tissue regeneration demonstrate that the optimum pore sizes are about 5 μm for neovascularization, 5-15 μm for fibroblast ingrowth, 20 μm for hepatocyte ingrowth, 20-125 μm for regeneration of adult mammalian skin, 40-110 μm for osteoid ingrowth

and 100-350 μm for regeneration of bone. Fibrovascular tissues require pores sizes greater than 500 μm for rapid vascularization and for the survival of transplanted cells. It should be noted that, the pore sizes obtained here have been performed for mentioned cell types up to 50 % porosities. [96, 97]

According to the study conducted in this thesis, combined effect of optimum pore size, porosity (%) and wall thickness could change these known pore size requisites. In this stuy, with the help of second generation pores obtained by double-networking method, the surface area/volume ratio of porous materials is not depend on the density and average diameter of the pores.

1.2 Hybrid Hydrogels

Within the second part of this thesis, multi-segmented hybrid hydrogels with two or three individual segments, which of each have chemically and physcially different properties were investigated from the stand point of designing and mechanical characterization.

As a novel part, for the first time, preparation step of monomer mixtures for the one-step synthesis of hybrid hydrogels by UV-initiated bulk polymerization was achieved by stratification method. Moreover, by this method, segments were integrated in the course of polymerization as a fused body of two or three individual segments with a stronger (than that of its individual segments), smooth interface region(s) in a few millimeters of thickness. Another exceptional properties of these hybrid gels are their self – healing ability and shape-memory behavior. Every single individual segments and the interface region(s) have these both extraordinary feature. Even if each of the segments have their own dual-shape memory behavior, as a combined behavior of these dual-shape memory segments, these materials have pseudo-triple- and pseudo-multiple- shape memory behavior in their whole fused body. This is the first time, that the terms of pseudo-triple- or pseudo-multiple- shape memory are used. By taking advantage of stratification, it was exhibited that, this method is available for a wide range of monomers. Therefore, several combination possibilities of different segments (with required physical and chemical properties) in a multi-segmented hybrid gel serves as a puzzle-like method to use in various desired applications. Additionally, according to the monomers used in this study, hybrid hydrogels are potentially biocompatible. Perspective of the design was established on introducing a brand new

artificial implant idea for load-bearing purposes like intervertebral disc (IVD), tendon, ligament, etc. applications. However, investigation on the biocompatibility of hybrid hydrogels is not a part of this thesis. Exclusively, three dimensional (3D) architectures of natural load-bearing structures (such as IVD, tendon and ligament) and the effect of these arhitectures on the mechanical properties were considered to get inspired. Inferences transfered to the design of hybrid hydrogels.

1.2.1 Hydrogels

Gel is a janus-faced state with its half solid-like and half liquid-like properties which causes many interesting relaxation behaviors that are not found in either a pure solid or a pure liquid. This extraordinary feature of gels originates from their elastic, cross-linked network structure which serves as a matrix for entraping the liquid in the structure [1,98,99].

Hydrogels are hydrophilic, cross-linked gels with a capacity to absorb large amounts of water or aqueous solutions, such as body fluids, without dissolving. Since the material has hydrophilic functional groups attached to the polymer backbone, name of the material takes the prefix “hydro”, in the meaning of “water” from Latin language. The reason why these materials called as “gel”, after the prefix of “hydro”, is because of their resistance against the dissolution by the help of cross-link points. Cross-links are the juctions wherein the polymer chains get together to form a three-dimensional (3D) network of polymers. Owing to the network chains connecting to each other, a hydrogel is by itself a one big molecule on a macroscopic scale with the ability to entrap water in its structure [1,98,99].

1.2.1.1 Hydrogels according to the cross-link type

In an attempt to understand the interesting mechanical properties of polymer gels, they should be considered at the molecular level. A dynamic, polymer network structure consists of several elements, including bridging strands (polymer chain that connects one cross-link to another), crosslinks (or junctions), dangling ends, and loops. are regarded as three dimesional (3D) networks of non-covalently bound polymer chains [100]. Here, “a physically-crosslinked hydrogel” is defined as a dynamic, network structure formed via reversible self-assembly of polymer chains in a non-covalent bonding manner or interactions. On the other hand, a chemically-crosslinked hydrogel

regards as a hydrogel of static network (permanent) with fixed mechanical properties due to their covolently bonded polymer chains.

The poor mechanical performance of chemically cross-linked hydrogels originates from their very low resistance to crack propagation due to the lack of an efficient energy dissipation mechanism in the gel network [101]. As schematically illustrated in Figure 1.4A, the energy focused around the crack tip cannot be dissipated properly in conventional, chemically-crosslinked hydrogels which causes the fracture of the whole material. In order to obtain a highly tough hydrogel, the overall energy dissipation along the gel sample has to be improved by introducing dissipative mechanisms at the molecular level as demonstared in Figure 1.4B [101].

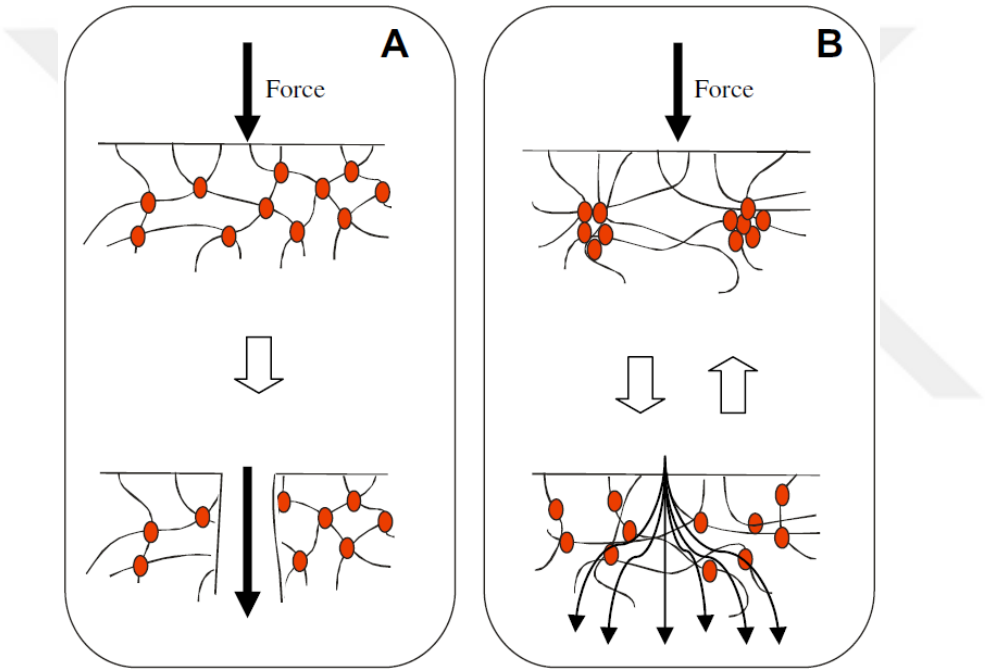

Figure 1.4 : Schematic illustration demonstrates: (A) the localization of applied energy in a conventional chemically-crosslinked hydrogels which results in a crack generation and (B) the dissipation of the applied energy in a physically-crosslinked hydrogel (e.g. hydrophobically modified hydrogel). Reprinted from "Design of high-toughness polyacrylamide hydrogels by hydrophobic modification.", by Abdurrahmanoglu, S., Can, V. and Okay, O., 2009, *Polymer*, 50, 5449–5455. Copyright 2009 by Elsevier Ltd. Reprinted with permission [101].

Significant progress has been achieved in recent years, in the design of mechanically strong and tough hydrogels [102] including: the topological hydrogels (sliding cross-link agents) [102], double network (DN) hydrogels [73,103,104], nanocomposite (clay filled) hydrogels [105] and supramolecular polymer network hydrogels [106]. These

designs of hydrogels were utilized in many mechanical performance-based approaches to mimic the biological systems.

A concept of chain crosslinking to form tophological hydrogels by using sliding crosslinking agents was reported by Okumura and Ito [107]. Within this concept, chemically crosslinked two cyclodextrin molecules were used as a sliding-double ring-crosslinking agent, to sustain their sliding along the different PEG chains (end-capped with a bulky group) of hydrogel structure. Results were outstanding with a high degree of swelling in water and a high stretching ratio without fracture [108].

Double networks (DN) are a subset of interpenetrating networks (IPNs) formed by two hydrophilic interpenetrated networks, the first polyelectrolyte network acting as a matrix for the subsequent network was brittle because of the highly crosslinked nature and the second neutral network was ductile by the help of loosely crosslinked structure [72]. The pionering study was made by Gong and co-workers. Although both networks are sequentially polymerized, some cross-linking between the two networks is possible due to the incomplete polymerization of the first network. Hydrogels containing about 90% water possessed an elastic modulus of 0.3MPa and fracture stress of ~10MPa, demonstrating both hardness and toughness. [108] Recently, Okay and co-workers achieved to obtain nonionic PAAm and PDMA hydrogels with extraordinary mechanical properties by the triple network (TN) approach (containing 89−92% water and exhibiting high compressive fracture stresses up to 19 MPa and compressive moduli up to 1.9 MPa) [85].

Nanocomposite hydrogels are organic–inorganic hybrids. They are based on N-isopropylacrylamide (NIPAAm) with hectorite as multifunctional crosslinker [105]. Exfoliated clay platelets are uniformly dispersed in an aqueous solution of NIPAAm monomer; polyNIPAAm chains are grafted on the clay surface by one or two ends. Here, up to 1500% elongation-at-break values were obtained. These hydrogels possessed extremely high surface hydrophobicities [109].

Hydrophobically modified hydrogels are supramolecular polymer networks. They are one of the very picture of tough, physically crosslinked hydrogels. As in large biological systems, which of their hydrophobic interactions play a dominant role in the formation, synthetic hydrogels can be generated by incorporation of hydrophobic

sequences within the hydrophilic polymer network chains [106]. Multi-segmented hybrid hydrogels presented in this thesis are also hydrophobically modified hydrogels.

1.2.1.2 Hydrophobically modified hydrogels

Conventional chemically-cross-linked hydrogels are covalently bonded, permanent shaped, hydrophilic 3D networks which are very brittle especially at their swollen state. Althoug they have a static network structure with their permanent crosslink, limited recovery can be obtained if the applied stress is low enough. Physically-crosslinked hydrogels are dynamic, reversible 3D networks based on their transient cross-links formed by interchain associations involving complementary functional groups that exhibit, for example, electrostatic interactions, hydrophobic interactions, and hydrogen bonding or produce crystallizing segments [110-116].

Since the physically cross-linked hydrogels possess a transient network structure rather than a permanent one, they represent relaxation in much longer periods than the application time of stress. When the stresses are either small, the temperature is sufficiently low, or the stress application is of short duration (i.e., short time or high frequency), it is possible to achieve that a physical gel may be mechanically indistinguishable from a covalent gel, and the network appears to be permanent. The reversible nature of the physcially cross-linked network structure provides unique properties, like viscous flow above a critical stress or time which favors the gel to be injectable and improved mechanical toughness compared with a covalent gel [117].

Garnier et al. synthesized hydrophobically modified polyelectrolyte hydrogels prepared by a complicated three step procedure [112]: a) introduction of double bonds onto a poly(acrylic acid) (PAAc) backbone, b) hydrophobic modification of PAAc with dodecyl amine, and c) crosslinking of double bonds using a dithiol. It was shown that hydrophobic modification of polyelectrolyte hydrogels provides a drastic increase in the viscous modulus G'' while the elastic modulus G' remains almost same [112]. This increase in G'' was generated by the help of energy dissipation mechanism obtained under the favor of the hydrophobic association formation as temporary junctions.

Okay and coworkers practiced on a simple, straightforward alternative for the preparation of such associative poymer materials is the free radical micellar polymerization technique, as first described by Candau and co-workers [118-125]. In

this technique, a water-insoluble hydrophobic monomer solubilized within the micelles is copolymerized with a hydrophilic monomer in aqueous solutions by free-radical addition polymerization. One limitation of this technique was that large hydrophobes cannot be solubilized within the micelles due to the very low water solubility of these monomers [126-128]. By means of the utilization of this technique in hydrogel synthesis, by Okay and coworkers, it was shown that n-alkyl (meth)acrylates with an alkyl chain length longer than 16, carbon atoms can be solubilized in a micellar solution of sodium dodecyl sulfate (SDS) by the addition of an electrolyte (such as NaCl) in a sufficient amount [106]. Salt leads to micellar growth which ensures the solubilization of hydrophobes. Copolymerization of acryl amide (AAm) with large hydrophobes solubilized within the wormlike SDS micelles produced physical hydrogels exhibiting unique characteristics such as insolubility in water, nonergodicity, high elongation ratios at break, and self-healing [106,129-132]. Hydrophobe content of the physical gels having the ability to self-heal was 2 mol % with respect to the total monomers while the self-healing ability disappeared as the hydrophobe content is increased [133]. Hydrogels formed via hydrophobic interactions in aqueous micellar solutions present two faces, depending on which state they are in. These states are (i) the preparation state, when the gels contain surfactant micelles, and (ii) the state in equilibrium with pure water, when the free surfactant micelles have been removed after preparation. With surfactants, the cross-links are reversible as a result of local solubilization of the hydrophobic associations, so that the hydrogels are weak. After removal of surfactant, however, direct exposure of the hydrophobic associations to the aqueous environment increases their lifetimes so that the hydrogels behave mostly like chemical gels with time-independent dynamic moduli [132].

Another study conducted by Okay coworkers was hydrophobically modified ionic hydrogels formed in oppositely charged surfactant solutions exhibit frequency-dependent dynamic moduli if they are in equilibrium in water after extraction of free surfactant micelles [134]. This is a result of complex formation between the ionic polymer and the oppositely charged surfactant, leading to polymer-bound surfactant counterions in the hydrogels. The mechanical strength of hydrogels were increased by use of hydrophobic acrylates rather than their methacrylate equivalents. This is due to the limited flexibility of the methacrylate backbones. Similarly, the length of the alkyl

side chain of the hydrophobes as well as the type of hydrophilic chains also affect the mechanical performance of hydrogels formed via hydrophobic interactions. For instance, replacing polyacrylamide (PAAm) by poly-acrylic acid (PAAc) provides mechanically stronger hydrogels as they have hydrogen bonding between carboxyl groups, which stabilize the hydrophobic associations. A similar improvement in mechanical performance is observed by replacing of PAAm with poly(N,N-dimethylacrylamide) (PDMA) with the help of additional hydrophobic interactions between the DMA units. By removing the surfactant micelles, similar changes are also observed in their mechanical properties. Most importantly, a remarkable decrease in the stretchability of such hydrogels is observed upon extraction of surfactant micelles. By tuning the preparation conditions, hydrogels formed via hydrophobic interactions in micellar solutions exhibit a high stretchability (up to 5000 %), high mechanical strength (up to 1.7 MPa tensile stress), and complete autonomous self-healing ability. Thus, hydrogels formed via hydrophobic interactions combine good mechanical properties with a high self-healing efficiency and are promising materials for new technologies [132,134,135].

Another interesting study of Okay and coworkers was conducting micellar copolymerization by using high amounts of hydrophobic monomers. In this study, supramolecular, semi-crystalline, hydrophobically modified, melt-processable hydrogels with shape-memory behavior and self-healing ability was achieved. The water content of hydrogel were between 60−80 wt % and they consist of PAAc chains containing 20−50 mol % crystallizable n-octadecyl acrylate (C18A) segments together with surfactant micelles. The key of this approach was that the hydrogels renders melt-processable are acquired under the favor of the absence of chemical cross-links and the presence of surfactant micelles. It was shown that, above the melting temperature (T_m) of the crystalline domains, the hydrogel liquefies and exhibits moldability to a desired form. Below the T_m and after removing the surfactant from the gel network, molded hydrogel in any permanent shape exhibit a high compressive strength of 90 MPa and a Young's modulus of 26 MPa. If the hydrogel was damaged on purpose e.g. by cutting into two pieces, the extraordinary mechanical properties can completely be recovered via temperature-induced healing process. The hydrogel also exhibits a complete shape fixity ratio and a shape recovery ratio of 97 ± 2% [133].

Okay and coworkers improved their hydrophopically modified hydrogel concept by exculuding the use of surfactants by taking the advantage of using UV-initiated bulk polymerization [3]. New approach was allowed to obtain hydrophobically modified hydrogels with a high hydrophobic monomer content which served for the generation of semicrystalline domains in the gel structure. The hydrogels consist of linear PDMA or PAAc chains containing (meth)acrylate units with long alkyl side chains. They have particularly high fracture energy of 20 ± 1 kJ m^{-2} and Young's modulus up to 308 ± 16 MPa. The mechanical properties of the hydrogels could be tailored by varying the degree of crystallinity by choosing suitable comonomer pairs and compositions. The hydrogels undergo up to 1000 fold change in their elastic moduli by changing the temperature between below and above the melting temperature of the crystalline regions. They also exhibit self-healing and shape memory functions triggered by heating above the melting temperature. Healed hydrogels sustain up to 138 ± 10 MPa compressive stresses, which are around 87% of the compressive stress of the virgin gel samples.

Multi-segmented hybrid hydrogels with self healing ability and shape-memory behaviors, will be represented as a second part of this thesis, are the result of this long journey on the hydrophobically modified hydrogels.

1.2.1.3 Self-healing ability

The use of synthetic, chemically crosslinked hydrogels in load-bearing applications is limited because of their brittle character. Therefore, design of hydrogels with good mechanical properties is crucial. Synthetic hydrogels representing high toughness with stimuli-responsiveness and self-healing ability are promising for the development of several new technologies [132].

With reference to the great potential, various approaches have been introduced for preparing self-healing gels, many of which are based upon the horizon of constitutional dynamic chemistry (CDC) [136-139]. CDC comprises both dynamic covalent- and non-covalent chemistry. The core of the CDC is comprised of ‘‘dynamic’’ and ‘‘reversible’’ terms. As they possess a dynamic/reversible nature with the reformation ability of broken bonds, dynamic polymer networks exhibit self-healing [140].

According to the physical and chemical character, self healing gels studied based on the CDC so far are schematically summarized in Figure 1.5.

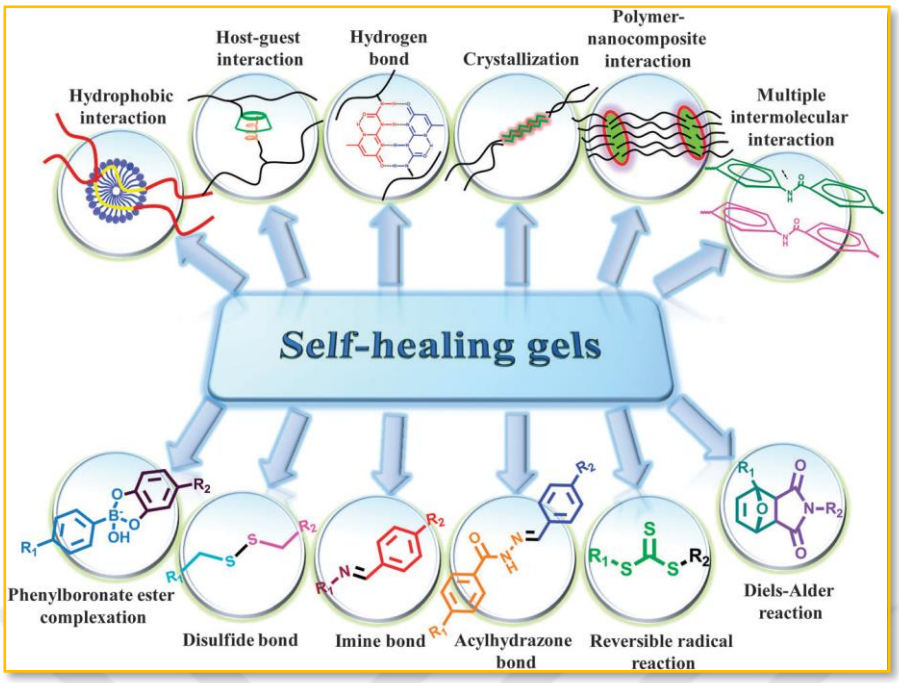

Figure 1.5 : Various strategies used to synthesize physical (upper) and chemical (down) self-healing gels based on CDC. Reprinted from "Self-healing gels based on constitutional dynamic chemistry and their potential applications.", by Wei, Z. et al., 2014, *Chem. Soc. Rev.*, 43 (23), 8114–8131. Copyright 2014 by Royal Society of Chemistry. Reprinted with permission [140].

Self-healing polymer materials can be achieved by means of two important features. Firstly, hydrogels can generate a ''mobile phase'' in or around the damaged zones by taking the advantage of captured solvent in the gel network which fills and bridges the crack zone to allow gel heal itself [141]. Secondly, self-healing gels are non-automatically or automatically self-healable depending on whether or not they need additional external energy, intervention or trigger (e.g., heat, light, pH or catalyst) to recover their original structures and properties [140].

Physical self-healing hydrogels restored networks via dynamic formation of attractive non-covalent interactions between molecules, oligomers or polymer chains, including hydrophobic interactions, host–guest interactions, hydrogen bonds, crystallization, polymer–nanocomposite interactions and multiple intermolecular interactions. Chemical self-healing gels restored networks via the dynamic formation of covalent bonds, including boron–oxygen bonds (phenylboronate ester), sulfur–sulfur bonds (disulfide), carbon–nitrogen bonds (imine, acylhydrazone), carbon–carbon/carbon–sulfur bonds (reversible radical reaction) and cyclohexenes (reversible Diels–Alder cycloaddition). For both physical and chemical self-healing gels, the reversible

equilibrium of the gel networks can dissociates and recombinates the physical interactions or chemical bonds. Therefore, for initiating the self-healing process, it is must that the functional groups of polymer chains should allow physical interactions or chemical reactions in damaged regions of gels [140].

Hydrophobic interactions are the dominant feature in the formation of self-healing hydrogels. The polymer chains containing hydrophobic monomer units result in the hydrophobic associations which yields a network with a transient crosslinks. Okay and coworkers introduced a micellar polymerization method for hydrogels to construct self-healing hydrogels which possess hydrophobic interactions among surfactant micelles as physcial junctions [106,129,130]. In this system, the reversible dissociation and association of the hydrophobic cross-links endow self-healing ability to the hydrogels. By this method, self-healing can be achieved by simply getting two pieces of cut micelle-based hydrogel samples in touch for a few seconds. The healing efficiency was almost 100% and the self-healed hydrogels can bear the applied strain up as the original one, with a maximum tensile strain of 3600%. Figure 1.6 exhibits the mentioned procedure of self healing.

Figure 1.6 : (a, b) Autonomous self-healing of HM PAAm hydrogels formed using 2 mol% of C17.3M hydrophobe in 7 % SDS + 0.5 M NaCl solution; (a) C_0 : 5 %. Reprinted from "Tough and self-healing hydrogels formed via hydrophobic interactions.", by Tuncaboylu, D.,C. et al., 2011, *Macromolecules*, 44, 4997-5005. Copyright 2011 by American Chemiacl Society. Reprinted with permission [106]. and (b) 10 %. Reprinted from "Dynamics and large strain behavior of self-healing hydrogels with and without surfactants.", by Tuncaboylu, D.,C. et al., 2012, *Macromolecules*, 45 (4), 1991-2000. Copyright 2012 by American Chemiacl Society. Reprinted with permission [129]. In (a), one of the hydrogel samples is colored for clarity.

The surfactant micelles (sodium dodecyl sulfate: SDS) were the key factor of this approach for sthe self-healing and mechanical properties. As a summary, the healing efficiency of surfactant-containing hydrogels depends on several factors, including the

healing time, the polymer and surfactant contents of the hydrogels, and the type and amount of the hydrophobes. The healing efficiency drasticly decreases with increasing polymer concentration of the gels. The efficiency also crucially depends on the comonomer feed composition; efficiency decreases as the amount of hydrophobe in the feed increases (i.e., as the fraction of dissociable cross-links decreases) [129,132].

Furthermore, Okay and co workers obtained self-healing hydrogels with improved mechanical strength by replacing the SDS micelles with mixed cetyltrimethylammonium bromide (CTAB)–SDS micelles. These hydrogels exhibit a maximum tensile strain of 5000% due to high solubility and hydrophobicity of the mixed micelles compared to SDS micelles and provide an ideal candidates for designing tough self-healable hydrogels for tissue engineering, such as artificial muscles [131].

Taguchi and coworkers developed a novel liposome based self-healing hydrogel [142]. The gelation obtained by means of hydrophobic interactions between the liposome and cholesterol (Chol)-end capped polyethylene glycol (PEG) (Chol-PEG-Chol). The liposome hydrogel possesses three possible binding types of Chol-PEG-Chol to the liposome. As a ‘‘bridge’’, two cholesterol end groups of Chol-PEG-Chol penetrate into the bilayers of two different liposome particles, as a ‘‘loop’’, two cholesterol end groups of Chol-PEG-Chol penetrate into the bilayers of a single liposome particle, as ‘‘dangling’’, only one cholesterol end group of Chol-PEG-Chol penetrates into the bilayers of the liposome particle while the other end group is exposed to the aqueous solution. Since the cholesterol groups of Chol-PEG-Chol may dynamically pull out and penetrate into the bilayers of liposomes, the liposome hydrogel could recover quickly from sol to the gel state [142].

Another important example of hydrophobically modified hydrogel study was conducted by Okay and coworkers with no use of surfactant. This study also constitutes the basis of multi-segmented hybrid hydrogels exhbited in this thesis. Within the scope of this study, 3D network of PDMA and PAAc chains were used to generate hydrophobic interactions. The key factor to obtain high strength hydrogels is the co-existence of crystalline domains and hydrophobic associations acting as strong and weak physical crosslinks, respectively. PAAc backbone provides a higher transition temperature and degree of crystallinity as compared to PDMA backbone due to the hydrogen bonds occur between the carboxyl groups. Stability of crystalline

domains in the hydrogels was revealed in an increasing order of: DMA/C17.3M < DMA/ C18A < AAc/C18A. The hydrogels exhibit self-healing function by heating trigger above the melting temperature of their crystalline domains. Healed hydrogels sustain up to 138 ± 10 MPa of compressive stress, which is around 87% of of the virgin samples [3].

1.2.1.4 Shape-memory behavior

Shape-memory is the ability to relax to ‘‘memorize’’ a macroscopic, permanent, stress-free form in their specific environmental conditions after they exposed to a manipulation in their form by an external trigger which forces the specific environmental conditions of shape-memory material to fix a new temporary, dormant form. Therefore a shape memory material can be defined as materials which have ability to response as relaxation to an external stimuli icluding: temperature [3], electricity [143-146], pH [147], magnetic field [148-150], ultra-sound [151], light [152-154] or etc. This relaxation is associated with elastic deformation stored during prior manipulation [155].

Osada et al. were mentioned that the isothermal conversiton of chemical energy into mechanical work underlies the moility of all living organisms [156]. They ground their idea to Katchalsky and colloborators work [157, 158] as they demonstrated that the collogen fibers changed dimension reversibly on transition from cyclic helices to rendom coils when they were immersed cyclically in salt and water and defined this system under the name of ‘mechanocehmical system’ (chemomechanical system) as athermodynamic system capable of transforming chemical energy o mechanical work.

Stimuli-responsive systems can be found in nature with numerous examples. For instance, the Venus flytrap, which has a leaf-shutting mechanism triggered by touching the hairs on the leaf surface. Figure 1.7 shows this reversible leaf-shutting mechanism of Venus fytrap as an example of stimuli-responsive system found in nature [159,160].

Figure 1.7 : Reversible leaf-shutting mechanism of Venus fytrap. Reprinted from “How the Venus flytrap snaps.”, by Forterre, Y., et al. 2005, *Nature*, 433 (7024), 421-425. Copyright 2005 by Springer Nature. Reprinted with permission [160].

Such examples in the nature inspires the design of synthetic smart materials which response to sitimuli, for various possible applications. Within the wide range scope of stimuli-responsive materials, much focus has been placed on the study and synthesis of soft stimuli-responsive polymeric materials due to their versatility, unique mechanical perfonmance and enhanced biocompatibility.

Early in the 1960s, the idea of shape memory effect in polymers has been applied in commercial use as wire wraps for the purpose of electrical insulation which of them were polyethylene tubes with ability to shrink through heat trigger [161]. From then on, several studies conducted in the past decades, focus on the stilimuli-responsiveness of polymer materials. Shape memory polymers are a class of stimuli-responsive polymers which of their shape can be programmed to shift reversibly by triggers. This is the most distinguishing feature of this materials in comparison with other stimuli-responsive ones [162]. Specifically, a typical shape memory polymer can be programmed to fix one temporary shape and subsequently recover to its permanent shape upon stimulation (typically heating), as illustrated in Figure 1.8.

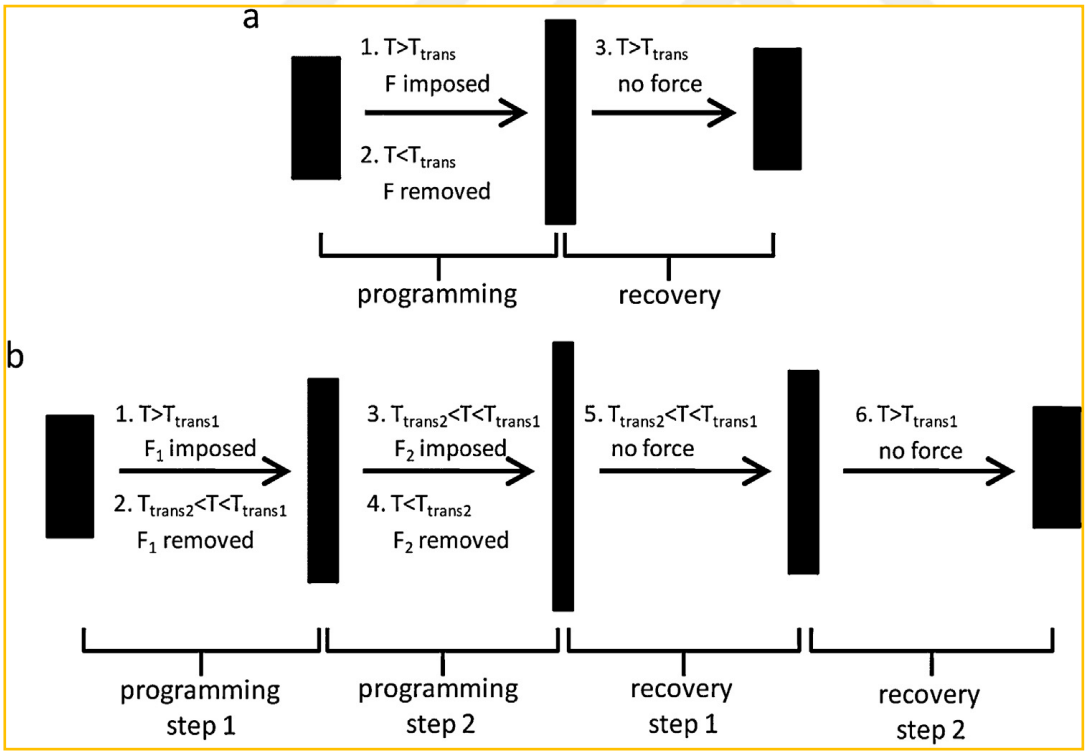

Figure 1.8 : Schematic illustrations of (a) Dual-shape memory effect; and (b) Triple-shape memory effect. Reprinted from "Recent progress in shape memory polymer: New behavior, enabling materials, and mechanistic understanding.", by Zhao, Q., et al. 2015, *Progress in Polymer Science*, 49 (50), 79-120. Copyright 2015 by Elsevier Ltd. Reprinted with permission [162].

Here, the temporary shape is usually defined by the applied force during the shape fixing step (programming step). The shape memory cycle in Figure 1.8(a) involves two shapes in total as one temporary and one permanent called as dual-shape memory effect. In a similar manner a triple-shape memory polymer cycle in Figure 1.8(b) involves three shapes in total as two temporary and one permanent shape. From a molecular structure standpoint, dual- or triple- shape memory effect is enabled by the combination of a reversible switching mechanism and a network structure [163]. These behavior can be obtained in such polymers as a crosslinked (chemically or physically), amorphous or crystalline polymer [164-168].

On the other hand, there is another significant accomplishment stood out during the past decade in shape memory polymers as multiple-shape memory polymers. According to our knowledge, yet there is no shape memory effect reported involving more than three shapes in total in their shape memory effect cycle as a material having a one permanent and three or more temporary shapes. Therefore, a mutiple-shape memory effect corresponds to the material possesses dual- or triple- shape-memory behavior responding to more than one external stimuli together, like pH and thermal [147].

Within the scope of this thesis, multiple-shape memory defines a material having more than three shapes in total in their shape memory effect cycle as one permanent and three (possibly more than three) permanent shapes. It is important that, a dual-, triple, or possible multiple- shape memory effect idetify that the memory effect should include a memory in whole body of material rather than a local.

Here in this study, a multi-segmented hybrid hydrogel refers a material having segments with distinctly different properties in their physical and chemical features. It was observed that every single segment of a hybrid hydrogel has their own dual shape memory effect locally. Since the hybrid material is fused body of this dual-shape memory segments, in example, two segmented-hybrids have one permanent and two permanent shapes.Similarly, a three-segmented hybrid hydrogels have one permanent and three temporary shapes in their shape memory effect cycle. Therefore, from this point of view, the shape memory behavior belonging to multi- or three- segmented hybrid hydrogels are termed as “pseudo multiple-“ and “pseudo triple-“ shape memory behavior, respectively.

The ability of a thermally-induced shape memory behavior in hydrogels was first represented in poly(acrylic acid)-based networks with short stearyl side chains [169]. Within this study, the hydrophilic main chain segments allow to swell in water, while the dangling stearyl units forming a crystalline aggregate structure below Ttrans as physical cross-links. After the heating above T_{trans}, the domains formed by stearyl units became amorphous causing the recovery of the permanent shape and, at the same time, might allow further swelling.

Hydrogels acts as a matrix which allow rapid diffusion of small molecules that may serve as triggers for the shape memory effect. Thus, hydrogen bonding [170], dipole−dipole interactions [171] or ion complexation can be used to fix a temporary shape as an alternative to crystallizable domains. For example, shape memory hydrogels having carboxylic acid enable the fixation of a temporary shape in the presence of Ca^{2+} solution, with shape recovery after addition of a complexing agent by dissociation of the Ca^{2+}−carboxyl complexes [172].

Shape memory hydrogels may also response to several stimuli when either one type of temporary cross-link is sensitive to different stimuli (alternative stimulation) or two types of temporary cross-links are incorporated in the polymer network structure that respond to independent stimuli (multi-stimuli response). Alternative stimulation was realized in a system consisting of PVA and boronic acid, where the formed boronate ester bonds acted as reversible cross-links [173]. These physical cross-links could be reversibly formed and dissociate by raising or lowering the pH either directly or via a PAG [174]. In addition, indirect heating by ultrasound treatment could initiate the shape recovery [151].

Multi-stimuli response was realized in shape memory hydrogels with temporary cross-links based on ionic/complex binding as well as salt-strengthened hydrophobic associations.

Most commonly reported shape memory polymers are thermally-triggered. Thermo-responsive shape memory polymers utilize the inherent thermal transitions of the polymers to accomplish the shape memory effect. These thermal transitions are either melting (T_m) or glass transition (T_g) temperatures. As the melting transition occurs over a much smaller temperature range as compared to a glass transition, melting transition is favored more as a shape transition temperature [159].

Recently, Okay and coworkers presented a non-covalent approach and bulk photo-polymerization method of hydrophilic (N,N-dimethylacrylamide and polyacrylic acid) and hydrophobic monomers ((meth)acrylate units with long alkyl side chains) to generate high-strength self-healing hydrogels with shape-memory effect arising from semi-crystaline domains formed by hydrophobic monomers. As they reported, hydrogels undergo up to 1000 fold change in their elastic moduli by changing the temperature between below and above the T_m of the crystalline regions. They exhibited hydrophically modified hydrogels with shape memory functions triggered by heating above the T_m [3].

Multi-segmented hybrid hydrogels represented in the scope of this thesis are also hydrophobically modified hydrogels utilizing the T_m for thermal inducing of shape memory effect.

1.2.2 Multi-segmented hybrid hydrogels

As a general meaning, "hybrid" term corresponds to a thing which combines two different elements to obtain a new, mixed character. Within hydrogel studies, hybrid is a common use to describe the material via their structural components' character in a chemical or physical manner. Within a chemical manner, a hybrid hydrogel may be a combination of a synthetic and a natural, organic and inorganic sources. On the other hand, in terms of physical manner, a hybrid hydrogel may be a combination of different components having different physical properties together, such as isotropy and anisotropy, amorphus and semicrystalline structure, rigidity and flexibility, etc. to create a new material with a new desired character.

Hydrogels resemble to biological systems in many aspects [175-177]. Many biological systems are anisotropic structures as combinations of hard and soft segments with extremely tough interfaces between their components. For instance, connective tissues such as tendon are joined to bone in a specialized interface known as the enthesis [178,179]. They serve as more than simple anchors, for in linking soft to hard tissue, entheses also minimize the risk of damage in the face of high levels of mechanical loading [180]. In contrast with such kind of biological systems, hydrogels having high strength reported so far are isotropic materials. In the past few years, to acquire anisotropy in the gel architecture, pioneering studies of interfacing soft and hard materials were reported. Hu et al. prepared "modulated hydrogels" by swelling the first

gel component in the excess of second monomer solution followed by cross-linking copolymerization [181]. Thus, by this technique, a harder interpenetrated network hydrogel component could be produced as merged with a softer single network hydrogel. However, a hydrogel comprising of two dissimilar gel components was for the first time called as "hybrid gel" by Raghavan et al. [182,183] Figure 1.9 represents the optical images of hybrid hydrogels synthesized by Ragvahan et al. They prepared a hybrid gel which of its components preserve the properties of each individual gel component with smooth and robust interfaces between dissimilar gel zones by bringing two high-viscosity monomer solutions into contact and then polymerizing the system. Different than the study conducted by Hu et al., the key of this approach was the limitation of diffusion between the monomer solutions at the gel/gel interface [182].

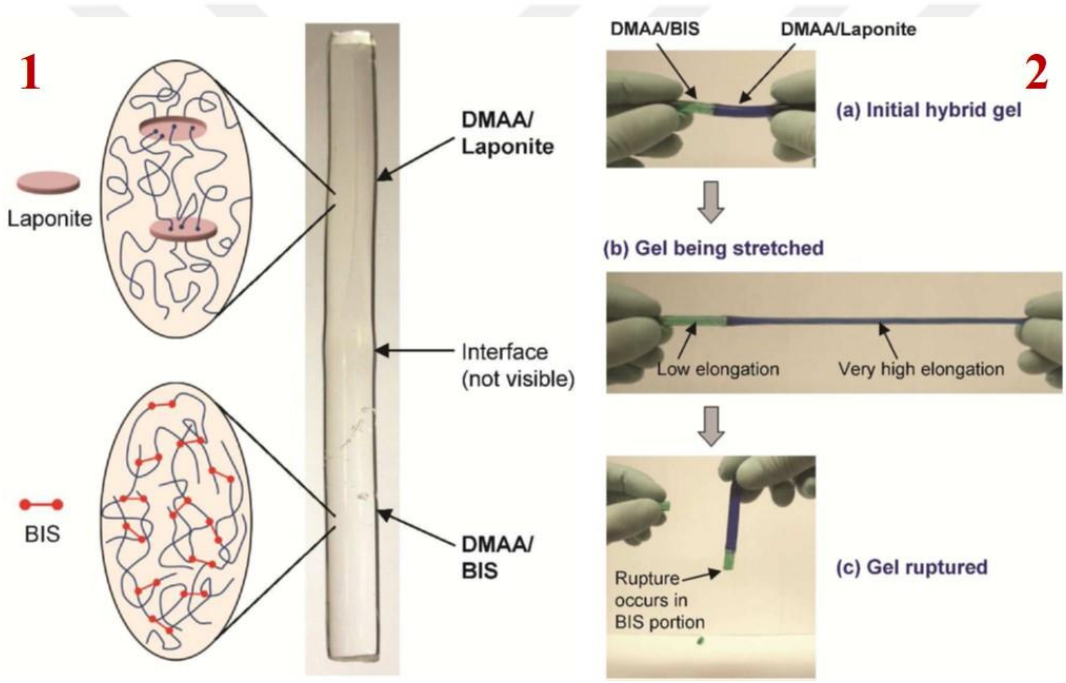

Figure 1.9 : (1) An optical image of hybrid gel. Interface regions is smooth and hence not visible. (2) Optical images showing mechanical differences between the zones of hybrid gel. The gel/gel interface is highly robust. Reprinted from "A New Approach for Creating Polymer Hydrogels with Regions of Distinct Chemical, Mechanical, and Optical Properties.", by Banik, S. J., et al. 2012, *Macromolecules*, 45 (14), 5712−5717. Copyright 2012 by American Chemical Society. Reprinted with permission [182].

Another method to create hybrid gel samples was introduced by Leibler et al. as "gluing" separate gel samples together by using nanoparticles as a binding agent to glue the dry or swollen hydrogels together [10]. This approach was extended by Yong et al. through the preparation of multilayered hydrogel sheets where the layers were

stacked and effectively glued together with chemical cross-links obtained by performing atom transfer radical polymerization between the successive layers [185,186]. Figure 1.10 demonstrates the representative optical images of soft-glued gels.

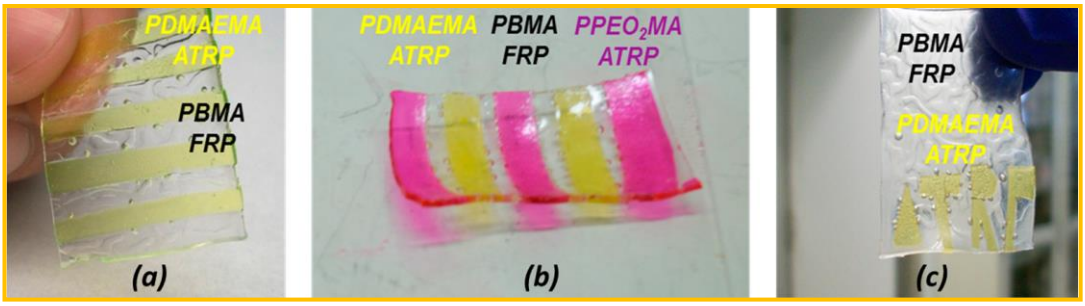

Figure 1.10 : (a) Ten-layer gel prepared by connecting gel slices together (b) Multi-layer gels obtained by connecting as a soft glue. (c) "ATRP" embedded letter made of and surrounding matrix. Reprinted from "Combining ATRP and FRP Gels: Soft Gluing of Polymeric Materials for the Fabrication of Stackable Gels.", by Beziau, A., et al. 2017, *Polymers,* 9 (6), 186-196. Copyright 2017 by MDPI AG, Basel, Switzerland. Reprinted with permission [186].

In order to fuse dissimilar materials in a body as macroscopic organo/hydrogel hybrids, another method was used by Deng et al. which originates from the rapid adhesion between polyethylene glycol hydrogels swollen in water and organogels swollen in anisole [187]. In this method, acylhydrazone dynamic bonds which are reversible and enable self-healing function in the hybrid were formed by condensation of the aldehyde and acylhydrazine groups between the macroscopic gels. However, either the method was applicable to a limited number of monomers or the tensile strengths of hybrids and their components were below 0.1 MPa [187]. In the past few years, Yuk et al. reported a strategy to design tough, optically transparent and electrically conductive bonding of hydrogels to nonporous solid surfaces which was achieved by anchoring the network chains of the hydrogels covalently to the silaneated surfaces [188].

Within this thesis, two- and three- (multi-) segmented hybrid hydrogels obtained by stratification method which exhibits self-healing and pseudo-triple shape memory effects. The inspiration of this work came from the water stream in the Istanbul strait (Bosphorus), a typical narrow sea strait connecting two seas, where more saline Mediterranean water flows at the bottom layer while the less saline Black Sea water flows at the top layer in the reverse direction. Similarly, by adjusting the densities of two monomer solutions, we were able to create layers of monomer solutions with

interfaces at which the solutions mix completely. Thus, another important point of this strategy is that the method introduced here is not limited with the monomers used in this study.

2. EXPERIMENTAL PART

2.1 Silk Fibroin Cryogels

Cryogels, based on crosslinked silk-fibroin with macropores, were prepared by our research group [7] and in the scope of this thesis, cryogels were subjected to MTT (3-(4,5-dimethylthiazol-2-yl)-2,5-diphenyltetrazolium bromide) cell growth assay to obtain cell viability results and visualized by confocal laser microscopy.

2.1.1 Materials

2.1.1.1 Materials and devices required for cell culturing

Clonetics™ Dermal Fibroblast Cell Systems (≥500.000 cells) coded as CC-2511 Normal Human Dermal Fibroblast (NHDF) cell line was supplied from LONZA in company with two kits:

1) CC-3132 FGM™-2 BulletKit™ comprised of:
    a) Fibroblast Basal Medium (FBM™)
    b) FGM™ SingleQuots™ (consists hFGF-B, Insulin, FBS and GA-1000)
2) CC- 5034 One ReagentPack™ subculture package containing:
    a) Trypsin/EDTA
    b) HEPES (4-(2-hydroxyethyl)-1-piperazineethanesulfonic acid)
    c) Trypsin Neutralizing Solution

T75 cell culture flasks (Z707503) were supplied from Sigma-Aldrich. Stericup-GP sterile vacuum filtration system (filter: 0.2μm) provided from Merck-Millipore.

All the procedures conducted with cell culture, which will be explained in following parts, were run in a microbiologic safety cabinet (Faster BH-EN 2003-Class II). Centrifugal requisities were compensated by Thermo Electron Corporation IEC CL10. Cells were counted by using a Fisher Scientific-0267110 hemocytometer and incubated in a Thermo Scientific 381 incubator.

2.1.1.2 Materials for cell viability assay

The MTT (3-(4,5-dimethylthiazol-2-yl)-2,5-diphenyltetrazolium bromide) cell growth assay kit CT02 was supplied from MILLIPORE while the polystyrene, flat bottom, sterile, lidded 96 well-plates (CLS3596) were obtained from Corning® Costar®, Sigma-Aldrich. Sterile-filtered, BioReagent Dimethylsulfoxide (DMSO) was provided from Riedel-de Haën and phosphate buffer solution (PBS) 1X w/o Ca, Mg (BE17-516F/12) was supplied from Lonza. Sterile Surgical Blades (22) from Broche were used to cut the materials to a proper size.

2.1.1.3 Materials for Laser Scanning Confocal Microscopy (LSCM)

Fluorescent dye Rhodamine–Phalloidin (R415) was used to stain actin filaments of cells in Laser Scanning Confocal Microscopy (LSCM) study while another fluorescent dye DAPI (62248) (diamidino-2-phenylindole) was used for nuclear counterstain. Besides these dyes, Formaldehyde (28906), Saponin (8047-15-2) and Bovine Serum Albumin (BSA) (15561020) were used by supplying from Thermo Fisher Scientific. LSCM was conducted in µ-Slides (chambered coverslip) with 8 wells (80826) which was provided from Ibidi.

2.1.2 Preperation of silk–fibroin cryogels

Synthesis of cryogels was not a part of this thesis but materials prepared according to the procedure improved in our research group [7] were subjected to biocompatibility tests. See reference "7" for further inquery in the synthesis of single network (SN), double network (DN) and triple network (TN) cryogels. Investigated cryogel samples are below:

i) Single-network (SN) cryogels: Obtained by varying the nominal fibroin concentration, C_{SF}, in the gelation solution as SN-4.2, SN-7, SN-12.5 and SN-22 wt%.

ii) Double-network (DN) and triple-network (TN) cryogels: DN and TN cryogels are denoted as DN-x/y and TN-x/y/z where x, y, and z are the fibroin concentration (C_{SF}) in the first, second and third gelation solutions, respectively, expressed in round numbers. DN-4/7, DN-4/14, DN-4/20, DN-4/29, TN-4/7/20.

2.1.3 Sterilization of cryogels

Cryogels, prepared by cutting in final sizes, were immersed in 70 % ethanol solution and shaked for 24 hours. Cryogel samples in ethanol were moved to a 96 well-plate to perform further sterilization. Ethanol was washed out of samples by adding distilled water (3 times) and PBS (3 times), respectively. After removing residual ethanol, samples are left for illumination under UV light for 30 mins. The sterilization step is over after these 30 mins.

In order to prepare samples to MTT assay, one more step is applied to cryogels, which is immersing them into full growth medium for obtaining the swelling equilibrium of cryogels. This step helps cryogels to be a proper media for cells.

2.1.4 Cell culturing

Cell line was cultured to use in further biocompatibility assays. Cells were passaged and cryopreserved. Cell passaging is a technique, which keeps cells alive and grows them under cultured conditions for an extended period of time. The aim of cryopreservation is to store the cells. Cell line was subcultured and cryopreserved according to the protocol given from Lonza. T75 cell culture flasks were used for culturing purposes. Culture flasks were placed into a 37 °C humidified incubator with 5% CO_2.

Additionally, in order to avoid the loss of cells, cells were subcultured before they reached 80% confluence. Obtaining a cell culture from cryopreserved cells by refereshing their full growth medium in every two or three day, generally takes two weeks. Passaged or cryopreserved cells were successfully reached to their 15^{th}.

2.2 Hybrid Hydrogels

2.2.1 Materials

Hybrid gels containg two or three distinct region composed of two or three induvidual gel components. Gels were obtained by hydrophobic associations of some monomers in a hydrophilic monomer. *N*,*N*-dimethylacrylamide (DMA) (99%, Sigma - Aldrih) and Acrylic acid (AAc) (99%, Sigma - Aldrih) were used as hydrophilic monomer. DMA was used as received (99%, Merck). AAc was freed from the inhibitor by

passing through an inhibitor removal column purchased from Aldrich Chemical Co. Figure 2.1 shows the hydrophilic monomers used in this study.

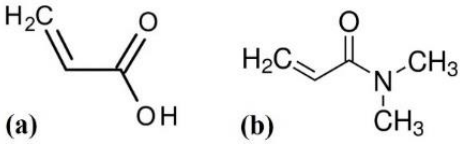

Figure 2.1 : Hydrophilic monomers, used in synthesis of hybrid hydrogels. (a) *N*,*N*-dimethylacrylamide (DMA), (b) Acrylic acid (AAc).

For each individual gel component different hydophobic monomer was used. Figure 2.2 shows the used hydrophobic monomers. These hydrophobes, lauryl methacrylate (C12M), stearyl methacrylate (C17.3M) which is a mixture of stearyl and cetyl methacrylates and octadecyl acrylate (C18A) were also used as received by supplying from Sigma - Aldrich.

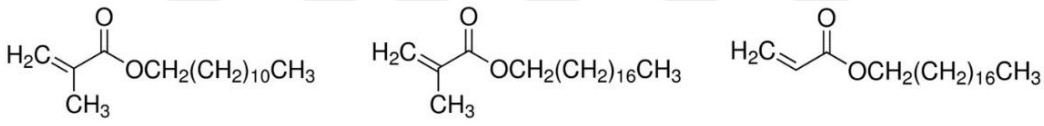

a) Lauryl Methacrylate (C12M) b) Stearyl Methacrylate (C17.3M) c) Octadecyl Acrylate (C18A)

Figure 2.2 : Hydrophobic monomers used in the synthesis of hybrid hydrogels.

Reaction was carried out by bulk polymerization of hydrophobic and hydrophilic monomers by using IRGACURE 2959 (2-Hydroxy-4′-(2-hydroxyethoxy)-2-methylpropiophenone, Sigma - Aldrich) as radical photoinitiator. Molecular formula of initiator is given in Figure 2.3. Reactions were carried out in plastic pipette and disposable syringes. Teflon pipe was used as a mold.

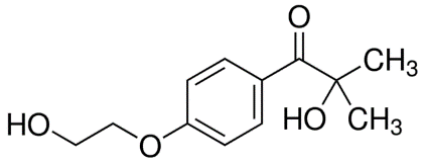

Figure 2.3 : Radicalic photoinitiator IRGACURE 2959.

2.2.2 Preperation of hybrid hydrogels

A hybrid hydrogel mentioned in the scope of this thesis is a material having two distinct region of different physical and chemical properties. The monolithic appearance of hybrid hydrogels with two distict, individual regions are created as a

fused body by the taking advantage of a strong interface region in between these regions.

Within this thesis, basicly, two kinds of hybrid hydrogels were sythesized. These types of hybrid hydrogels were classified according to the number of regions they have. Therefore, preperation of these two hybrid gels will be explained in this part under two subtitles as two- segemented hybrid hydrogels (H2) and three-segmented hybrid hydrogels (H3). Hybrid hydrogels will be expressed by using the H2 and H3 denotations. In this notification, "H" symbolizes "hybrid hydrogel" where the numbers 2 or 3 denote the number of segments these hybrid hydrogels have.

2.2.2.1 Two-segmented hybrid hydrogels

Two segmented hybrid gel samples were obtained in two different shapes and compositions. Shapes of hybrid gels will be named as flat hybrid hydrogels and interbedded hybrid hydrogels through this thesis. H2 samples according to their shapes are shown in Figure 2.4.

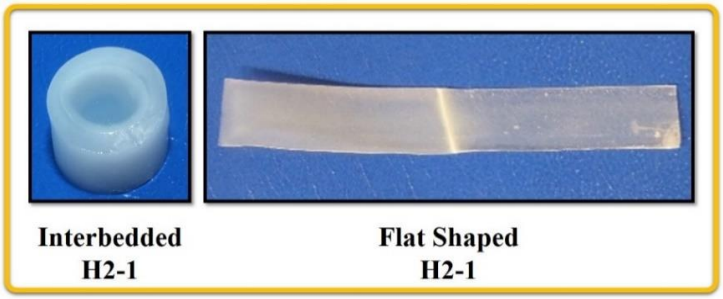

Figure 2.4 : Optical images of an example interbedded and flat shaped H2.

Hybrid hydrogels differs from each other with their composition will be denoted as H2-1 and H2-2 hydrogels. H2-1 and H2-2 have a common component "C1" which of its details will be given within this part. "C" denotes "component" and "1" is the code of the segment. Except the common segment C1, varying components of H2-1 and H2-2 will include C2-1 and C2-2, respectively. Figure 2.5 shows the optical images of H2-1 and H2-2 samples.

Here, preperation of hybrid hydrogels will be explained under two title according to the shapes and compositions of hybrid gels. Additionally, mixture gels, simulating the interface regions formed between two segments of hybrid gels, and each segments of hybrid gels were prepared individually and details will be given under the "preparation of hybrid hydrogels according to their compositions" part.

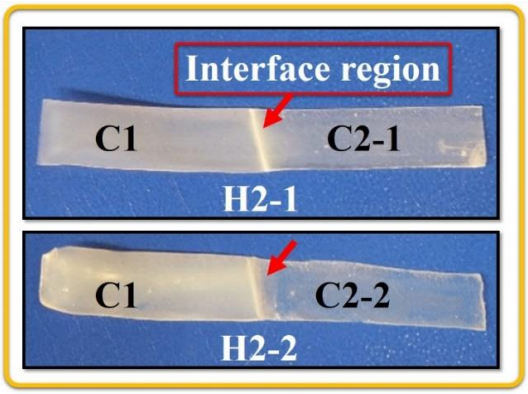

Figure 2.5 : Optical images of H2-1 and H2-2 hydrogels.

Preperation of hybrid hydrogels according to their shapes

- *Interbedded hybrid hydrogels*

Interbedded hybrid hydrogel saples are cylinder in shape with two distinct region, which of softer one is bedded in a tire-like outer hard cylinder, with a smooth interface in between these two gel components. The template, with sizes, arranged for to obtain an interbedded hybrid hydrogel and expected sample's illustrations are given in Figure 2.6.

Template was made out of a teflon pipe inside and a disposible plastic syringe around, which is wider in diameter and encircles the area around this teflon mold, to obtain a tire - like outer space.

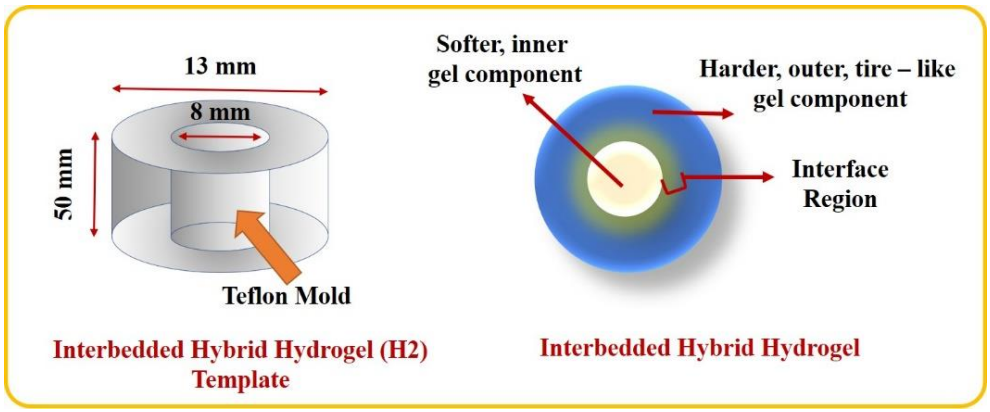

Figure 2.6 : Illustration of interbedded hybrid hydrogel template and expected shape of final interbedded hybrid hydrogel.

Preperation of interbedded hybrid polymer network with an expected interbedded shape as shown in Figure 2.6 was summarized with illusturation in Figure 2.7 in 6 steps.

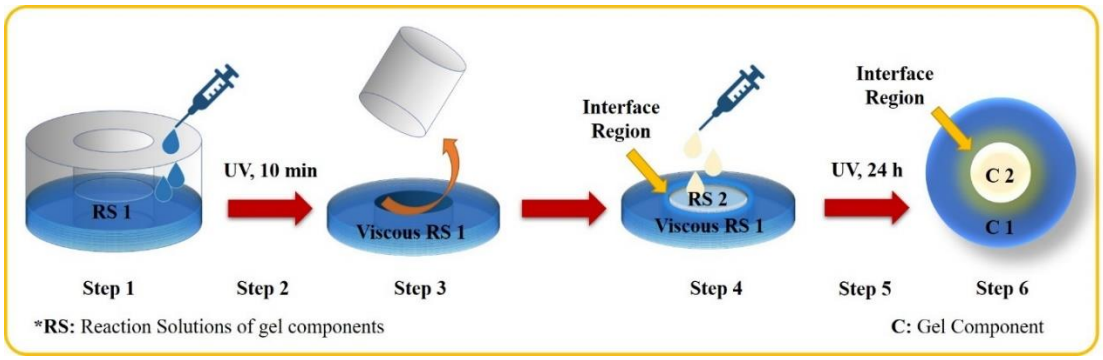

Figure 2.7 : Illustration of interbedded hybrid hydrogel preparation in 6 steps.

As summarized on illustration, preperation of interbedded hybrid hydrogel can be explained under six easy steps.

1) Addition of first reaction solution (RS1) to the area around the teflon mold. RS1 was the same, C18A/DMA, for both of two hybrid hydrogels H2-1 and H2-2.

2) UV irradiation of RS1 for 10 min to obtain a partially self-standing, viscous RS1.

3) Removing the teflon pipe mold out of the template to obtain a hollow viscous RS1 structure.

4) Filling of RS2 to the inner space of viscous RS1 area according to the type of hybrid gel (C2-1 of H2-1: C17.3M/DMA or C2-2 of H2-2: C12M/DMA) desired to acquire.

5) UV irradiation of whole reaction solutions for 24 h.

6) Releasing the interbedded hybrid polymer network from the template. Reaction was carried out as a bulk polymerization, meaning that no water was included in the after synthesis structure of polymer network. In order to call these networks as hydrogel, polymer networks at after synthesis step were submerged in water bath at 50 °C for 2 days to reach a swelling equilibrium. Thus, samples synthesized here at a swelling equilibrium state called as interbedded hybrid hydrogels.

- *Flat shaped hybrid hydrogels*

Flat shaped hybrid hydrogel samples are also composed of two distinct region, which of these follow each other individually in a rectangular shape with smooth transition area between these two gel components. Template set for flat shape hybrid hydrogel and preperation steps of synthesis were given in Figure 2.8.

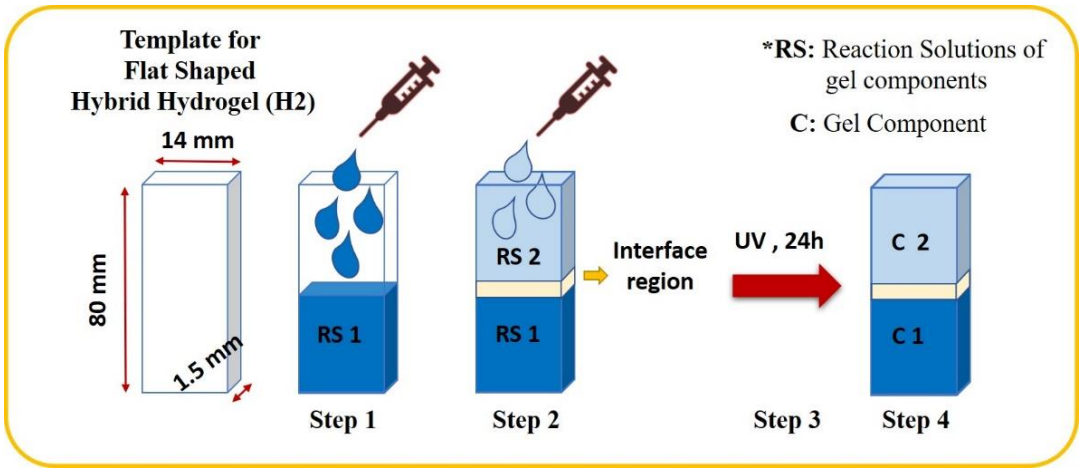

Figure 2.8 : Template and the preparation steps of flat-shaped hybrid hydrogels.

Reactions were carried out in a plastic pipette template which is given as an illustration with sizes in the very left side of Figure 2.8. Different than interbedded hybrid gels, there is no need to introduce any viscosity difference to prepare flat hybrid gel. For this purpose, stratification* of reaction solutions were used to combine gel parts in a fused body of flat hybrid gels. Stratification will be explained below this part.

1) Addition of first reaction solution (RS1). RS1 was the same, C18A/DMA, for both of two hybrid hydrogels H2-1 and H2-2.

2) Addition of RS2 directly onto the RS1 according to the type of hybrid gel (H2-1: C17.3M/DMA or H2-2: C12M/DMA) desired to acquire. This step is performed with the help of stratification*.

3) UV irradiation of whole reaction solutions for 24 h.

4) Releasing the flat hybrid polymer network from the template and let this polymer network reach to a swelling equilibrium by submerging it in a water bath at 50 °C for 2 days to call this polymer network as flat shaped hybrid hydrogel.

* *Stratification of reaction solutions*

Stratification of fluids occurs due to the temperature variations, concentration differences or the presence of different fluids of different densities. A well-known example of this behaviour can be observed in the Istanbul strait (Bosphorus), a typical narrow sea strait connecting two seas, where more saline Mediterranean water flows at the bottom layer while the less saline Black Sea water flows at the top layer in the reverse direction.

Here, preparation of hybrid hydrogels in flat shape with two distinct gel component achieved with density difference of the reaction solutions (RS). The basis of method is simply using two solution (at least) with two differrent densities, one of which with a low density floats on top of another solution of higher density whereas the interface between layers acts as a barrier to prevent monomers from diffusion between layers. By stratifying the layers of RS, it is achived to fuse these layers in a single material, by UV-initiated bulk copolymerization, as two individual component and a mixture of them in a few millimeters of thickness as a stronger interface region in between.

Preparation of hybrid hydrogels according to their compositions

Preperation of hybrid hydrogels, classified according to their compositions, are given below in details under the "Hybrid 1 and Hybid 2" subtitle. Interface regions located between individual components of Hybrid 1 (H2-1) and Hybrid 2 (H2-2) gels were simulated by preparing mixtures of reaction soltions (RS) and their preparation methods will be explained in details under the subtitle as "Mixture 1 and Mixture 2" at this part. Additionally, gels forms distinct zones of hybrid gel samples as C1, C2-1 and C2-2 were synthesized on an individual basis to compare with hybrids and mixtures.

All gel samples will be explained hereunder were synthesized by UV initiated bulk copolymerization of reaction solutions. For this purpose, 0.1 wt.% IRGACURE 2959 photoinitiator (with respect to the monomers) was added to each reaction solutions (RS) . Then, RS are exposed to UV irradiation in a UV reactor, which is equiped with light sources at 360 nm, for 24h, at room temperature. While the method of copolymeization was bulk, polymer networks were obtained but a hydrogel. Acquired polymer networks after UV irradiation were let to reach an equilibrium swelling state in a water bath at 50 °C for 2 days. Thus, hydrogel samples were obtained.

- *Hybrid 1 and Hybrid 2*

Hybrid 1 (H2-1) and Hybrid 2 (H2-2) in both shapes, interbedded and flat, were synthesized with photoinitiated bulk copolymerization method by using two different reaction solution. Reaction solution 1 (RS1) consists of 70 mol % hydrophilic monomer *N*,*N*-dimethylacylamide (DMA) and 30 mol % hydrophobic monomer octadecyl acrylate (C18A). Mol % values of monomers were calculated with respect to total monomer concentration (C_o). RS1 solutions were the same solution, which of

its gel state is named as C1, for H2-1 and H2-2. RS 2 was prepared with the same calculation at the concentrations and compositions below:

a) RS2 for H2-1: 50 mol % DMA and 50 mol % steryl methacrylate (C17.3M).

b) RS2 for H2-2: 50 mol % DMA and 50 mol % lauryl methacrylate (C12M).

UV-initiated bulk copolymerization of the monomer mixtures were performed by addition of 0.1 wt.% IRGACURE 2959 photoinitiator (with respect to the monomers). RS are exposed to UV irradiation in a UV reactor (according to the processes of its required shape explained in details above) which is equiped with light sources at 360 nm. Hybrid polymer network samples were released to swelling in a water bath at 50 °C up to an equilibrium state, so hybrids can be named as hybrid hydrogel samples.

- *Mixture 1 and Mixture 2*

Hybrid 1 (H2-1) and Hybrid 2 (H2-2), hydrogel samples, in both shapes, interbedded and flat, have transition areas between components C1-C21 and C1-C2-2, respectively. To mimic the properties of the transition areas, mixture gels were prepared by mixing reaction solutions (RS) RS1 and RS2 of H2-1 or H2-2 gel, before the onset of copolymerization. The polymerization was then conducted as described above. To acquire Mixture 1 (M1), RS1 (70DMA/30C18A) and 50DMA/50C17.3M (RS2 for H2-1) were completely mixed and solved in each other by using same weight amounts of these RS1 and RS2, then copolymerized under UV light as carried out for hybrid gels. By the same way, Mixture 2 (M2) was prepared by mixing RS1 and 50DMA/50C12M (RS2 for H2-2). IRGACURE 2959 was added to RS at a same concentration (0.1 wt.%), copolymerized by UV irradiation and let to reach a swellig equilibrium as explained before for hybrids.

- *Individual gel samples (C1, C2-1 and C2-2 samples)*

Hybrid 1 (H2-1) and Hybrid 2 (H2-2) gel samples are comprised of three different components in total as C1, C2-1 and C2-2 segments. As explained above, H2-1 comprised of C1 and C2-1 segments and H2-2 comprised of C1 and C2-2 segments. In order to compare the properties of hybrids with their own segments, C1, C2-1 and C2-2 segments were synthesized in individual basis by the same UV initiated bulk polymerization method. Besides the compositions of C1, C2-1 and C2-2, compositions of Mixture 1 (M1: C1+C2-1) and Mixture 2 (M2: C1+C2-2) are given in Table 2.1.

Table 2.1 : Table of all synthesized hydrogels in different compositions.

Sample Name	Composition (mol %, respect to C_O)
C1	70DMA/30C18A
C2-1	50DMA/50C17.3M
C2-2	70DMA/30C18A
M1 (C1+C2-1)	70DMA/30C18A+50DMA/50C17.3M
M2 (C1+C2-2)	70DMA/30C18A+50DMA/50C12M
H2-1 (C1-C2-2)	70DMA/30C18A - 50DMA/50C17.3M
H2-2 (C1-C2-2)	70DMA/30C18A - 50DMA/50C12M

2.2.2.2 Three-segmented hybrid hydrogels

The preparation of hybrid hydrogels with three distinct gel zones is based on the density difference of the monomer mixtures, measured using a calibrated glass pycnometer at 25 °C. The solution with low density floats on top of another solution of higher density whereas the interface between layers acts as a barrier to prevent monomers from diffusion between layers.

Two kinds of three segmented hybrid hydrogels, denoted as H3-1 and H3-2, were synthesized in a rectengular, flat shape. Within this part, hybrid hydrogels differs from each other with their composition will be denoted as H3-1 and H3-2 hydrogels. H3-1 and H3-2 have a common component "C1" which of its details will be given within this part. "C" denotes "component" and "1" is the code of the segment. Except the common segment C1, varying segments of H2-1 and H2-2 will include C2-1, C3-1 and C2-2 and C3-2, respectively. "1" and "2" next to the C2 and C3 segments are codes exhibiting to which H3 kind (H3-1 or H3-2) they are belonging to. C2-1 is the middle part of H3-1, while the C1 and C3-1 are the end parts of H3-1. C2-2 is the middle part of H3-2, while the C1 and C3-2 are the end parts of H3-1.

Hybrid hydrogels were prepared by UV-initiated bulk copolymerization of the monomer mixtures using 0.1 wt % Irgacure 2959 photoinitiator (with respect to the monomers). The polymerization reactions were then conducted at 24 ± 3 °C for 24 h under UV light at 360 nm. Figure 2.9 is an illustration of the H3 synthesis prescription. As in two-segmented flat hybrid hydrogel synthesis, stratification method was used to obtain three layers of reaction solutions before the onset of polymerization.

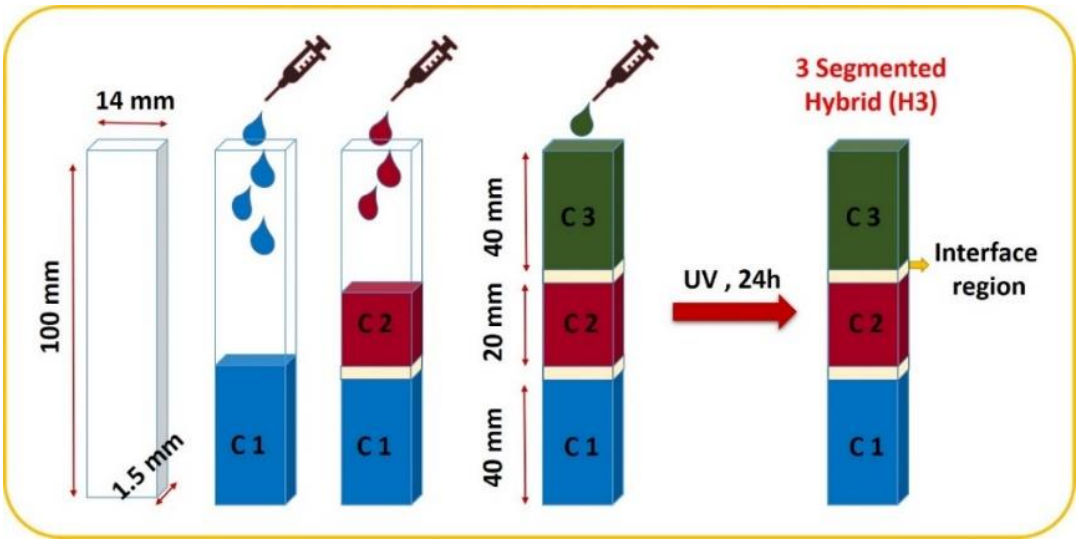

Figure 2.9 : Schematic illustration of three-segmented hybrid hydrogel synthesis through the stratification of monomer mixtures.

Plastic molds of 100 × 14 × 1.5 mm dimension were used to prepare flat rectangular shaped hybrids. As can be seen in Figure 2.9, length of middle segment was 20 mm which is shorter than that of other two parts. Thus, during the tensile tests of three segmented hybrids, initial sample length between the jaws, in other words grip-to-grip separation, was fixed to 60 mm consisting of three segments of hybrid which of each were in 20 mm for providing the equal attendance of segments to the tensile measurement. Additional 20 mm of two end segments were used to grab the hybrid sample in jaws.

The molar ratios and the densities (at 25 °C) of monomer mixtures coded as C1, C2 and C3 in blue, red and green colors, respectively, in Figure 2.9, are collected in Table 2.2. To compare the properties of hybrids with their gel components, bulk polymerizations of C1, C2, and C3 monomer mixtures were also carried out separately using 0.1 wt % Irgacure 2959, as described above.

Table 2.2 : Table of molar ratios and densities (at 25 °C) of monomer mixtures which create the components of three segmented hybrids.

H3-1				H3-2			
Code	**Content**	**MolarRatio (mol %)**	**Density (g/mL)**	**Code**	**Content**	**Molar Ratio (mol %)**	**Density (g/mL)**
C1	DMA/C17.3M	70/30	0.895	**C1**	DMA/C17.3M	70/30	0.895
C2-1	DMA/C18A	60/40	0.888	**C2-2**	DMA/C18A/17.3 M	60/15/25	0.887
C3-1	DMA/C17.3M	50/50	0.881	**C3-2**	AAc/C18A	60/40	0.880

To compare the results of H3-1 and H3-2, two segmented hybrids derivated from the H3-1 and H3-2 were also synthesized and subjected to elongation tests. Two segmented hybrids derivated from H3-1 and H3-2 as H1 and H2 were shown through an illustration in Figure 2.10.

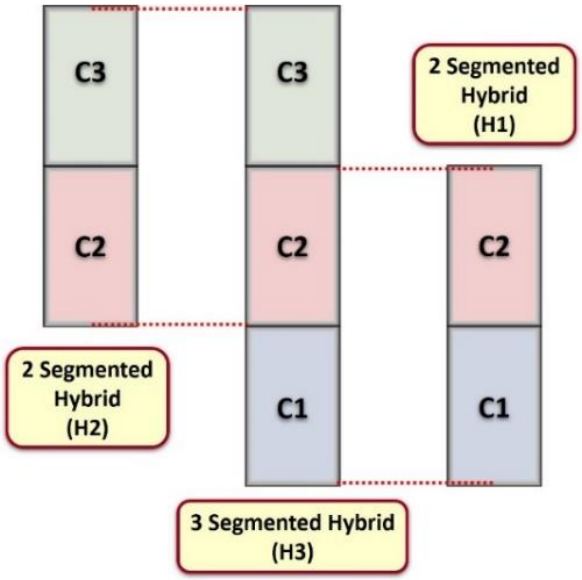

Figure 2.10 : Schematic illustration of three- and two-segmented hybrid hydrogels.

3. CHARACTERIZATION METHODS OF GELS

Within the scope of this thesis, two kinds of gels were chracterized. These gels are listed below.

1- Silk-Fibroin Cryogels
   a) Single Network (SN) Cryogels
   b) Double Network (DN) Cryogels
   c) Triple Network (TN) Cryogel
2- Hybrid Hydrogels
   a) Two-Segmented Hybrid Hydrogels
   b) Three-Segmented Hybrid Hydrogels

First kind of gels, silk-fibroin cryogels, were characterized in the point of biocompatibility view while the second group of gels, Hybrid Hydrogels, were subjected to mechanical characterization.

3.1 Characterization of Silk Fibroin Cryogels

3.1.1 Determination of proper cell/well amount for MTT asssay

Normal Human Dermal Fibroblast (NHDF) cell line was used for the present to optimize the cell numbers used for MTT assay in 96 well-plates. For the purpose of determining proper amount of cell/well, 20.000, 15.000, 10.000 and 7500 cells/well were examined. This preliminary experiments were applied either in empty wells as control group or in wells containing cryogel samples. Single network cryogels were used for this optimisation study. In order to decide on a reliable proper cell amount/well, MTT assays were conducted. Besides the quantitative results of MTT assays, qualitative results were considered as well to support the decide. Therefore, confluency states of cells were followed for 3, 7 and 10 days by using optical microscope (Olympus CK40-F200).

3.1.2 Biocompatibility – MTT cell viability test

The MTT (3-(4,5-dimethylthiazol-2-yl)-2,5-diphenyltetrazolium bromide) reduction assay is a homogeneous cell viability assay applied for a 96 well-plate which was suitable for high throughput screening (HTS). For the set of this experiment, aimed for cell viability measurements of cryogels, samples were placed in 96 well-plates for three other days as 3, 7 and 10. As given before in the part 2.1.2.

Investigated cryogel samples were:

i) Single-network (SN) cryogels: Obtained by varying the nominal fibroin concentration, C_{SF}, in the gelation solution as SN-4.2, SN-7, SN-12.5 and SN-22 wt%.

ii) Double-network (DN) and triple-network (TN) cryogels: DN and TN cryogels are denoted as DN-x/y and TN-x/y/z where x, y, and z are the fibroin concentration (C_{SF}) in the first, second and third gelation solutions, respectively, expressed in round numbers. DN-4/7, DN-4/14, DN-4/20, DN-4/29, TN-4/7/20.

7500 cells/well was applied according to the preliminary tests of which explained in details before. For each experiment day, a new well plate was used. Cryogel samples were placed in wells and cells were seeded. Every other plate had its own control groups to evaluate relative cell viability. Four control groups existed for each experiment day's 96 well-plate. Control groups include only cells in full growth medium solution while other wells have samples too. Figure 3.1 illustrates a representative experiment set (e.g. SN cryogels) for these three days.

The MTT substrate was prepared in a physiologically balanced solution (e.g. Phosphate buffered saline solution), added to cells in culture, at a final concentration of 0.2 mg/ml, and incubated for 4 hours. Viable cells with active metabolism convert MTT into a purple colored formazan product. When cells die, they lose the ability to convert MTT into formazan, thus color formation serves as a useful and convenient marker of only the viable cells. The formazan product of the MTT tetrazolium accumulates as an insoluble precipitate inside cells as well as being deposited near the cell surface and in the culture medium. The formazan must be solubilized by dimethylsulfoxide (DMSO), prior to recording absorbance readings.

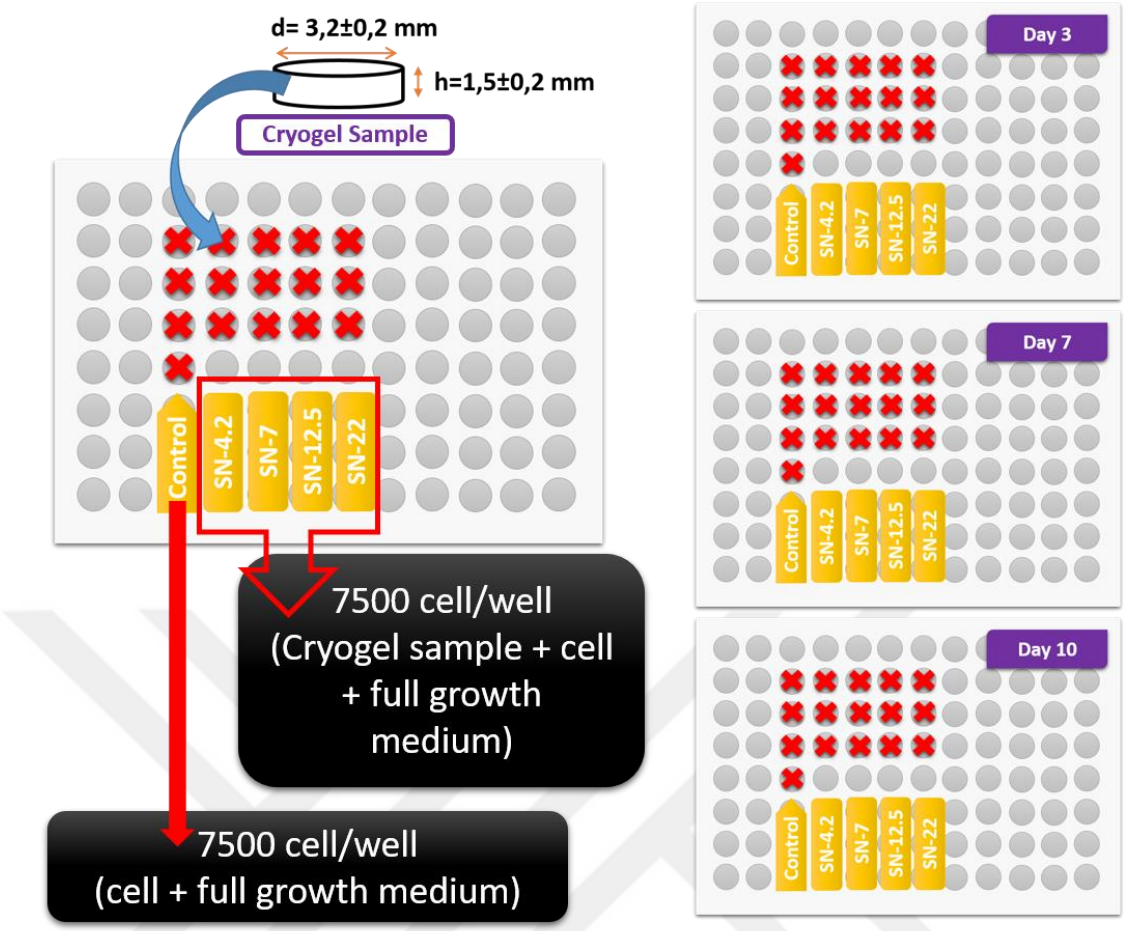

Figure 3.1 : Representative illustration of MTT assay setup for single network (SN) cryogels for 3^{rd}, 7^{th} and 10^{th} day. Red "X" symbols: loaded wells.

Figure 3.2 simply illustrates the application of MTT assay protocol for the SN cryogel set, on the example of "3^{rd} day MTT assay", which was specially planned for this study. Experiments for the 7^{th} and 10^{th} day were also conducted as explained for 3^{rd} day. Conditions were optimized according to the MTT assay protocol of the used brand.

The amount of signal generated is dependent on several parameters including the concentration of MTT, the length of the incubation period, the number of viable cells and their metabolic activity. Culture conditions that alter the metabolism of the cells will likely affect the rate of MTT reduction into formazan. For example, when adherent cells in culture approach confluence and growth becomes contact inhibited, metabolism may slow down and the amount of MTT reduction per cell will be lower [94]. Therefore, number of cells used for these experiments were determined by preliminary assays by performing in different number of cells.

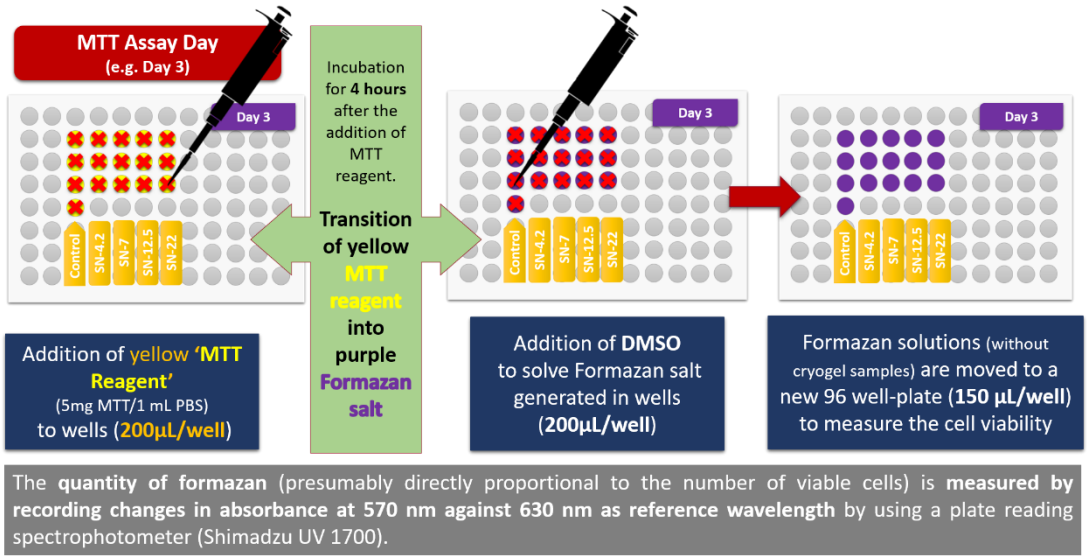

Figure 3.2 : Representative illustration of a running MTT assay at its 3^{th} day. Red "X" symbols: loaded wells.

3.1.3 Scanning laser confocal microscopy (LCSM)

Cell proliferation studies using the Normal Human Dermal Fibroblast (NHDF) cell line on fibroin cryogels were conducted by confocal microscopic technique. Briefly, at prerequisite time points the cell-seeded scaffolds were harvested and washed two times with PBS (1x, pH 7.4). Cells were fixed for 20 min by incubating in 4% formaldehyde in PBS (20 mins) followed by further washing (4 times, for 5 mins). The cells were permeabilized using 0.1% Saponin for 15 min and followed by preincubation with 0.1% Saponin + 3% bovine serum albumin (BSA) for 1.5 h. Incubation with Rhodamine–Phalloidin was carried out for 30 min at room temperature and then followed by washing with PBS (2 times for 5 mins). Finally stained with DAPI for 2 min. After two more washing with PBS for 5 mins, cryogel samples were transfered to new empty wells of µ-Slide (chambered coverslip) with 8 wells for a reliable monitoring. For cell proliferation, fluorescence images from stained samples were obtained by using a confocal laser scanning microscope (LCSM Leica, TCS SP2) equipped with Argon (488 nm) and HeNe (534 nm) lasers. The scaffolds being large in size (3.2±0.2 mm diameter), smaller areas were individually scanned and finally combined together by using Adobe Photshop CC 2017 to form a composite image for analysis.

3.2 Characterization of Hybrid Hydrogels

Hybrid gels, mixture gels and individual gels were subjected to mechanical tests which of their methods are explained in details under this part. Pycnometer measurements used for stratification of reaction solutions were also explained. Additionally, characterization of gels' outstanding properties were expressed under the self healing and shape memory subtitles.

3.2.1 Pycnometer measurements

Stratification of reaction solutions were achieved by intoducing density differences between the reaction solutions of expected hybrid gels. For this purpose, a calibrated pycnometer with capacity of 10 mL in volume was used to measure the densities of reaction solutions. Every measurement was performed at 25°C and repeated for at least three times.

In order to measure density of reaction solutions (RS), weight of pycnometer was recorded before every weighing. Then, pycnometer was filled up to overflowing of RS at 25°C and covers were closed. Gross weight of pycnometer was recorded. By using gross weight and pycnometer weight, net weight obtained and density was calculated. This way of density determination was used for segments of both H3 and H2 hydrogels. All resuts were collected acquiered from every sample. Mean values and standart deviations of densities were calculated. According to these results, stratification of reaction solutions were carried out.

3.2.2 Swelling measurements

All samples were synthesized by photoinitiated bulk copolymerization method, meaning that reaction solutions include no water. Thus, samples after synthesis state are just polymer networks but a hydrogel sample.

The copolymer samples thus obtained were immersed in excess of water at 50 (for H2) 70 (for H3) and 23±2 °C for the first and following days, respectively, by replacing water every day to extract any soluble species. By this way, samples as polymer networks turn into hydrogel samples at swelling equilibrium state. After equilibrium swelling, the amount of water in the gel samples was calculated as H_2O % = 10^2 x (m – m_o)/m, where m_o and m are the initial and swollen mass of the gel samples. Then, the gel samples were freeze-dried and the gel fraction w_g, that is, the conversion of

monomers to the water-insoluble polymer was calculated from the masses of dry polymer network and from the comonomer feed.

3.2.3 Uniaxial elongation and compression tests

- **Tests for two segmented hybrid hydrogels**

Uniaxial compression and elongation measurements were performed on swollen hydrogel samples by using Zwick Roell and Devotrans test machines with 500 N and 10 kN load cells. All the tests were conducted at 23±2 and 37±1 °C. Load and displacement data were collected during the experiments. The Young's modulus E was calculated from the slope of stress–strain curves between 5-15% and 1-3% deformations for compression and elongation tests, respectively.

For uniaxial compression measurements, cylindrical hydrogel samples of 6±1 or 13±1 mm in diameters and 7±1 mm in length were compressed at a strain rate of $3.8x10^{-2}$ s^{-1}. Before the test, an initial compressive contact to 0.01 ± 0.002 N was applied to ensure a complete contact between the gel and the plates. The stress was presented by its nominal σ_{nom} or true values σ_{true} (= $\lambda\sigma_{nom}$), which are the forces per cross-sectional area of the undeformed and deformed gel specimen respectively, while the compressive strain is given by λ, the deformation ratio (deformed length/initial length). The strain is also given by ε, the change in the sample length relative to its initial length, i.e., ε = 1- λ or ε = λ -1 for compression and elongation tests, respectively. Because the σ_{true}–λ plots pass through maxima before a macroscopic fracture of the gel samples, the nominal fracture stress σ_f and the compression ratio λ_f at failure were calculated from the maxima in σ_{true}–λ plots (Figure 4.16). Uniaxial elongation measurements were performed on dumbbell-shaped hydrogel samples with the standard ISO-37 type 2 (ISO 527-2) [194] under following conditions: Strain rate = $3.8x10^{-2}$ s^{-1}; sample length between jaws = 50±3 mm.

- **Tests for three-segmented hybrid hydrogels**

Uniaxial elongation measurements were performed on swollen hydrogel samples by using Zwick Roell test machine equiped with 500 N load cells. Since theree-segmented hybrids (H3) were just ynthesized in flat shaped, no compression test was performed on H3. All the tests were conducted at 23±2°C. Load and displacement data were collected during the experiments. The Young's modulus *E* was calculated from the slope of stress−strain curves between 1−3% deformations. The stress was presented

by its nominal σ_{nom} values, while the strain is given by ε, which is the change in the sample length relative to its initial length. Uniaxial elongation measurements were performed on rectangular-shaped hydrogel samples under the following conditions: strain rate = 3.8×10^{-2} s^{-1}; for two segmented hybrids (H1-1, H2-1 and H1-2, H2-2) and for each individual components of hybrids (C1, C2-1, C3-1 and C2-2, C3-2) sample length between jaws = 40 ± 3 mm, for three segmented hybrid samples (H3-1 and H3-2) = 60 ± 3 mm.

3.2.4 Self - healing tests

This test was just conducted for the set of samples explained as two-segmented hybrid hydrogels. Self-healing behavior of dumbbell-shaped gel specimens was investigated by first cutting them at both gel zones locating 6 mm away from the interface region. For cylindrical gel specimens, they were cut in the middle into two equally sized pieces. The damaged gel samples were then self-healed by keeping the cut surfaces in contact for 1 h at 80 °C in a water vapor-saturated glass chamber. Thereafter, uniaxial compression and elongation tests were conducted as described above. The results were compared with those of the virgin gel samples.

3.2.5 Uniaxial cyclic elongation tests

This test was just conducted for the set of samples explained as two-segmented hybrid hydrogels. Uniaxial cyclic elongation measurements were performed on swollen hydrogel samples by using Zwick Roell universal testing machine with 500 N load cell. All the tests were conducted at 23±2 °C. Load and displacement data were collected during the experiments as explained above, under the “Uniaxial elongation and compression tests” subtitle.

Cyclic elongation tests performed at a strain rate of $3.8x10^{-2}$ s^{-1}. The stress was presented by its nominal σ_{nom}, while the strain is given by λ, the deformation ratio (deformed length/initial length). The strain is also given by ε. Uniaxial cyclic elongation measurements were performed on dumbbell-shaped hydrogel as in elongation tests. Sample length between jaws = 50±3 mm. Based on the parameters given above, cyclic elongation tests were carried out for both of the hybrid gels.

To show the recovery potential of gels, 4 sets of cyclic elongation was performed for Hybrid 1 (H2-1). For the first 3 of these 4 sets of cyclic elongation, H2-1 sample was

subjected to λ at 1.3 for 20 times per each set of cycle. Then, the last (4^{th}) set of cycle was performed for 7 times by gradually increased λ values (rise of λ per each cycle was 0.05) between 1.3 and 1.6. After these 4 sets of cycles, comprised of 67 cycles in total, sample was retaining its structural integrity. For the last time after 67 cycles, sample was subjected to deformation up to rupture. Result was compared with the virgion sample. In order to recover deformations, generated by first and follwing sets of cyclic elongation tests, H2-1 hydrogel was released in a water bath at 50 °C for 1 min and followingly cooled down to room temperature before new set of cycle.

However, for Hybrid 2 (H2-2), 2 sets of cyclic elongation tests were performed which of each was comprising of 20 cycles at the λ value of 4. Result was compared with the virgin sapmle's rupture curve. In order to recover deformations, generated by first and follwing sets of cyclic elongation tests, H2-2 hydrogel was released in a water bath at 23±2 °C for 1h.

3.2.6 Rheological measurements

Cylindrical gel samples of 12 and 25 mm in diameters and about 1 mm in thickness were used for the rheological tests. The measurements were carried out between the parallel plates of the rheometer (Gemini 150 Rheometer system, Bohlin Instruments) equipped with a Peltier device for temperature control. The upper plate (diameter 20 mm) was set at a distance of 1000 to 1250 μm, depending on the swelling degree of the hydrogels.

During all rheological measurements, a solvent trap was used to minimize evaporation. Further, the outside of the upper plate was covered with a thin layer of low-viscosity silicone oil to prevent evaporation of solvent. A frequency ω of 6.3 rad·s^{-1} and a deformation amplitude γ_o = 0.001 (0.1%) were selected to ensure that the oscillatory deformation is within the linear viscoelastic region.

Thermal behavior of the gels was investigated by first keeping the samples at 80 °C for complete melting of crystalline domains and then, cooling down to 5 °C, after keeping for 10 min at 5 °C, heating back to 80 °C. The cooling/heating steps were carried out at a fixed rate of 1 °C·min^{-1}. The changes in the dynamic moduli of gels were monitored during the course of the cycle as a function of temperature. The gel samples were also subjected to frequency-sweep tests at γo = 0.001 over the frequency range 0.06 to 180 rad·s^{-1}.

3.2.7 Differential scanning calorimetry (DSC) measurements

DSC measurements were conducted on a Perkin Elmer Diamond DSC under nitrogen atmosphere. The gel samples sealed in aluminum pans were scanned between 5 and 80 °C with a heating and cooling rate of 5 °C·min^{-1}. From the DSC curves, enthalpy changes during melting, ΔH_m, were calculated from the peak areas. The degree of crystallinity, f_{cry}, that is, the fraction of polymer units in crystalline domains, was estimated by $f_{cry} = \chi_{HM}\, \Delta H_m^\circ / \Delta H_m^\circ$, where χ_{HM} is the mole fraction of the hydrophobic monomer in the comonomer feed and ΔH_m° is the melting enthalpy of crystalline C17.3M and C18A units. ΔH_m° was taken as 71.2 kJ·mol-1 from previous works studied in our colleaques on the melting behavior of long n-alkyl chains exhibiting a hexagonal crystal structure [191,192].

3.2.8 Shape memory tests

- *Two-segmented hybrid hydrogels*

Segments of Hybrid 1 (H2-1) hydrogel, have semicrystalline structures. Individual segments belonging to H2-1, C1 and C2-1, exhibit dual shape memory seperately by the advandage of Tm's at 48 and 35 °C, respectively. Therefore, fused body of C1 and C2-1 components in a single H2-1 exhibits pseudo-triple-shape-memory effect. Figure 8 demonstrates triple shape-memory capability of a H2-1 gel specimen. C1 zone was blue-violet colored with crystal violet for clarity. The gel is first heated to 70 °C (above both Tm's), and its C1 zone is deformed. When the gel is cooled to 42 °C, i.e., between the two Tm's of the gel zones, the first temporary shape is fixed due to the formation of crystalline domains in C1 zone. In the second step, the still melted C2-1 zone at 42 °C is deformed into the second temporary shape which is then fixed by cooling to 25 °C, i.e., below Tm of C2-1 zone. For the shape recovery, the gel is first heated to 42 °C to recover the first temporary shape while further heating to 70 °C recovers the permanent shape.

In the present hybrid hydrogel, H2-1, the switching domains are localized in the gel zones, and thus, although each zone has dual shape-memory function, the whole hybrid exhibits triple-shape-memory effect, which may be termed as "pseudo triple-shape-memory" behavior. Shape-memory tests conducted on H2-2 gel revealed existence of shape-memory function only at C1 zone while the C2-2 zone was unable to fix the temporary shape due to the absence of crystalline domains.

- *Three-segmented hybrid hydrogels*

Segments of H3-1 and H3-2, C1, C2-1, C3-1 and C1, C2-2, C3-2, respectively, have semicrystalline structures. Each of the individual segments belonging to H3-1 and H3-2 exhibit dual shape memory seperately.

Therefore, fused body of segments in a single H3-1 and H3-2 exhibits pseudo-triple-shape-memory or pseudo-multiple-shape-memory effect, respectively. For the clarity, C2-1 zone of H3-1 was blue-violet colored with crystal violet and the rest, end segments released non-colored. End segments, non-colored segments, C1 and C3-1 have T_m's of 37 and 35 °C, respectively, which are so close. Middle segment, clue-violet colored, C2-1 have Tm at 51 °C which is far different than the rest segment's T_m. Therefore, H3-1 exhibited pseudo-triple-shape-memory.

Firstly, the H3-1 gel is heated to 60 °C (above all of the three T_m's), and all segments were deformed into their temporary shapes. When the gel is cooled to 25 °C (below all of the three T_m's), temporary shapes are fixed. For the shape recovery, the gel is first heated to 40 °C to recover the first temporary shapes of end segments to their own permanent shapes, while further heating to 60 °C recovers the whole permanent shape of H3-1.

In order to follow the shape memory effect in H3-2 specimen,middle segment C2-1 zone released non-colored, while the end segments C1 and C3-2 was colored in red and, respectively. C1, C2-1 and C3-1 segments of H3-2 gel have Tm values at 37, 46 and 56 °C which are far different than each other. Therefore, H3-2 exhibited pseudo-multiple-shape-memory.

Firstly, the H3-2 gel is heated to 60 °C (above all of the three Tm's), and all segments were deformed into their temporary shapes. When the gel is cooled to 25 °C (below all of the three Tm's), temporary shapes are fixed. For the shape recovery, the gel is first heated to 40 °C to recover the first temporary shape of C1 segment, further heating to 50 °C recovers the permanent shape of C2-2 segment. As the last step, heated specimen to the 60 °C recovers the permanent shape of C3-2. Thus, the complete shape memory in the H3-2 specimen was reached.

4. RESULTS AND DISCUSSION

4.1 Silk-Fibroin Cryogels

Silk fibroin derived from *Bombyx mori* has been used by our research group to obtain silk fibroin based single network (SN), double network (DN) and triple network (TN) cryogels. As silk fibroin derived from *Bombyx mori* is a fibrous protein exhibiting extraordinary material properties such as good biocompatibility, biodegradability, high strength and toughness, and ease of processability, cryogels based on this protein promise potential application areas in bone tissue engineering, regenerative medicine, etc. Gelation of aqueous fibroin solutions mainly takes place through self-assembly of fibroin molecules induced by hydrophobic associations to form intermolecular ß-sheet crystallites acting as physical cross-link zones [7]. In this study, 3D interconnected macroporous, tough cryogel samples, obtained by the low-temperature gelation technique known as cryotropic gelation or cryogelation- with double network concept, were investigated within the point of biocompatibiliy view.

As given before, investigated cryogel samples were:

i) Single-network (SN) cryogels: Obtained by varying the nominal fibroin concentration, C_{SF}, in the gelation solution as SN-4.2, SN-7, SN-12.5 and SN-22 wt%.

ii) Double-network (DN) and triple-network (TN) cryogels: DN and TN cryogels are denoted as DN-x/y and TN-x/y/z where x, y, and z are the fibroin concentration (C_{SF}) in the first, second and third gelation solutions, respectively, expressed in round numbers. DN-4/7, DN-4/14, DN-4/20, DN-4/29, TN-4/7/20.

Within the scope of this thesis, biocompatibility assays comprising of MTT assay for cell viability and imaging of proliferating cells by confocal microscopy were conducted. Following sub-parts of this title will include the determination of proper cell amount for MTT assay procedure, cell viability capability results of cryogel samples and proliferation behavior of cells in cryogel architecture in details. Through

the bicompatibility tests of cryogel samples, Normal Human Dermal Fibroblast (NHDF) cell line was used.

4.1.1 Determination of cell/well amount

Within the biocompatibility investigation, Normal Human Dermal Fibroblast (NHDF) cell line was planed to subject to MTT assay for examining the cell viability on cryogel samples. According to the literature, culture conditions that alter the metabolism of the cells will likely affect the rate of MTT reduction into formazan. For example, when adherent cells in culture approach confluence and growth becomes contact inhibited, metabolism may slow down and the amount of MTT reduction per cell will be lower [193]. Therefore, optimisation of cell amount for the wells, where the cryogel samples will be tested in, is having critical importance. A higher amount of cell, than that of the used well's capacity to mediate cells until the termination of MTT assay (for example 10^{th} day), would cause an early cell deaths because of the high rates of confluences, while the lower amount of cell would cause insufficient signaling among cell agregates to proliferate and spread on the well surface. Both case would result in inadequate cell viability results which will not reflect the real viability ratios. Mismatching in cell amount for the used well surface area would come out as the material tested are not biocompatible.

Thus, here we examined a scale of cell/well amounts in a concentration of 20.000,15.000, 10.000 and 7500 cells per 200 µL of medium. Amounts were tested for 96 well plate. Application of these amounts were followed by using optical microscope. Quantitative cell viability results were obtained through the reading of absorbance (A) values after the MTT application by use of UV-Vis plate reader. Cell viability was calculated from the A values which are directly proportional to the cell viability. Control group results were assumed as 100% viable ratio of cells. Optical microscopy observations and MTT assay results were considered together to reach a reliable decision on proper cell amount. Figure 2.13 exhibits the trends of change in cell viability % of SN cryogel samples aaccording to the various cell amounts. Results of cell viability % (Figure 4.1) are relative ratios to the control groups of each assay's own. Samples subjected to this optimisation experiment were belonging to single-network (SN) cryogel series formed at silk fibroin concentrations between 4.2 and 22

wt%. Experiments were carried out for three different assay termination times as 3rd, 7th and 10th days.

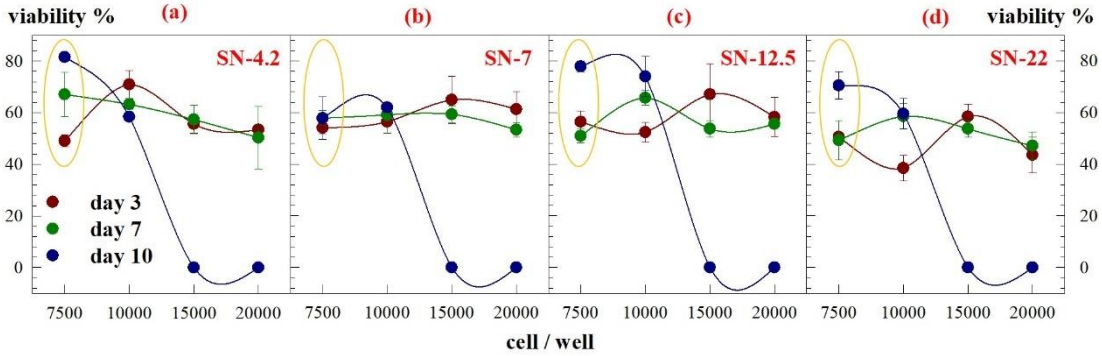

Figure 4.1 : Viable cell percentages are plotted against the cell amounts (in 200 µL of full growth medium) per well of a 96 well plate. Termination times of MTT assays are denoted by red, green and blue symbols for 3rd, 7th and 10th days, respectively. Results of most proper cell amounts are indicated by yellow hoops for each cryogels of single network (SN) sample series. (a) SN-4, (b) SN-7, (c) SN-12.5, (d) SN-22.

According to the pursuit of optical microscopy, it was seen that, as well as the wells containing cryogel samples, control wells were full with cells even at 3rd day of MTT assay for 20.000, 15.000 and 10.000 cells/well. Control group cells have been found as they are sustaining to die in following days of assay because of the exceeding of harvesting confluence state (80% confluency) of cell culture.It was seen that the attached cell number to the cryogel samples was already high enough for 3rd day of 10.000 cells/well assay and it provided to obtain higher values than 3rd day of MTT assay with 7500 cells/well. At 7th and 10th day, results of MTT assay were found virtual for 10.000 cells/well because of the relative drastic increase of dead cells in control wells than wells with samples. Thus, cell deads served as an increasing virtual viability for results and general view of results misleadingly show that 10.000 cells/well is better than 7500 cells/well. In order to avoid from contact inhibition of cells, cell numbers per well was planned to be choosen as cells would not be in contact inhibition until 10th day of the assay. In this way, 7500 cells/well was detected as the most proper amount for these experiments. From that decision on, all MTT assays with fibroblast cell line were performed by using 7500 cells/well.

4.1.2 Cell viability results by use of MTT assay

Normal Human Dermal Fibroblast (NHDF) cell line was used for investigations. As explained above, proper cell number was determined as 7500 cells per well and

experiments performed for this amount of cells. Figure 4.2 represents the results of cell viability (%) ratios for cryogels, with their specific pore sizes (μm) and porosities (%). Pore size and porosiy results of samples were obtained from the study conducted by our research group [7] to interpret the effect of cryogel structure in cell viability.

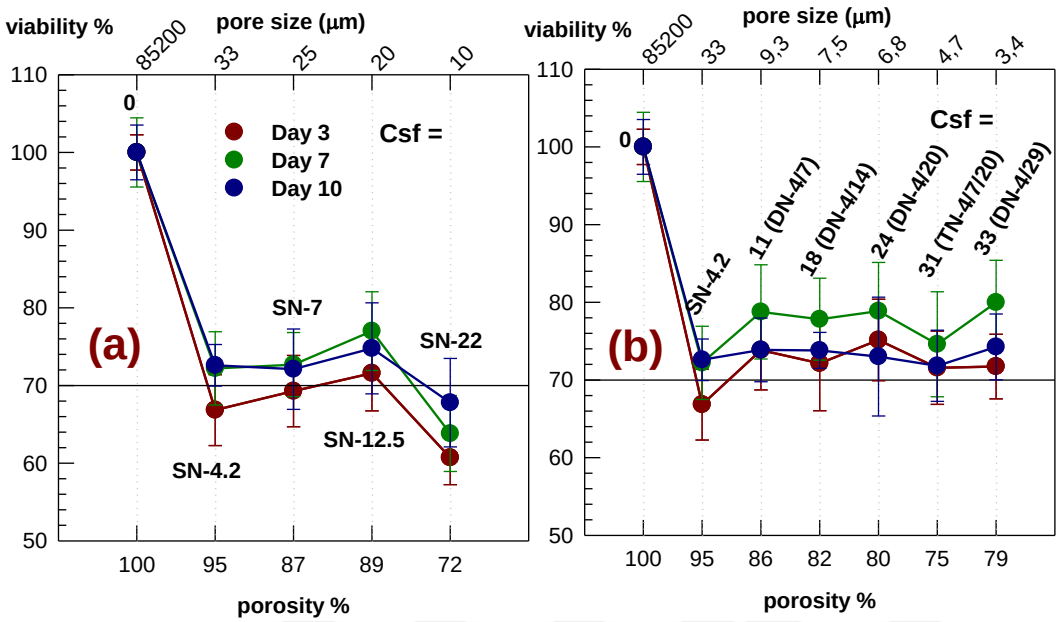

Figure 4.2 : Change in cell viability results are plotted against the pore size and porositiy values of (a) Single network (SN) cryogels, (b) SN-4.2, double network (DN) cryogels and triple network (TN) cryogel. Total silk-fibroin concentrations (C_{SF}) of DNs and TN are stated on graph for the consideration purposes. (For example, TN-4/7/20 has total C_{SF} of (4+7+20=33) 33). Control groups denoted as "0". Porosity of "0" assumed as 100% and the pore size taken as 85200μm (well diameter).

Investigations made for silk fibroin % concentrations (C_{SF}) at 0 (Control), 4.2, 7, 12.5 and 22 (Figure 4.2, a) and at 0, 4.2, DN-4/7, DN-4/14, DN-4/20, DN-4/29), TN-4/7/20 (Figure 4.2, b) for three different days. Cell viability was calculated according to absorbance (A) values which are directly proportional to the cell viability. Control group results were assumed as 100 % viable ratio of cells. As explained before, different cryogel series as SN and DN, TN series were examined for this study. Both of these series have been synthesized by our research group at two different date to beware of mistakes possibly caused by synthesis of cryogels. Therefore, two different synthesis of SN cryogels and two different synthesis of DN, TN cryogels were investigated seperately. Moreover, at least two assays were performed for each synthesis. As a summary, in total, four set of experiments were made for two different synthesis of SN cryogels and four set of experiments were performed for DN, TN

cryogels as well. Viabiliy (%) results of assays were merged and ploted against pore size (μm) and poreosity (%) in Figure 4.2, a, b by the help of variance calculation for each cryogel series.

It is seen that, the cell viability of SN cryogels formed over the whole range of silk fibroin concentrations is higher than that of the lethal dose of 50 %, stated as LC50 in toxicology. This means that all SN cryogels do not show any acute toxicity. Another point seen in Figure 4.2, a and b is that there is no significant dependency of cell viability (%) on the silk fibroin concentration of cryogels. Moreover, SN cryogels formed at 7 and 12.5 % fibroin concentrations denoted as SN-7 and SN-12.5, respectively, exhibit cell viability above 70% indicating that they are "not cytotoxic" for MTT assays of medical devices as emphasised in the standart called "Biological evalution of medical devices/ Part 5: Tests for in vitro cytotoxicity" with the code of ISO 10993-5 [194]. As to Figure 4.2, b, it is seen that the results obtained from DN and TN cryogel series show absolutely no acute toxicity for all experiment days (3^{rd}, 7^{th} and 10^{th}) of the MTT assay. The ratios of cell viability for all cryogels are above the lower limit of cytotoxicity level as well as stated in ISO 10993-5 [194] standart for the MTT assays of medical devices.

Figure 4.3 represents the all cell viability (%) results together, as ploted against the pore size and porosity (%), in the order of increasing total (C_{SF}). Results on Figure 4.3 indicates that, compared to the SN series, DN and TN cryogels show much better biocompatibility. The higher biocompatibility of the cryogels with double and triple-network structures as compared to the SN cryogels is attributed to the increasing internal surface area of the former cryogels due to the presence of a second generation of smaller pores.

DN and TN cryogels were prepared by conducting the cryogelation reactions within the pores of SN and DN cryogels, respectively, providing the formation of two generations of pores. Increasing internal surface area and porosity of DN and TN cryogels enable cells to access nutrients much easier and provide them much proper waste exchange capacity. The pore size and the total porosity of SN cryogels are between 10-33 μm and 95-72%, respectively. Increasing the silk fibroin concentration during the preparation of SN cryogels, pore walls are becoming thicker whereas pore sizes are becoming smaller. In contrast, second generation pores of 1μm in diameter

appear in DN and TN cryogels. For instance, DN-4/20 and SN-22 cryogels have similar silk fibroin concentrations and similar porosities (80 vs 72%).

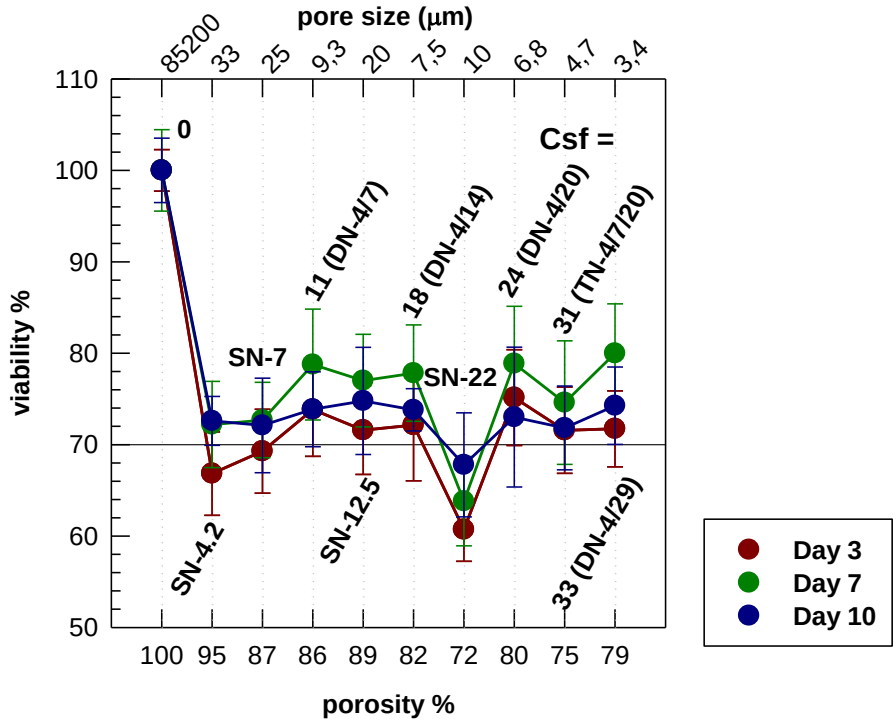

Figure 4.3 : Change in cell viability (%) rates are ploteted against the pore size (µm) and porosity (%) values of SN, DN and TN cryogels. Graph exhibits all the results shown in Figure 2.14 "a" and "b" together. Viability results are given in the order of increasing total silk-fibroin concentration (C_{SF}).

Cell viability results of SN-22 for the 3^{rd}, 7^{th} and 10^{th} day are 61±3.5, 64±5 and 68±6 %, respectively, while DN-4/20 cryogels show 72±4.1, 80±5 and 74±4 % cell viability in the same day order. Thus, although both fibroin concentration and the total porosity are almost the same for these samples, double-networking results in an increase of cell viability. It was reported that increasing cell viability is mainly due to enhanced nutrient supply and more efficient metabolic waste removal from the interior regions of scaffold constructs [91,92,94,195]. Due to the formation of smaller pores in DN cryogels, specific surface area increases, providing a more favourable environment in which cells could remain viable and therefore proliferate to a greater extent.

4.1.3 Imaging by Laser Scanning Confocal Microscopy (LSCM)

In order to obtain a scaffold for biomedical applications, material clustering, pore size, surface area, wall thickness and homogeneity etc. have critical importance. For the study we explained here, we have two kinds of materials to clarify the relationships

between cell viability and pore size, surface area and wall thickness. SN crogels synthesized by increasing fibroin concentrations represents decreasing pore size and porosity while wall thickness is increasing. The other set of cryogels, named as DN and TN in this report, are formed by double-networking method as sequential synthesizing of networks inside a single network cryogel, represents increasing fibroin concentrations by penetration of new networks inside the single network. However, DN and TN cryogels exhibit no increase in wall thickness with the help of formed pores inside the bigger pores of single network pores, called as second generation pores. Moreover, decreasing in pore size occasioned by second generation pores and incresing fibroin concentration cases were run with increasing surface area. Besides all, both of two cryogel type have an advantege for biomedical applications as they have interconnected pores. It has reported in the literature that, pores of adequate size allow cells to migrate or adhere to the surface of a material, but interconnecting pores are necessary to permit cell growth into the scaffold interior [38].

To study cell proliferation, spreading and actin development on cryogel samples, confocal microscopy was carried out. Figure 4.4 and Figure 4.5 represents the confocal laser micrographs of NHDF cells cultured on SN-4.2 and TN-4/7/20, repectively.

It can be interpreted from confocal micrograms (Figure 4.4 and 4.5) that, profuse cell growth was observed in TN-4/7/20 cryogel compared to SN-4.2. These findings are in relation to MTT assay results. Cells were covered the scaffold surface and cells were observed to attach on to scaffold walls for support. Cells with nuclei and filaments were observed throughout the matrix surface suggesting normal growth of fibroblast cells on these cryogel. Confocal laser micrographs and MTT assay results supported that porosity plays a significant role in the overall function of cryogels. Reported studies in the literature mention that, there are limits of acceptable scaffold architecture (VF, pore size) that influence in vitro cellular responses. Additionally, pore size and VF (volume fraction) can affect cellular adhesion, viability, ingrowth, distribution, and the formation of an ECM by specific cell types. A high VF (and thus large surface area/volume ratio) was necessary for in vitro cell attachment, proliferation, and subsequent matrix deposition. It was stated in the literature that the optimum VF for engineering homogeneous tissues may be greater than 90% or between 75% and 90% and generalized as, if engineering tissues in vitro using any of the cell types studied, scaffolds with the largest VF (90%) are likely to support greater cellular metabolism

and infiltration and production of collagens and glycosaminoglycans compared to scaffolds with 75% VF [95].

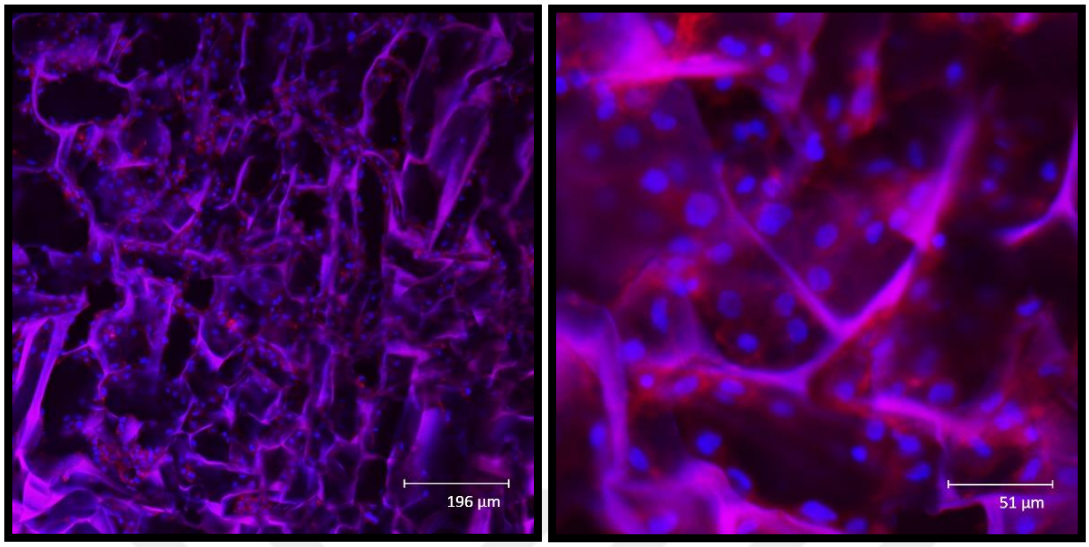

Figure 4.4 : Confocal laser micrographs of Normal Human Dermal Fibroblast (NHDF) cells cultured on SN-4.2 which were stained with Rhodamine–phalloidin for detecting actin filaments (red) and DAPI for nuclei (blue). Micrograms were obtained from the 7^{th} day culture.

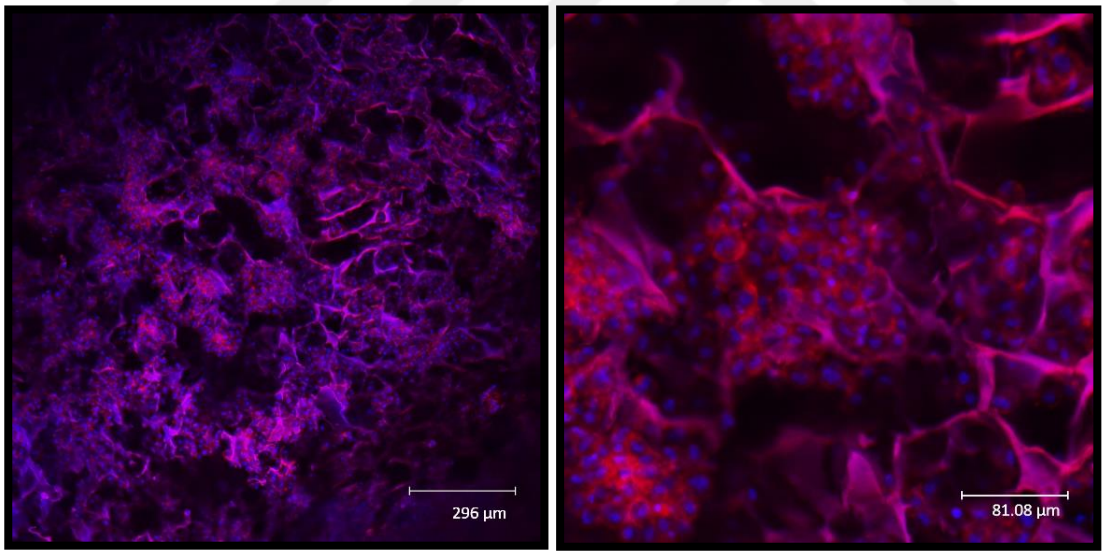

Figure 4.5 : Confocal laser micrographs of Normal Human Dermal Fibroblast (NHDF) cells cultured on TN-4/7/20 which were stained with Rhodamine–phalloidin for detecting actin filaments (red) and DAPI for nuclei (blue). Micrograms were obtained from the 7^{th} day culture.

For the set of cryogels we exhibited the results in this report, viability (%) results of MTT assays represent a corelation with literature. Viability (%) results show that, cryogels with the porosity (%) ratios between 90 and 75% reveal better results. Scaffold porosity in particular controls the key processes of nutrient supply to cells,

metabolite dispersal, local pH stability and cell signaling. The size of the pores can affect how close the cells are at the initial stages of cultivation (allowing for cell-cell communication in three dimensions), but also influences the amount of space the cells have for 3-D organization in the later stages of tissue growth. In addition, a porous surface is known to improve mechanical interlocking between the implanted scaffolds and the surrounding natural tissue, providing greater mechanical stability at this critical interface [38,57].

Former papers in the literature were declared that the surface area/volume ratio of porous materials depends on the density and average diameter of the pores. Nevertheless, the diameter of cells in suspension dictates the minimum pore size, which varies from one cell type to another. Depending on the envisioned applications, pore size must be carefully controlled. The effect of implant pore size on tissue regeneration is emphasized by experiments demonstrating optimum pore size of 5 μm for neovascularization, 5–15 μm for fibroblast ingrowth, close to 20 μm for the ingrowth of hepatocytes, 20–125 μm for regeneration of adult mammalian skin, 40–100 μm for osteoid ingrowth and 100–350 μm for regeneration of bone. Fibrovascular tissues appear to require pores sizes greater than 500 μm for rapid vascularization and for the survival of transplanted cells [96,97]. It was informed that, the pore sizes obtained here have been performed for mentioned cell types up to 50 % porosities. However, according to the study we made here shows that, a property obtained by the combination of optimum pore size, porosity% and wall thickness could change these known pore size requisites. In this stuy, with the help of double networking method, the surface area/volume ratio of porous materials is not depend on the density and average diameter of the pores. In an example, porosity% ratio and pore size seen as 87% and 25μm for SN-7 while they were 86% and 9,3μm for DN-4/7, repectively. In contrast with claimed in literature, we succeded to obtain high cell viabilities and cell attachment on cryogels, having second generation pores, even for very small sizes as 3,4 μm (DN-4/29).

Here, we claim that these DN, TN cryogels can increase the cell viability and be protected from any loss on mechanical properties as well. For this reason, these “second generation pores” make DN, TN cryogels a good candidate for load bearing biomedical applications.

4.2 Hybrid Hydrogels

Hybrid hydrogels mentioned in this thesis are materials with two or three distict zones, in a fused body, of which have different physical and chemical features. The aim of the study is achieving to create a multi-segmented hybrid hydrogel with tunable and switchable segments according to the requisites possibly we can face in its wide range of application areas.

Within the scope of this part, mechanical and thermal measurement results of hybrid hydrogels will be discussed. For this purpose, results were collected under two main title according to the number of zones hybrids include.

These hybrids are:

i) Two-segmented hybrid hydrogels

ii) Three-segmented hybrid hydrogels

4.2.1 Two-segmented hybrid hydrogels

The most proper hybrid hydrogels with two segments having different physical and chemical properties were prepared by considering of several characteristics. Preliminary experiments reveal three requirements for preparing mechanically strong hybrid hydrogels with smooth and robust interfaces:

i) Since the preperation of hybrid gels in this study based on the simultaneous synthesis of two individual components in a fused body, reaction solutions of hybrid hydrogel components have to be suitable for stratification.

ii) In order to obtain hybrids with reproducible mechanical properties, the interface region in hybrids should exhibit a smooth transition from one to another gel zone (Figure 4.6).

iii) Swelling ratios of the gel components of hybrids should not differ significantly from each other. Otherwise, the mismatch in the swelling ratios resulted in their rupture in aqueous environment (Figure 4.6).

Examples of feasible and unfeasible hybrid gels in interbedded and flat shapes are demonstrated in Figure 4.6. Feasible hybrid gels are also exhibit superior behaviors such as self-healing and shape memory.

Figure 4.6 : Optical images of feasible and unfeasible hybrid gels in interbedded and flat shapes.

Two-segmented hybrid hydrogels composed of the following gel components in two different compositions satisfied these requirements in both of the shapes obtained within this study as interbedded and flat types. Compositions of hybrid segments satisfying the requirements are given in Table 4.1.

Table 4.1 : Compositions of hybrid segments.

Hybrid 1 (H2-1)	Hybrid 2 (H2-2)
C1: 70 mol % DMA / 30 mol % C18A	C1: 70 mol % DMA / 30 mol % C18A
C2-1: 50 mol % DMA / 50 mol % C17.3M	C2-2: 50 mol % DMA / 50 mol % C12M

Figure 4.7 shows the optical images of H2-1 and H2-2 gels in both interbedded and flat shapes.

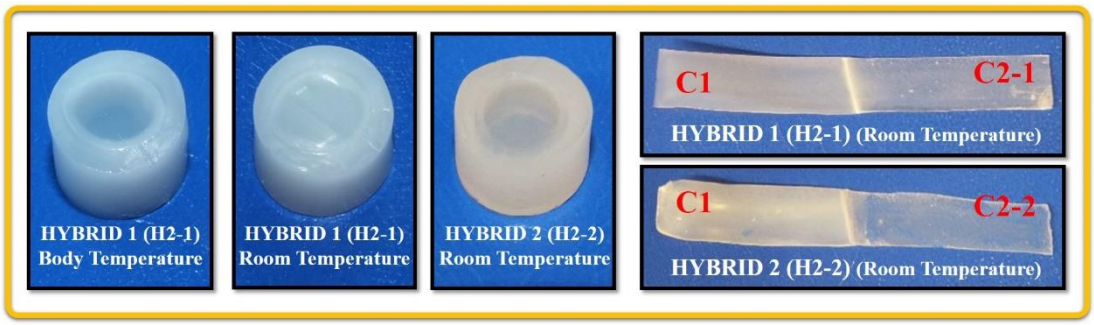

Figure 4.7 : Optical images of hybrid gels in interbedded and flat shapes.

As can be seen, inner part of interbedded H2-1 gel (Figure 4.7) is opaque at room temperature, however, it turns into a transparent look at body temperature. Even if the C2-1 for H2-1 gel exhibits hard texture at room temperature, it is getting softer at body

temperature and the appearance turns into transparent. On the other hand, C2-2 segment of H2-2, can be found soft in a wide range of temperature scale encompassing room and body temperature.

Within this section, facts in determining proper hybrid gels will be clarified and properties of these hybrid gels will be investigated in details.

4.2.1.1 Stratification Study

Preparation of hybrid hydrogels in a flat shape with two distinct gel zones, based on the density difference of the monomer mixtures, were achieved in terms of stratification of reaction solutions (RS). Densities of RS were measured by using a calibrated glass pycnometer at 25 °C. By stratification method, the RS with a low density floats on top of another RS of higher density whereas the interface between layers (transition area) acts as a barrier to prevent monomers from diffusion between layers. Figure 4.8 shows an example of stratification study performed for RS components of H2-1 samples.

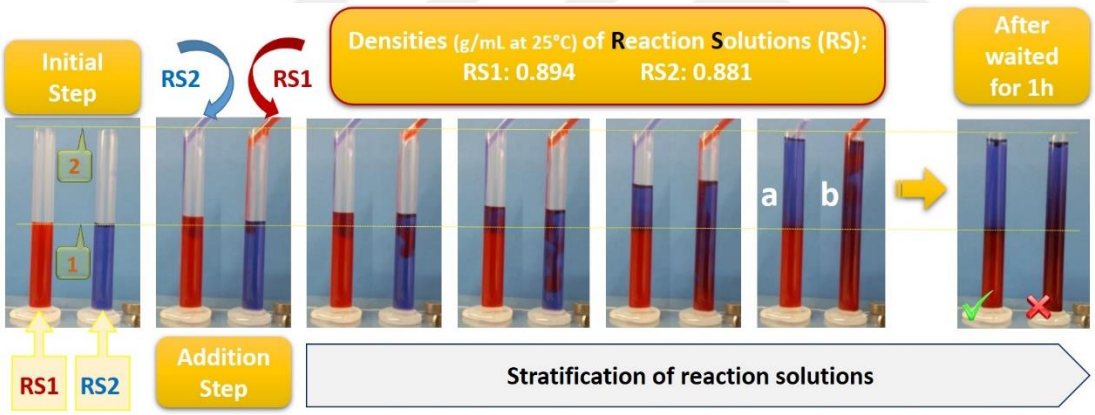

Figure 4.8 : Illustration of stratification study performed for H2-1 samples' reaction solutions (RS). (RS 1: monomer mixture of C1, RS 2: monomer mixture of C2-1).

Red and blue RS, shown in Figure 4.8 as the initial step, were denoted as RS1 and RS2 with the densities of 0.894±0.021 and 0.881±0.002, respectively. Pipettes were poured with two different RS as shown in initial step up to half level of their heights. At the addion step, the plastic pipettes with red RS1 and blue RS 2 were subsequently poured with vice versa colored solutions as blue RS2 and red RS1, respectively; thus, whether the stratification succeeded or not can be made apparent. By using solution-dyed RS, as in Figure 4.8, it was proved that, according to densities measured by pycnometer, stratification of RS is possible even for the little differences in desities. In addition, it

was seen that the transition area (interface region) occurs apparent in just a few millimeters in thickness. It was demonstrated with yellow dashed lines and these lines are named as "1" and "2" in Figure 4.8. Yellow dashed line, stretch across the pictures at the top level of pipettes (Figure 4.8, 2), shows the coequal heights of pipette. The secant line above the half heights of pipettes (Figure 4.8, 1) demonstrate that there is no change in the location of transition area by any jumble for a successfully stratified RS combination. A successfully stratified solution combination has to be as seen on "a" of 6th photo in Figure 4.8. It was clear that, the vice versa combination of these solutions causes jumble of solutions ("b" of 6th photo in Figure 4.8), resulting in not to obtain a stratified combination of RS.

In order to obtain right combination for stratification of RS, densities of three sets of RS comprising of dimethylacrylamide (DMA) and one of three different hydrophobic monomers (octadecy acrylate (C18A), stearyl methacrylate (C17.3) or lauryl methacrylate (C12M)) in various concentrations were measured. Densities of RS are collected in Table 4.2. Molar ratios of monomers in RS given in table are calculated with respect to total initial monomer concentration (C_O). Mean and standart deviation (SD) values are given in the Table 4.2. SDs can be found in brackets.

Table 4.2 : Densities of reaction solutions belonging to hybrid segments.

	RS Composition (mol % - with respect to C_O)	**Density** at 25 °C (g/mL)
Set 1 (DMA / C18A)	50 DMA – 50 C18A	0.881 (0,003)
	70 DMA – 30 C18A	0.894 (0,021)
Set 2 (DMA / C17.3M)	50 DMA – 50 C17.3M	0.881 (0,002)
	70 DMA – 30 C17.3M	0.895
	80 DMA – 20 C17.3M	0.912
Set 3 (DMA / C12M)	50 DMA – 50 C12M	0.889 (0,001)
	70 DMA – 30 C12M	0.907
	80 DMA – 20 C12M	0.921

Stratification with solution-dyed RS were examined for various combinations. Photos of all resulting views are shown together in Figure 4.9. Red solutions symbolize RS containing 30 (upper box of Figure 4.9) or 50 (lower box of Figure 4.9) mol % C18A. Blue solutions denote RS with C17.3M or C12M in concentrations of 50, 30 and 20 mol %, in the order of left to right in Figure 4.9. Every single photo in Figure 4.9

contains two filled pipettes with two different colors of solutions. Left sides of every single photos show the addition order of C18A and followingly C17.3M or C12M while the right sides performed as vice versa.

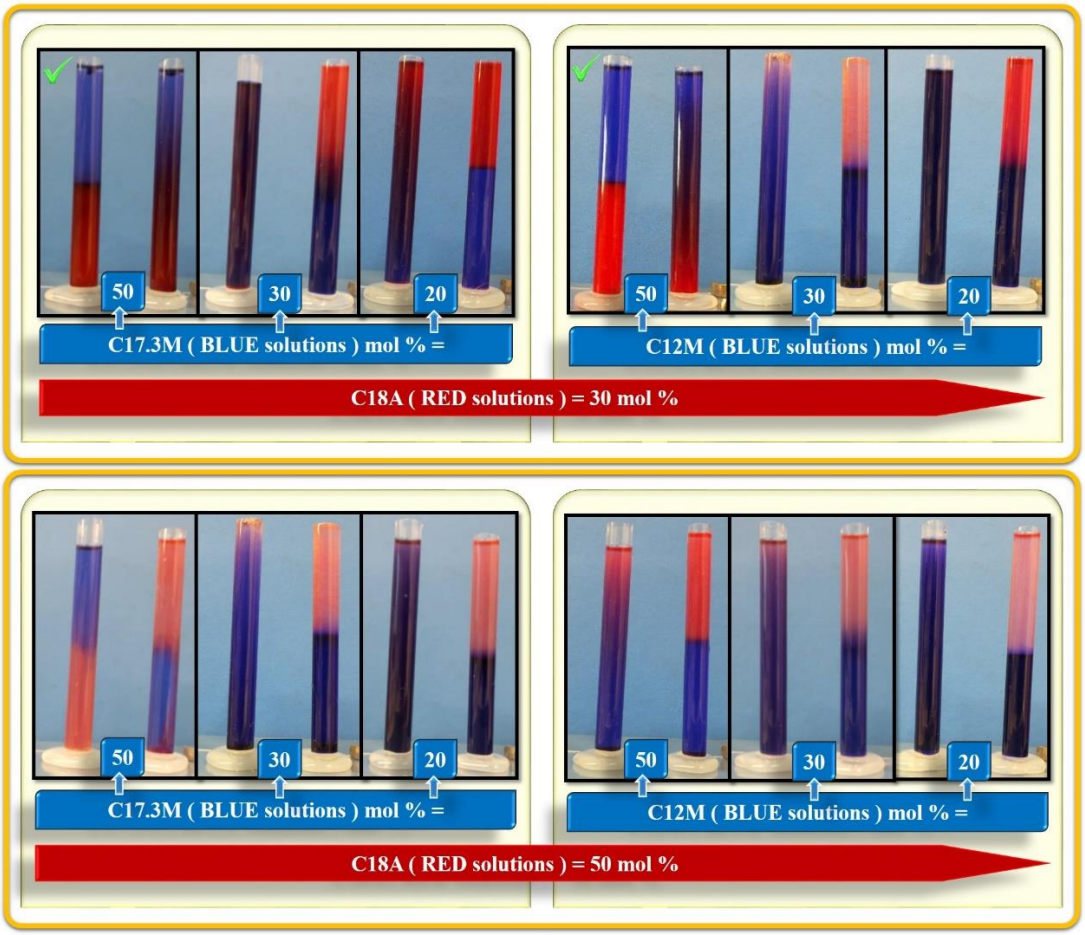

Figure 4.9 : Illustration of stratification study performed for solution-dyed reaction solutions.

Obtaining an optimum hybrid gel was achieved by following the stratification method. However, apart from stratification, properties like swelling rate, rigidity, etc. were considered as well. Ticked up RS combinations on photos were selected to synthesize hybrid gels in the light of the stratification and other properties which of them will be mentioned under following parts.

4.2.1.2 Differential Scanning Calorimetry (DSC)

Differential Scanning Calorimetry (DSC) traces of waterswollen hybrid hydrogel samples reveal melting and crystallization transitions by changing the temperature. Figure 4.10 shows the sampling method for DSC measurements of hybrid gels. Obtained intersections were labeled as 1 to 6 and colored in various colors in Figure

4.10 to define the plots of Figure 4.11 and Figure 4.12. DSC measurements were also performed for individual gel samples of each component and their mixture to compare with transition area of hybrid gels.

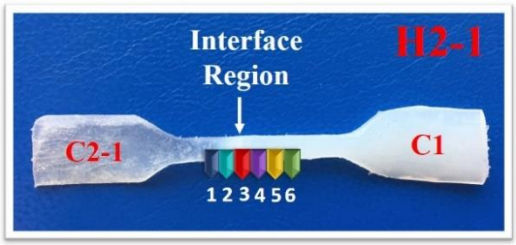

Figure 4.10 : Sampling method on an optical image of Hybrid 1 (H2-1) gel as an example for DSC measurements of hybrid gel samples.

Numbered intersections include a range of samples in hybrids from soft component, transition area to soft component. Figure 4.11 shows the DSC measurement results of Hybrid 1 gel (Figure 4.11, (a)) and their comparison with individual gel samples and the mixture of them (M 1/Mixture 1) (Figure 4.11, (b)), having same composition with the components of Hybrid 1 gel and its transition area.

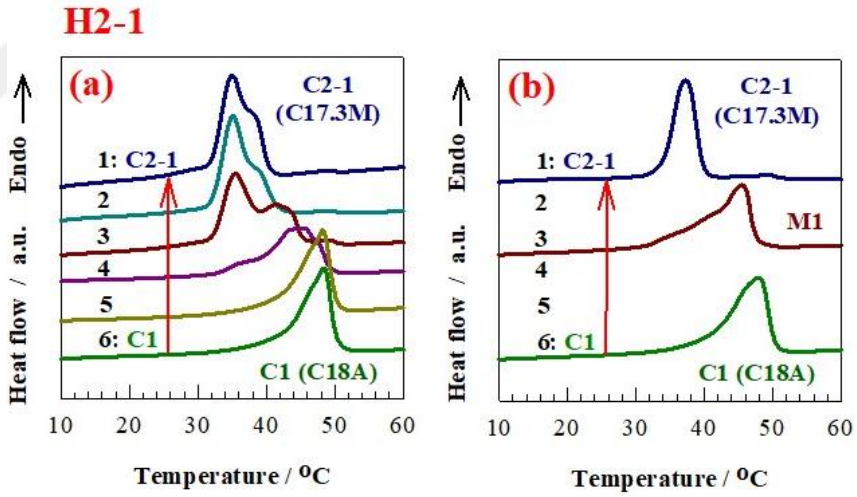

Figure 4.11 : DSC results of Hybrid 1 (H2-1) gel. DSC results obtained from (a) H2-1 gel sample, (b) Individual C1, C2-1 and Mixture 1 (denoted as M1) gel (C1+C2-1) samples.

DSC measurements reveal that as the locations of sample change, from C2-1 (labeled as 1 in Figure 4.10) to C1 (labeled as 6 in Figure 4.10), T_m values were gradually increased from 35 to 48 °C. DSC results of individual components C1, C2-1 and their mixture M1which mimics the interface region of Hybrid 1 (H2-1) gel given in Figure 4.11. C1 gel component, consisting of DMA and C18A, is a semicrystalline hydrogel with a melting temperature (T_m) of 48 °C. The C2-1 component, comprasing of DMA

and C17.3M, has a lower T_m of 35 °C, due to the limitation of side alkyl chain alignment which originates from the methyl group on the backbone of C17.3M units [3]. See Table 4.3 for the complete list of T_m values for Hybrid 1.

In contrast, C2-2 component, consisting of DMA and C12M, is in amorphous state due to the shorter alkyl chain length of C12M units [130]. Figure 4.12 shows the DSC measurements conducted for Hybrid 2 (H2-2) gel (Figure 4.12, (a)) and their comparison with individual gel samples having same composition with the components of H2-2 (Figure 4.12, (b)).

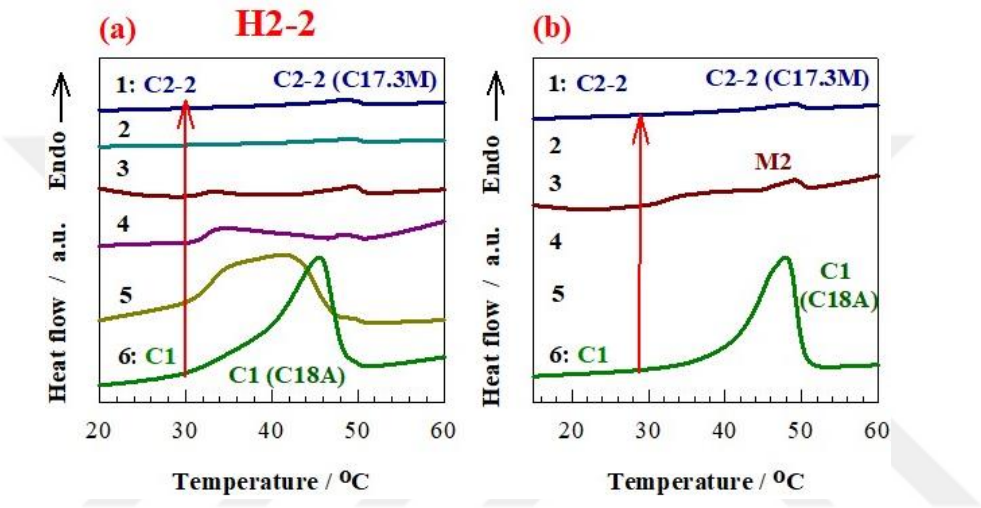

Figure 4.12 : DSC results of Hybrid 2 (H2-2) gel. DSC results obtained from (a) H2-2 gel sample, (b) Individual C1, C2-1 and Mixture 2 (denoted as M2) gel (C1+C2-2) samples.

Figure 4.12, (a) shows that the melting peak appearing at 48 °C in C1 zone first broadens and then gradually disappears as the sample position approaches to the amorphous C2-2 zone of H2-2, indicating complete mixing of the gel components at the interface. By using the DSC measurements, results collected in Table 4.3 were calculated.

Table 4.3 : Thermal mechanical properties of hybrid segments and mixture gels.

Code	Composition (mol %)				T_m (°C)	T_{cry} (°C)	f_{cry} (%)
	DMA	C18A	C17.3M	C12M			
C1	70	30	-	-	48	41	12
C2-1	50	-	50	-	35	23	12
C2-2	50	-		50	-	-	0
C1+C2-1 (M1)	60	15	25	-	46	36	16
C1+C2-2 (M2)	60	15	-	25	-	-	0

Shape memory experiment of H2-1 was carried out by using the T_m results obtained from DSC.

4.2.1.3 Shape memory

T_m results obtained from the DSC measurement were used to examine shape memory behavior of Hybrid 1 (H2-1) and Hybrid 2 (H2-2). Relative to C18A and C17.3M, C12M monomer has shorter alkyl chain with 12 C length.

DSC results represent that, C2-2 segment in H2-2 gel, composed of C12M monomer, has no crystalline domain. Therefore, C2-2 segment was flexible at room temperature. Its known that, shape memory behavior arise from the existence of high cystalline domains in the gel network, so that no shape memory behavior observed on C2-2 segment as it has been foreseen with the help of DSC results. H2-2 gel has C1 and C2-2 segments. C1 segment has dual-shape memory ability due to the semicrystalline structure originated from the C18A while the C2-2 segment has no shape memory ability. Thus, shape memory test was not performed on H2-2 hydrogel.

In contrast with H2-2 hydrogel, H2-1 hydrogel, having C1 (includes C18A) and C2-1 (includes C17.2M) segments, has dual shape memory ability in both of its segments. It means that, fused body of C1 and C2-1 segments in a single H2-1 hydrogel has capability to have two temporary shapes arising from its individual segments. Whole, single, fused body of H2-1 hydrogel has also a permanent shape. In total, an H2-1 hydrogel can have three shapes. Therefore, H2-1 hydrogel has triple-shape memory. As explained, in order to call a material that it has triple-shape memory ability, material should exhibit two temporary and a permanent shape in a whole body of material [196]. Different from a material having conventional triple-shape memory ability, H2-1 hydrogel has its two temporary shapes by taking the advantage of its individual segments' own temporary shapes. Since these two different temporary shapes are local on the segments but a spreading shape on a whole material, shape memory ability of H2-1 is specifically called as "pseudo-triple shape memory". Figure 4.13 shows the pseudo-triple shape memory ability of H2-1 hydrogel.

Images in Figure 4.13 are labeled from "a" to "e" to ease the follow of procedure. The image labeled as (a) is the permanent shape of H2-1 where the C1 zone was colored in blue for clarity.

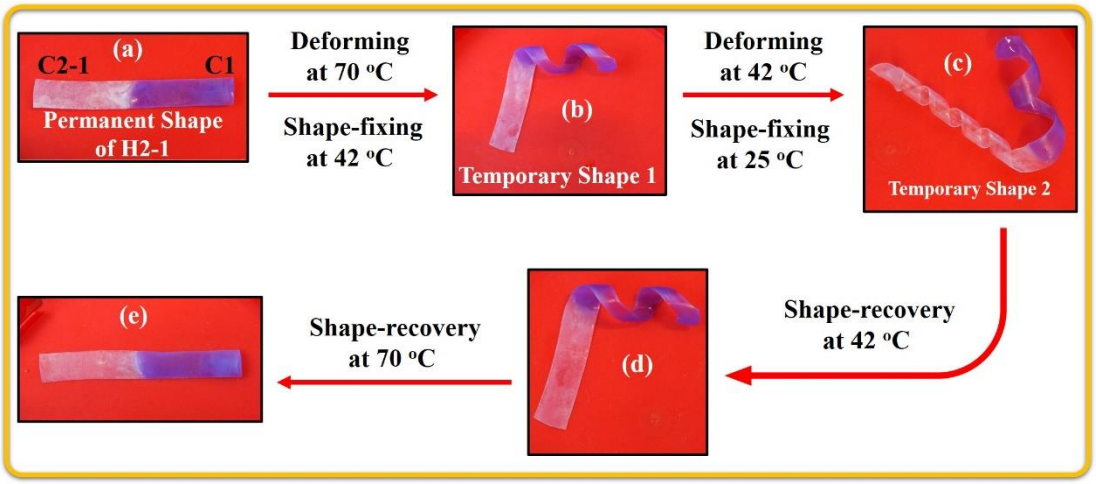

Figure 4.13 : Images demonstrating pseudo triple-shape-memory behavior of H2-1 hydrogels. Permanent shape (a), temporary shapes 1 and 2 (b, c), and successive shape recoveries at 42 and 70 °C (d, e).

The gel is first heated to 70 °C (above both T_m's), and its C1 zone is deformed. Then the gel is cooled to 42 °C (which is a temprature between the two Tm's of the gel zones) for forming the temporary shape 1. Shape is fixed due to the formation of crystalline domains in C1 zone (Figure 4.13, b). In the second step, the still melted C2-1 zone at 42 °C is deformed into the temporary shape 2 which is then fixed by cooling to 25 °C (a temperature below T_m of C2-1 zone) (Figure 4.13, c). In order to recover the shape, the gel is first heated to 42 °C for testing the recovery of the temporary shape 1 (Figure 4.13, d). Followingly, further heating to 70 °C recovers the permanent shape (Figure 4.13, e).

For the H2-1 hydrogel, hydrophobic associations and crystalline domains acts as netpoints and switching segments, respectively, which are responsible for the shape memory effect. At temperatures above T_m, hydrophobic associations formed by melting of alkyl crystals determine the permanent shape of the hydrogel. In this state, the hydrogel can easily be deformed under loading to assign temporary shapes to its gel zones. Upon cooling below T_m, side alkyl chains forming crystalline domains fix the temporary shapes of the hydrogel. Shape memory tests conducted on H2-1 revealed the existence of pseudo- triple shape-memory function.

4.2.1.4 Uniaxial compression and elongation

Uniaxial elongation tests of flat shaped hybrid hydrogels and uniaxial compression tests of interbedded shaped hybrid hydrogels at room and body temperature were performed. Results will be demonstrated and discussed under this part.

- *Uniaxial elongation tests*

The Hybrid 1 (H2-1) gel is composed of two individual segments as C1 and C2-1. In between the segments of H2-1, there is an interface region in a few millimeters of thickness. Hybrid 2 (H2-2) gel is also comprised of two individual segments as C1 and C2-2 with an interface region of a few millimeters of thickness. Flat shaped hybrid hydrogels were subjected to elongation tests. Figure 4.14 shows the tensile test results and optical images of H2-1 and H2-2.

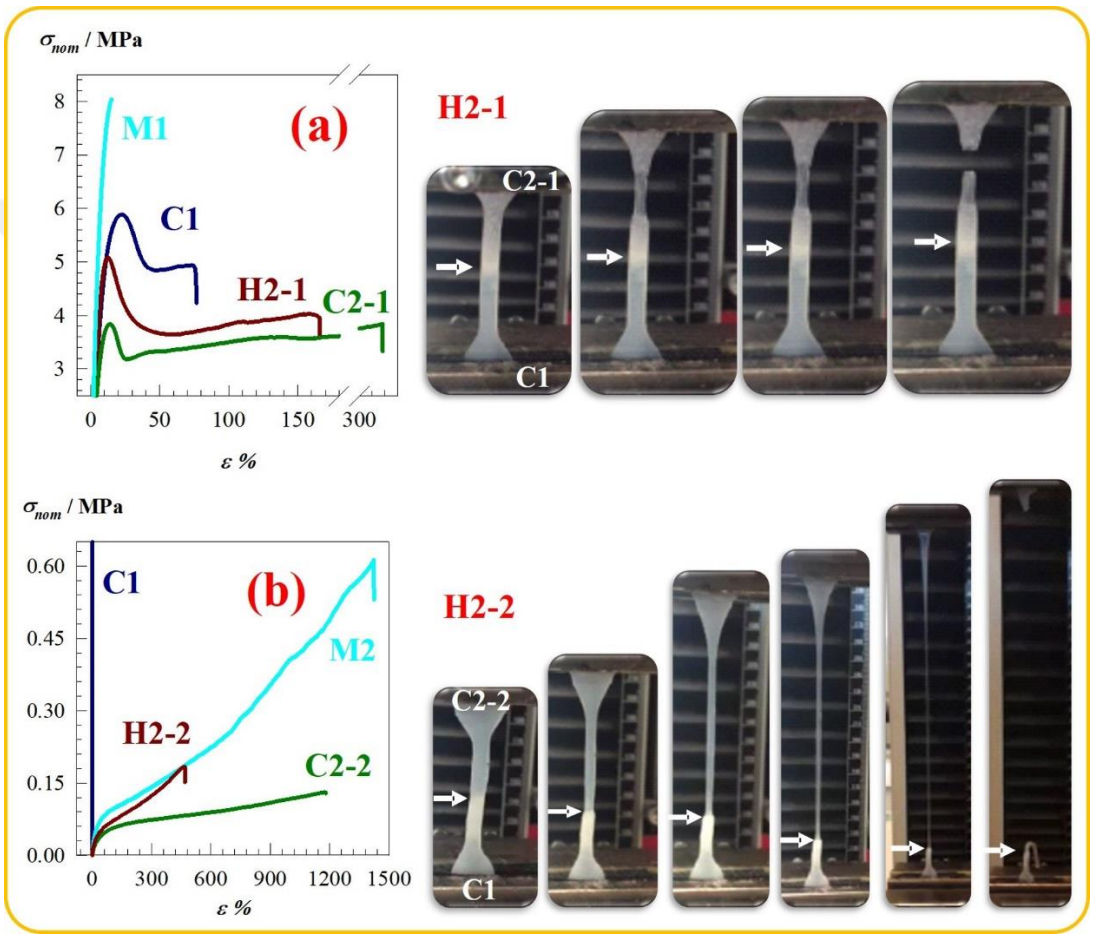

Figure 4.14 : Uniaxal test results and optical images of H2-1 and H2-2 at room temperature. White arrows on optical images indicate the interface region. (a) Stress (σ_{nom})-strain (ε %) curves of H2-1, C1, C2-1 and M1 (b) Stress (σ_{nom})-strain (ε %) curves of H2-2, C1, C2-2 and M2.

All tests shown in Figure 4.14 were conducted at room temperature. Besides the hybrid specimens (H2-1 and H2-2), their individual segments C1, C2-1 and C2-2 were also tested separately. Mixtures of reaction solutions belonging to the segments of hybrids, which mimic the interface regions, were separately synthesized (M1 of H2-1 and M2 of H2-2) and subjected to elongation tests to compare the results.

Measurements repeated for many times revealed that, H2-1 and H2-2 gel never break at the interface region and the tensile mechanical properties of hybrids represent the average of those of their components (Figure 4.14, a, b). H2-1 hybrid has a Young's modulus of 79 ± 9 MPa and tensile strength of 3.9 ± 0.2 MPa while H2-2 hybrid exhibits a lower modulus and tensile strength (Table 4.4) but a higher stretch at break (457% vs 113%) due to the contribution of its highly stretchable C2-2 component.

As seen on the optical images in Figure 4.14, the interface regions indicated by white arrows remain intact under stress for both of the hybrid samples. The intactness of the interface region of hybrids at their fracture reveals higher mechanical strength of the interface as compared to one or both of their individual segments. The Young's modulus and tensile strength of M1 are 92 ± 2 and 8.2 ± 0.9 MPa, respectively, which are much higher than those of the gel components. This is due to the higher degree of crystallinity of the mixture gel as compared to the gel components (16% vs 12%, Table 4.3) as well as due to the formation of more ordered crystalline domains in the presence of mixed hydrophobes leading to increased strength of hydrogels [197]. This explains why the interface of H2-1 is stronger than both of its C1 and C2-1 segments.

Several tests showed that H2-1 always breaks at the necking zone of C2-1 region, as illustrated in the optical images on Figure 4.14 (a), likely because C2-1 segment yields and weakens before yielding of the C1 segment due to the relatively small Young's Modulus (E) value.

Figure 4.14, (b) show tensile stress−strain curves and mechanical parameters of the interface of H2-2 together with its C1 and C2-2 components. Both the modulus and strength of the interface are higher than the C2-2, suggesting that C2-2 segment of the hybrid would rupture under stress while the interface remains robust.

The optical images shown in Figure 4.14, (b) indeed demonstrate that the rupture of the hybrid occurs at its C2-2 segment. Young's modulus (E) (Figure 4.15, a, b), nominal stress (σ_{nom}) (Figure 4.15, c, d) and strain % (ε %) (Figure 4.15, e, f) results of hybrids, H2-1 and H2-2, and their components, C1, C2-1 and C2-2, are shown in the graphs.

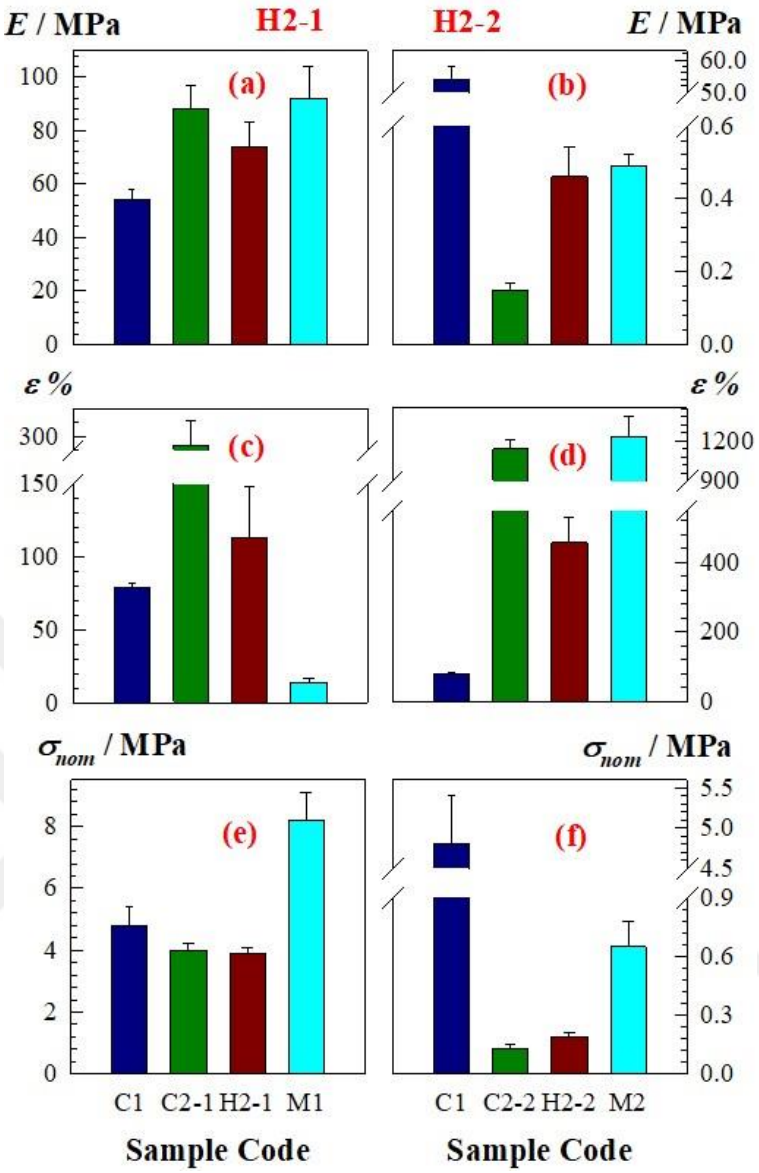

Figure 4.15 : Tensile mechanical properties of hybrids, H2-1 and H2-2, and their components, C1, C2-1 and C2-2, mixtures mimicking the interface regions, M1 and M2 are given. Graphs on left side demonstrates the results of H2-1 and related gels' results, while the graps on right side show H2-2 and related results. (a, b) Young's modulus (E), (c, d) strain % (ε %) (e, f) nominal stress (σ_{nom}).

- *Uniaxial compression tests*

Interbedded shaped hybrid hydrogels were subjected to compression tests. Tests were conducted at room and body temperature. Besides the hybrid specimens (H2-1 and H2-2), their individual segments C1, C2-1 and C2-2 were also tested separately.

For the mentioned hybrid gels, gel specimen can sustain its structural integrity even after the complete compression. Thus, an actual fracture deformation ratio (λ) and nominal stress (σ_{nom}) values require further evaluation by using the true stress (σ_{true})-

deformation ratio (λ) curves of raw data. (ε=1–λ and σ_{true} = λ x σ_{nom}) Results demonstrated in this part will be given as corrected by using this method. An example of this correction is exhibited in Figure 4.16, (a). Figure 4.16, (b) shows the compression test results of H2-2.

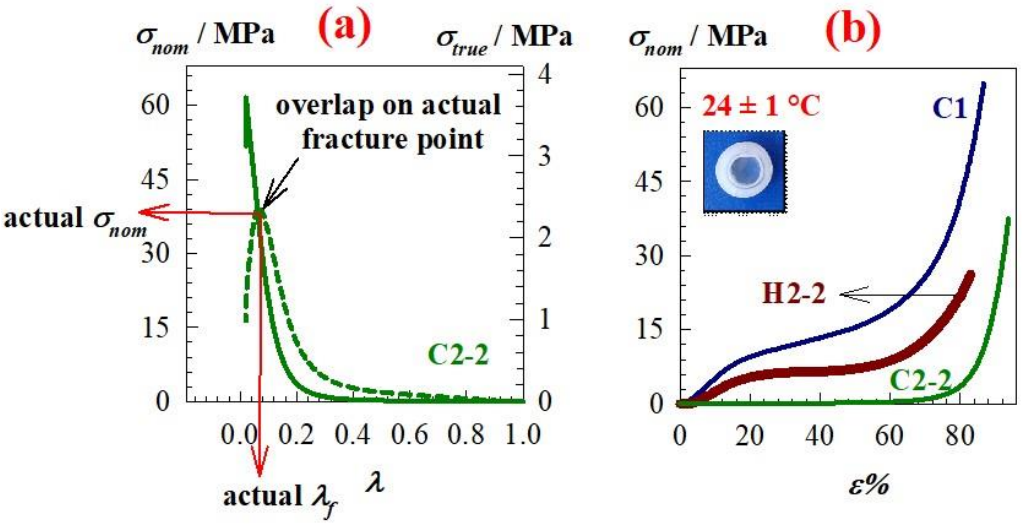

Figure 4.16 : (a) An example of compressive correction method applied on C2-2 sample. Dashed line shows the true stress (σ_{true})-deformation ratio (λ) curve. λ_f denotes deformation ratio at break and ε = 1- λ. σ_{true} can be read on right axis, while the σ_{nom} is on the left side. (b) Compressive σ_{nom} − strain % (ε %) curves of H2-2 and its components (C1 and C2-2) at 24 ± 1 °C.

H2-2 has two segments as C1 and C2-2. In contrast with C1 segment, having highly semicrystalline structure, but, as evidenced by DSC results, C2-2 with C12 hydrophobic monomer has no crystalline domain which results in C2-2 a soft texture both at room and body temperature. Therefore, H2-2 and its components C1 and C2-2 were tested only at room temperature (Figure 4.16, (b)).

On the other hand, segments belonging to H2-1 gel, C1 and C2-1, have crystalline domains which affect the texture difference at room and body temperature. Since the T_m of C2-1 segment is around the body temperature, compression tests performed at both room and body temperature. Besides the texture, opacity difference was observed in C2-1 segment. Figure 4.17 demonstrates compressive stress−strain curves of H2-1 and their gel components at room and body temperature. Additionally, optical images of H2-1 samples at room and body temperature were also given in the graphs.

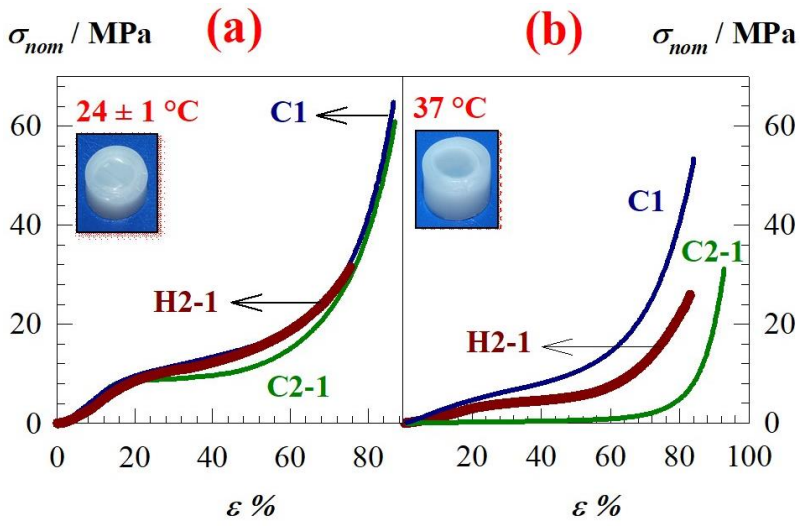

Figure 4.17 : Compressive σ_{nom} (MPa) − strain % (ε %) curves of H2-1 and its components (C1 and C2-1) at (a) room temperature (24 ± 1 °C) and (b) body temperature (37 ± 1 °C).

The general trend is that the hybrids (H2-1 and H2-2) exhibit lower compressive strength as compared to their gel components (Table 4.4). This is attributed to the easier appearance of microcracks in the hybrid due to the pressure of the hard shell on the soft core. The Young's modulus and compressive strength of H2-1 gels are 47 ± 6 and 30 ± 4 MPa while those of H2-2 samples are 32 ± 5 and 24 ± 3 MPa, respectively. Figure 4.17, (a) also shows that the initial mechanical properties of H2-1 gel and its components are similar; i.e., their moduli are between 47 and 62 MPa. The inset to Figure 4.17, (b) presents stress−strain curves of C1, C2-1, and H2-1 gels measured at 37 °C which is between the melting temperatures of the C1 and C2-1 zones. Because the crystalline domains in C2-1 zone melts at 37 °C, as also seen from opaque-to-transparent transition in C2-1 segment (see optical images of interbedded hybrid gels niched in graphs), the modulus of this zone decreases from 62 ± 7 to 0.34 ± 0.04 MPa, thus producing at the body temperature a hybrid hydrogel consisting of a soft core surrounded by a hard tire-like shell.

4.2.1.5 Self healing

Self-healing behavior in flat shaped hybrids was investigated by cutting them at both gel zones locating 6 mm away from the interface region. For interbedded gel specimens, they were cut in the middle into two equally sized pieces. The damaged gel samples were then self-healed by keeping the cut surfaces in contact for 1 h at 80 °C in a water vapor-saturated glass chamber. Thereafter, uniaxial compression and

elongation tests were conducted. The results were compared with the virgin gel samples. Figure 4.18 shows the tensile test results of healed hybrid samples.

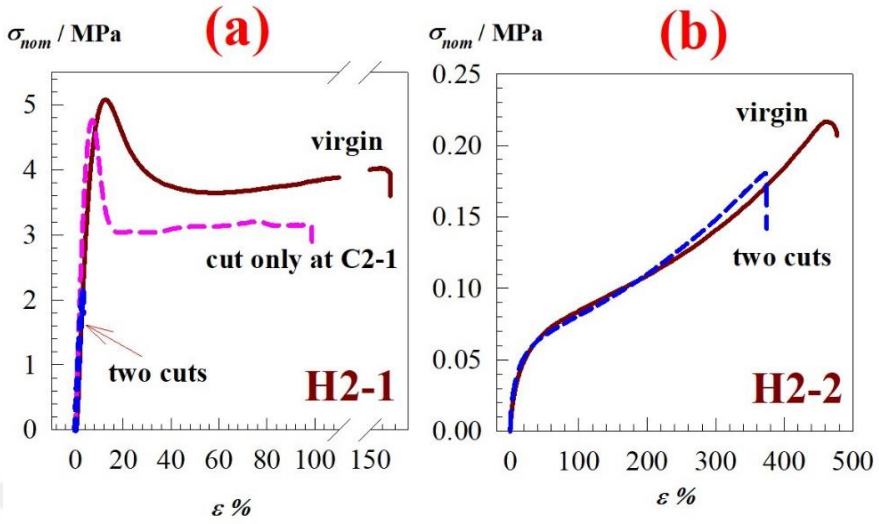

Figure 4.18 : Stress (MPa)−strain (%) curves of virgin (solid curves) and healed (a) H2-1 and (b) H2-2 gel samples (dashed curves) obtained from tensile tests.

Self healing behavior of hybrid samples (H2-1 and H2-2) were examined by elongation test. Optical images of healing examination for H2-1 and H2-2 gels are given in Figure 4.19.

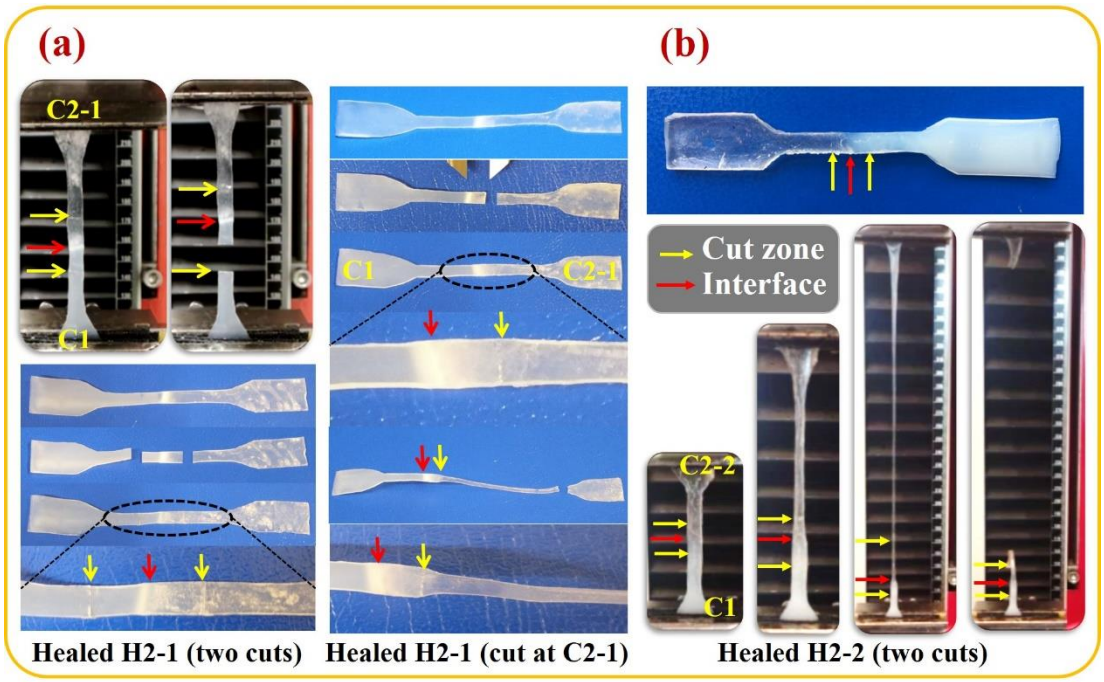

Figure 4.19 : (a) Images of a H2-1 gel specimen before and after cutting and after repairing. (b) Images of a H2-2 gel specimen after repairing. Yellow arrows indicate the cut regions while red arrow is the interface region.

Healing ability of both hybrids were tested by two cuts. Cutting at both gel zones of H2-1 gel specimen followed by healing at 80 °C significantly reduces the ultimate mechanical properties, and the sample broke at the cut region before the yield point. However, when cut is created only at C2-1 zone, the healed sample again shows yielding behavior, and the healing efficiency with respect to fracture stress and strain becomes 73 ± 7 and 62 ± 5%, respectively.

Moreover, the fracture always occurred at C2-1 segment of the hybrid but at a different location than the cut region (Figure 4.19, a). The H2-2 gel exhibited above 80% healing efficiencies independent of the location of the cuts, and the fracture always occurred at the C2-2 segment but at a different location (Figure 4.19, b).

Compression tests were also conducted by cutting interbedded hybrid gel specimens in the middle into two equally sized pieces and then bringing the cut surfaces together, as described above. Figure 4.20 shows the stress-strain curves for comparing the compression results of virgin H2-1 and H2-2 gels with their healed states.

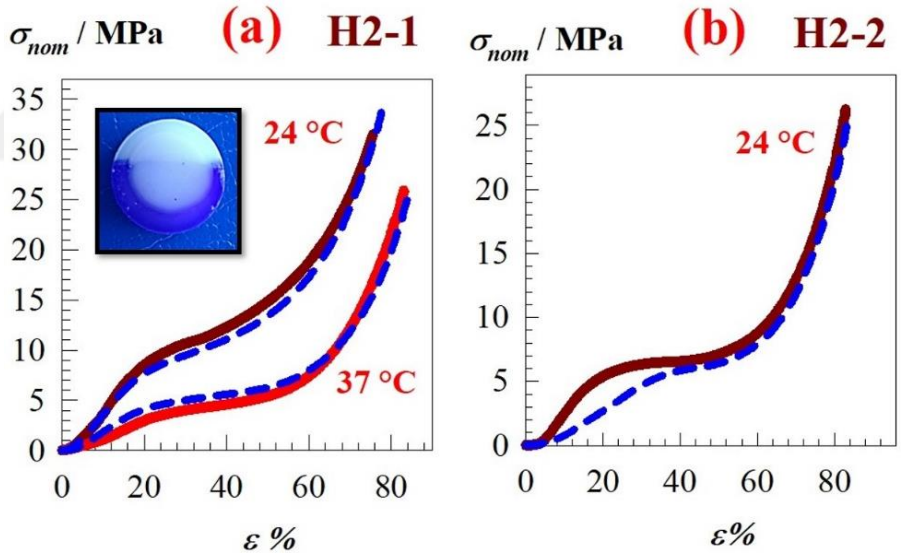

Figure 4.20 : Stress (MPa) –strain (%) curves of virgin (solid curves) and healed (a) H2-1 gel samples (at room and body temprerature) and (b) H2-2 gel sample (at room tempretature) (dashed curves) obtained from compression tests.

As seen in Figure 4.20, complete healing could be obtained on both H2-1 and H2-2 hydrogels. All results of compression and elongation tests were collected in Table 4.4. Standard deviations are given in brackets.

Table 4.4 : Tensile and compressive mechanical properties of gels.

Elongation Results									
Code	**DMA**	**C18A**	**C17.3M**	***E* (MPa)**	**ε %**	**λ_f**	**σ_f (MPa)**	**λ_y**	**σ_y (MPa)**
H2-1	(C1/C2-1) virgin			74 (9)	113 (35)	2.1 (0.2)	3.9 (0.2)	1.12 (0.03)	4.7 (0.7)
H2-1	healing-one cut at C2-1			78 (7)	3 (0.5)	2 (0.2)	2 (0.3)	-	-
H2-1	healing- two cuts			79 (6)	102 (22)	1 (0.01)	3.2 (0.1)	1.1 (0.01)	4.7 (0.1)
C1	70	30	-	54 (4)	79 (3)	1.8 (0.03)	4.8 (0.6)	1.23 (0.04)	5.8 (0.1)
C2-1	50	-	50	88 (9)	287 (35)	3.9 (0.3)	4 (0.2)	1.13 (0.03)	4.4 (0.6)
M1	60	15	25	92 (12)	14 (3.1)	1.14 (0.03)	8.2 (1)	-	-
M1	(C1+C2-1) healing			85 (5)	8 (0.9)	1.1 (0.01)	6.2 (0.4)	-	-
Code	**DMA**	**C18A**	**C12M**	***E* (MPa)**	**ε %**	**λ_f**	**σ_f (MPa)**	**λ_y**	**σ_y (MPa)**
H2-2	(C1/C2-2) virgin			0.46 (0.03)	457 (73)	5.6 (0.7)	0.19 (0.02)	-	-
H2-2	(C1/C2-2) two cuts			0.43 (0.03)	431 (60)	5.3 (.6)	0.17 (0.03)	-	-
C1	70	30	-	54 (4)	79 (3)	1.8 (0.03)	4.8 (0.6)	1.23 (0.04)	5.8 (0.1)
C2-2	50	-	50	0.15 (0.02)	1137 (67)	12.4 (0.7)	0.13 (0.02)	-	-
M2	60	15	25	0.49 (0.03)	1227 (160)	13.3 (16)	0.65 (0.13)	-	-
M2	(C1+C2-2) healing			0.44 (0.07)	893 (122)	10 (1.2)	.53 (0.1)	-	-
(*) Healing Results				**Compression Results**					
	24±1 °C					**37 °C**			
Code	***E* (MPa)**		**ε %**	**λ_f**	**σ_f (MPa)**	***E* (MPa)**	**ε %**	**λ_f**	**σ_f (MPa)**
H2-1	47 (6)		76 (6)	0.24 (0.6)	30 (4)	15 (0.5)	84 (2)	0.16 (0.02)	27 (4)
H2-1	*50 (2)		*79 (1)	*0.21(0.01)	*31 (5)	*19 (4.5)	*85 (1)	*0.15(0.01)	*26 (1)
C1	54 (7)		80 (5)	0.2 (0.05)	59 (15)	27 (4)	84 (2)	0.16 (0.02)	50 (11)
C2-1	62 (7)		85 (1)	0.15 (0.01)	56 (8)	0.34 (0.04)	93 (0.4)	0.07(0.004)	30 (3)
M1	102 (3)		82 (0.4)	0.18(0.004)	71 (11)	61 (6)	85 (2)	0.15 (0.02)	60 (10)
24±1 °C									
Code	***E* (MPa)**		**ε %**		**λ_f**		**σ_f (MPa)**		
H2-1	32 (5)		80 (5)		0.2 (0.05)		59 (15)		
H2-1	*19 (1.5)		*84 (1)		*0.16 (0.01)		*24 (1)		
C1	54 (7)		80 (5)		0.2 (0.05)		59 (15)		
C2-1	0.27 (0.03)		93 (1)		0.07 (0.01)		24 (3)		

4.2.1.6 Rheology

Presence of crystalline domains in both C1 and C2-1 segments of H2-1 hydrogels resulted in drastic changes in their mechanical properties depending on the temperature. This feature is presented in Figure 4.21, a where the storage (*G'*) and loss moduli (*G''*) data are plotted against temperature.

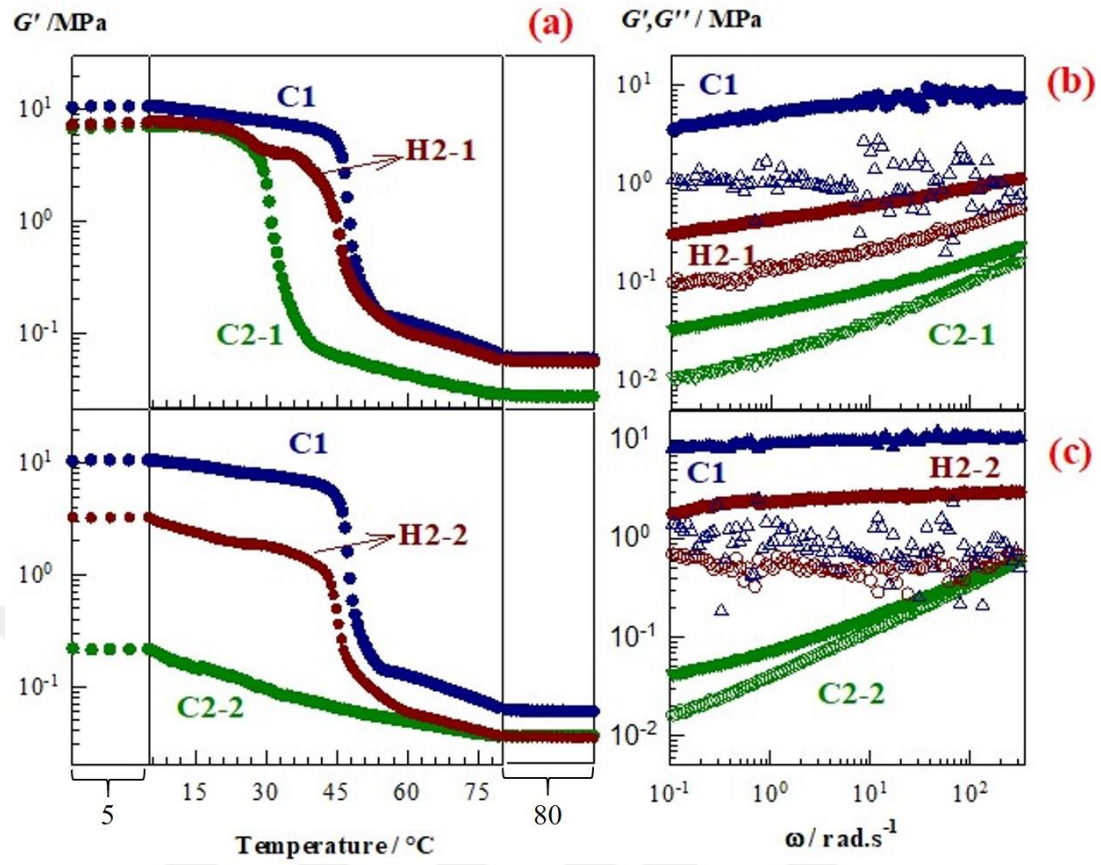

Figure 4.21 : (a) Storage modulus G' (MPa) of H2-1 (upper panel) and H2-2 (bottom panel) and their gel components during heating from 5 to 80 °C at a rate of 5 °C min^{-1}. ω = 6.3 rad s^{-1} and γ_0 = 0.1%. (b, c) Frequency dependences of G' (filled symbols) and the loss modulus G''(MPa) (open symbols) of H2-1 (b) and H2-2 hybrids (c) and their components. Temperature = 37 °C (b) and 25 °C (c). γ_0 = 0.1%.

The storage moduli G' of hybrids, H2-1 and H2-2, during heating from 5 to 80 °C at a heating rate of 5 °C min^{-1} are shown in Figure 4.21, a. G' of the C1 component is 10 MPa at 5 °C, while it rapidly decreases at around its T_m, 48 °C, and finally becomes 0.06 MPa at 80 °C. More than 2 orders of magnitude decrease in the modulus of the C1 upon heating is totally reversible with a thermal hysteresis due to the lower recrystallization temperature, as also reported before for semicrystalline hydrogels [198,199]. A similar change in G' is observable for the C2-1 component except that the drastic decrease in G' occurs at its T_m of 35 °C. In contrast, G' of the C2-2 component only slightly decreases with temperature due to the absence of crystalline domains. The results also show that the modulus−temperature curves of hybrid hydrogels locate between those of their components, indicating that they both contribute to their overall viscoelastic response. Frequency sweep tests conducted on

C1, C2-1, and H2-1 gels at 25 °C (Figure 4.22, a), i.e., below their T_m's, show similar viscoelastic spectra with the spectra at 37 °C (Figure 4.22, b).

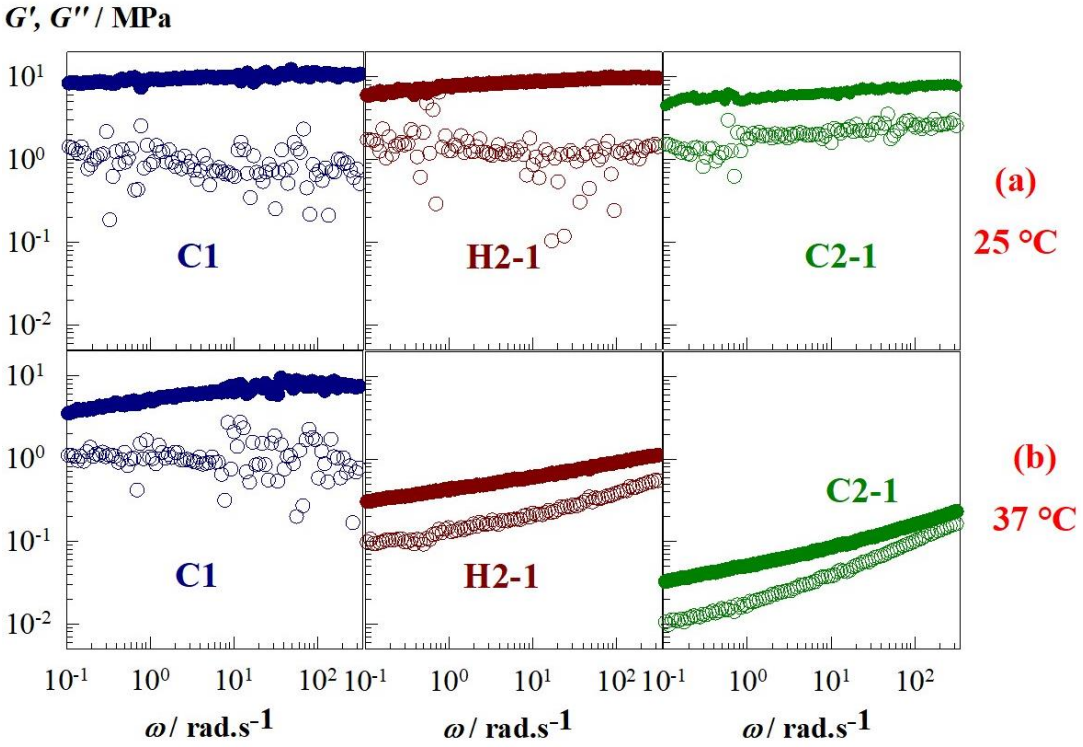

Figure 4.22 : Frequency dependences of *G'* (MPa) (filled symbols) and *G''* (MPa) (open symbols) of C1, C2-1, and H2-1 hydrogels at (a) 25 °C and (b) 37 °C. γ_0 = 0.1%.

G′ is independent of frequency, and it is much larger than the loss modulus *G″* at 25 °C (Figure 4.22, a), as typical for strong gels. However, at 37 °C, i.e., between the T_m's of C1 and C2-1 gels, C1 gel is still a strong gel with a weak frequency dependence while C2-1 becomes a weak gel with a *G″* approaching to *G′* at high frequencies (Figure 4.22, b). Similar viscoelastic spectra but at 25 °C were obtained on H2-2 hybrids composed of semicrystalline C1 and amorphous C2-2 segments (Figure 4.21, c).

As a preliminary experiment, another rheological measurement was performed to understand the synthesis stage of a proper hybrid gel. Polymerization times of individual segments belonging to hybrids were investigated. Viscosity (η) changes, during the polymerization, against the reaction time were plotted in Figure 4.23.

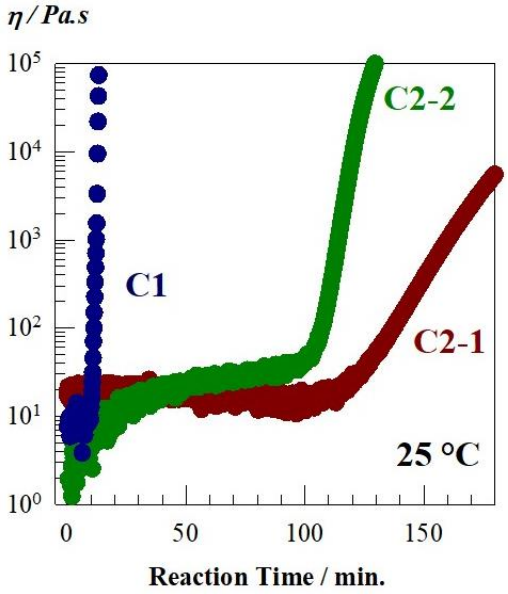

Figure 4.23 : Viscosity (η/Pa.s) changes of C1, C2-1, C2-2 segments of H2-1 and H2-2 during the course of polymerization s plotte againt reaction time. Results were collected at 25 °C.

Synthesis method of this hybrid gels were UV-initiated bulk polymerization. To follow the polymerization depending on time, rheometer was externally equiped with two UV lamp which were also used for the UV reactor and the temperature of plate was fixed at 25 °C. As seen on Figure 4.23, during the polymerization, viscosity of reaction solution belonging to C1 was increased much more rapidly as compared to that of the other solutions, and reaction solution of C1 turned to a gel after 10 min, while both of the reaction solutions belonging to C2-1 and C2-2 formed gels after more than 1 h. This difference in the gelation times between the layered solutions also prevented their mixing during the course of polymerization.

4.2.1.7 Cyclic elongation

Because of the supramolecular nature, hybrid hydrogels have the ability to self-heal on both of their gel zones. Cyclic mechanical tests are a mean to detect the self-healing ability of cross-linked materials via monitoring the reversible nature of their cross-links. The cyclic tests were carried out by stretching H2-1 gel specimens at a strain rate of 3.8×10^{-2} s^{-1} up to a maximum strain ε_{max} and then unloading at the same rate up to zero strain, followed by repeating these loading and unloading steps at the same strain rate. Figure 4.24 shows the cyclic elongation test resuls of H2-1.

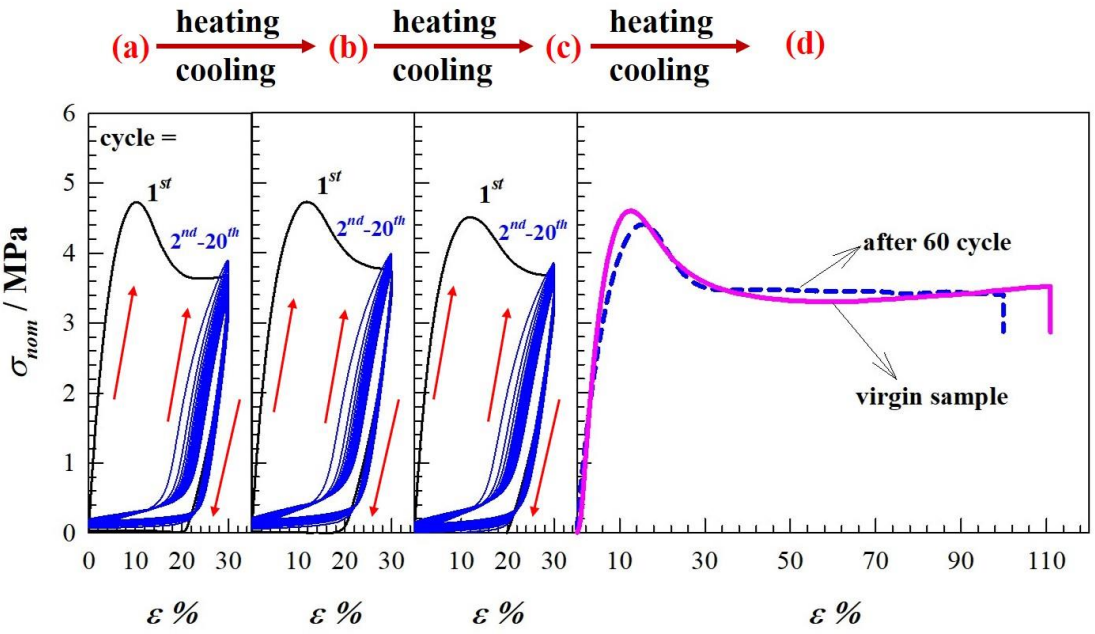

Figure 4.24 : Stress (MPa)−strain (%) (a−c) 3 sets of successive 20 tensile cycles separated by the thermal treatment for a H2-1 gel specimen. ε_{max} = 30%. (d) Stress−strain curve of H2-1 after subjecting 60 tensile cycles is shown by dashed line. For comparison, stress−strain curve of a H2-1 gel sample is also shown by the solid curve.

Figure 4.24, a shows 20 successive tensile cycles composed of loading (upward curves) and unloading steps (downward curves) up to ε_{max} of 30%. It is seen that the neck region shown during the first loading step disappears in the following loadings, indicating a significant damage in the gel. Indeed, the hysteresis energy U_{hys} which is proportional to the number of bonds broken during a mechanical cycle is 0.92 MJ m^{-3} for the first cycle while it reduces to 0.45 MJ m^{-3} in the second cycle. U_{hys} further gradually decreases with increasing cycle number and becomes 0.24 MJ m^{-3} after 20^{th} cycle, revealing that around 70% of intermolecular bonds in the gel specimen are broken. The damaged gel specimen was then taken out of the tensile tester and immersed in a water bath at 50 °C for 1 min followed by bringing to the test temperature of 24 °C. The sample was again subjected to 20 successive tensile cycles. This procedure was repeated twice, and the results are shown in Figures 4.24 b, c. It is seen that heating the gel above T_m of the gel components and subsequent cooling to 24 °C recover the neck region so that similar hysteresis energies could be obtained. For instance, U_{hys} energies for the first cycles in Figures 4.24, b and c are 0.86 and 0.90 MJ m^{-3}, respectively, revealing that 93−98% bonds broken could be recovered by heating at 50 °C for 1 min. The damaged gel sample after subjecting to 60 tensile

cycles was again repaired by the thermal treatment as described above and then stretched up to the fracture point. The solid and dashed curves in Figure 4.24, d present stress−strain curves of the repaired sample and the virgin one, respectively. The repaired sample fractures at a stretch ratio of 97% under around 3.4 MPa stress, which are close to that of the virgin sample (113 ± 35% at 3.9 ± 0.2 MPa), revealing thermally induced self-healing ability of H2-1 hybrid hydrogels.

Besides the H2-1 ydrogel, H2-2 hydrogel was also subjected to cyclic elongation test. Figure 4.25 demonstrates the results of cylic elongation test of H2-2 hydrogel.

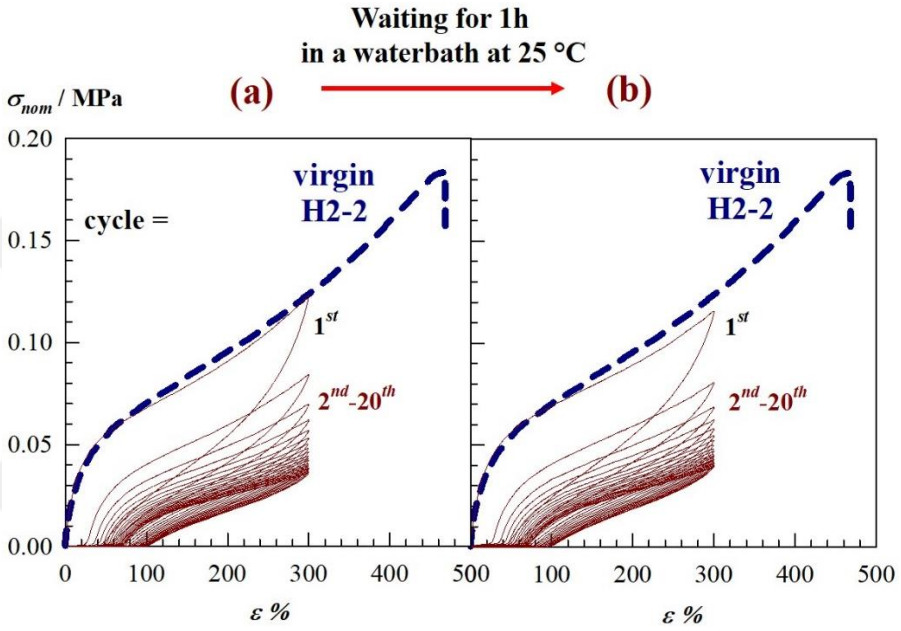

Figure 4.25 : Uniaxial cyclic elongation test of H2-2 gel at room temperature. (a) 20 successive cycles at strain ratio of 300%, (b) 20 more successive cycles in same strain ratio, after a waiting time of 1h in a water bath at 25 °C.

Elongation test results of H2-2 and its segments C1 and C2-2 hydrogels demonstrated that C2-2 segment has a lower Young's modulus and fracture strength than that of C1 segment (Figure 4.25, Table 4.4). Additionally, drastically higher Young's modulus and fracture stress of C1 was attributed to its semicrytalline structure at room temperature and evidenced by DSC measurements. Since there is a distict texture difference between the segments of H2-2, H2-1 hydrogel, subjected to first set of 20 successive elongation cyles, was waited in a water bath for 1h to recover itself. In other words, no further heating-cooling was required for the reason that there was no change in C1 segment. It was in Figure 4.25 that, after the first of 20 cycles (Figure 4.25, a) and following recovery time, there was already no residual deformation left behind (Figure 4.25, b).

4.2.2 Three-segmented hybrid hydrogels

It was introduced in the two-segmented hybrid hydrohel study that there were three requirements for preparing mechanical strong hybrid hydrogels with smooth and robust interfaces:

i) Since the preperation of hybrid gels in this study based on the simultaneous synthesis of two individual components in a fused body, reaction solutions of hybrid hydrogel components have to be suitable for stratification.

ii) Swelling ratios of the gel components of hybrids should not differ significantly from each other. Otherwise, the mismatch in the swelling ratios resulted in their rupture in aqueous environment.

iii) In order to obtain hybrids with reproducible mechanical properties, the interface region in hybrids should exhibit a smooth transition from one to another gel zone.

Here, in this study, preliminary experiments of three segmented hybrids reveal one more additional requirement that

iv) The monomer mixture with the higher density should be the solution with the shorter or the similar reaction time than that of the monomer solution of lower density's reaction time. Otherwise, the monomer mixture with lower density reacts to form polymer and begin to immerse in the monomer mixture of higher density, thus result in the formation of non-smooth transition in the interface region.

For the first Three Segmented Hybrid (H3-1), components are: component 1 (C1) component 2 (C2-1) and component 3 (C3-1). For the second Three Segmented Hybrid (H3-2), components are: component 1 (C1) component 2 (C2-2) and component 3 (C3-2). Molar ratios of segments belonging to H3-1 and H3-2 are given in Table 4.5 .

4.2.2.1 Stratification Study

Preparation of hybrid hydrogels in a flat shape with three-distinct gel zones based on the density difference of the monomer mixtures, were achieved in terms of stratification of reaction solutions (RS) as also acquired in two-segmented hybrid hydrogel study. Stratification is performed by taking the advantage of densitiy difference. Densities of RS were measured by using a calibrated glass pycnometer at

25 °C. By stratification method, the RS with a low density floats on top of another RS of higher density whereas the interface between layers (transition area) acts as a barrier to prevent monomers from diffusion between layers.

Within this three-segmented hybrid hydrogel study, through deriving the benefit of two segmented hybrid hydrogel experience, it was aimed to improve a concept of multi-segmented hybrid hydrogel with multiple-shape memory effect. Different from two segmented hybrid hydrogel, the use of hydrophilic monomer was varied in the compositons of segments. Compositions of reaction solutions and their densities were given in Table 4.5 with the T_m values of the three-segmented hybrid hydrogel's segments.

Table 4.5 : Compositions (mol %) and densities (g/mL) of reaction solutions with T_m (°C) values of their gel states.

Code	Composition (mol %)				Density (g/mL) (at 25 °C)	T_m (°C)
	DMA	AAc	C18A	C17.3M		
H3-1						
C1	70	-	-	30	0.895	37
C2-1	60	-	40	-	0.888	51
C3-1	50	-	-	50	0.881	35
H3-2						
C1	70	-	-	30	0.895	37
C2-2	60	-	15	25	0.887	46
C3-2	-	60	40	-	0.880	56

Here, beside the DMA, AAc was used to obtain new combinations for new segments. Since the molecular weight (MW) of AAc (72.06 /mol) is lower than the DMA's MW (99.13 g/mol), in the same hydrophobic monomer content, it was achieved to obtain a segment with lower density and significantly higher T_m which is directly related to the shape memory characteristics of gel sample. For instance, C2-1 segment coprised of DMA and C18A was used in the synthesis of H3-1 which of this segment was in the same molar ratio with the C3-2 segment of H3-2 with an only difference in hydrophilic monomer as AAc. By just switching the hydrophilic monomer in the rection solution from DMA into AAc, the density is apperantly decreased from 0.888 to 0.880 which is a significant difference for this stratification method. Moreover, the T_m value was 51 °C for DMA/C18A combination while this value incrased in 56 °C for AAc/C18A combination in the same molar ratio (Table 4.5). Therefore, through the method improved in this study, it is possible to decide the place of stretchable and rigid parts with different T_m values in a multi component hybrid structure, according to the

requisite, by using the monomers in different densities and chemical properties. By means of the concept studied here as multi-segmented hybrid hydrogels with nultiple-shape memory effect, it is possible to obtain multi-segmented hybrid hydrogels for spesific requisites with segments of accuretly determined places like a puzzle which of these segments would have exact T_m values, stretchabiliy, toughness, healing ability, etc. in a wide range of monomer scale.

4.2.2.2 Differential scanning calorimetry (DSC)

Thermal properties of these hybrids were also investigated. It was known from the several studies made by our research group, that semi-crystalline hydrogels acquired by use of hydrophobic monomers with long *n*-alkyl chains have a great potential to exhibit self-healing and thermally induced shape-memory behaviors [3,198]. For the investigation of shape-memory behavior, hybrids were subjected to differential scanning calorimetry (DSC) measurements. Sampling was made from the segments of H3-1 and H3-2 hydrogels. Figure 4.26 shows the DSC results of individual gel components belonging to H3-1 and H3-2 hybrid gels.

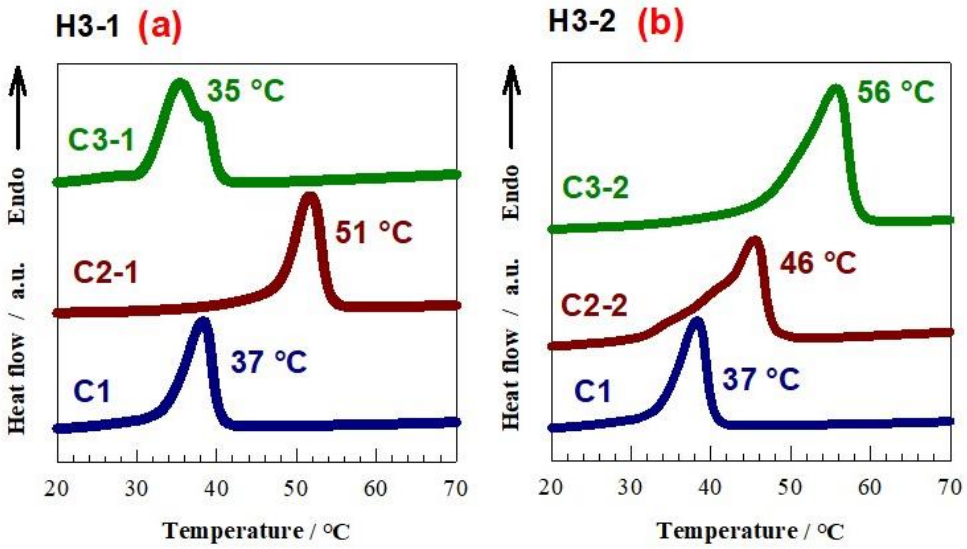

Figure 4.26 : DSC scans conducted on the individual components of (a) H3-1 and (b) H3-2 hybrids.

DSC results of H3-1 segments are presented in Figure 4.26, (a). Tm values were obtained as 37, 51 and 35 °C for individual C1, C2-1 and C3-1 segments of the H3-1, respectively. Similar measurements were also conducted on individual segments of H3-2 hybrid gel specimen. Figure 4.26, (b) shows that the melting peak appearing at 37 °C in C1 zone and increases to 46 and 56 °C for the C2-2 and C3-2, respectively.

From the DSC curves, enthalpy changes during melting, ΔH_m, were calculated from the peak areas. The degree of crystallinity, f_{cry}, that is, the fraction of polymer units in crystalline domains, was estimated by $f_{cry} = x_{HM}\Delta H_m/\Delta H_m°$, where x_{HM} is the mole fraction of the hydrophobic monomer in the comonomer feed and $\Delta H_m°$ is the melting enthalpy of crystalline C17.3M or C18A units. $\Delta H_m°$ was taken as 71.2 kJ mol^{-1} from previous works on the melting behavior of long n-alkyl chains exhibiting a hexagonal crystal structure [200, 203]. Thermal properties belonging to H3-1 and H3-2 are collected in Table 4.6.

Table 4.6 : Composition, water content and thermal properties of gels.

Code	Composition (mol %)				H_2O (%)	T_m (°C)	T_{cry} (°C)	f_{cry} (%)
	DMA	AAc	C18A	C17.3M				
H3-1								
C1	70	-	-	30	36	37	26	8
C2-1	60	-	40	-	21	51	42	19
C3-1	50	-	-	50	10	35	23	12
H3-2								
C1	70	-	-	30	36	37	26	8
C2-2	60	-	15	25	18	46	36	16
C3-2	-	60	40	-	5	56	43	29

DSC measurements reveal that the C2-1 and C3-2 gel components consisting of same mol % of DMA and AAc, respectively, and C18A at same mol % are semicrystalline hydrogel with a melting temperature of 51 °C for C2-1 of H3-1 and 56 °C for C3-2 of H3-2 (Table 4.6). Even though the hydrophobic monomer mol % ratios are the same for both of these different segments, a marked difference in between the T_m values as 5 °C was observed. This is because the poly-acrylamide (PAAc) backbone produces a higher transition temperature and degree of crystallinity as compared to poly-dimethylacrylamide (PDMA) backbone. It was attributed to the cooperative hydrogen bonding between the carboxyl groups of AAc units stabilizing the alkyl crystals in the former research of our research group [3]. The results reveal that the stability of crystalline domains in the hydrogels increases in the following order: DMA/C17.3M < DMA/C18A < AAc/C18A.

The C1 and C3-1 components composed of DMA and C17.3M has lower melting temperature values than that of the components with C18A, 37 and 35 °C, due to the methyl group on the backbone of C17.3M units limiting the alignment of side alkyl chains [132].

C2-2 segment of H2-2 hydrogel is differ from other segments with its hydrophobic monomer mixture content. This segment comprises of two hydrophobic monomers of C17.3M and C18A. C17.3M/C18A ratio of this segment is 25/15 (mol %). Even if the C17.3M content is higher than that of the C18A content, higher Tm value of 46 °C was observed. It means that, the T_m value of this mixture component is dominated by crystalline domains of C18A. It was attributed to the higher stability of C18A crystalline domains than that of the C17.3M's.

4.2.2.3 Uniaxial elongation

For the first three-segmented hybrid (H3-1), components are: component 1 (C1) component 2 (C2-1) and component 3 (C3-1). For the second Three Segmented Hybrid (H3-2), components are: component 1 (C1) component 2 (C2-2) and component 3 (C3-2). Molar ratios of segments belonging to H3-1 and H3-2 are given in Table 4.7. C1 is the same for both of three segmented hybrids. Figure 4.27 shows the elongation results of H3-1 (a) and H3-2 (b) hybrid gels and their individual segments C1, C2 and C3.

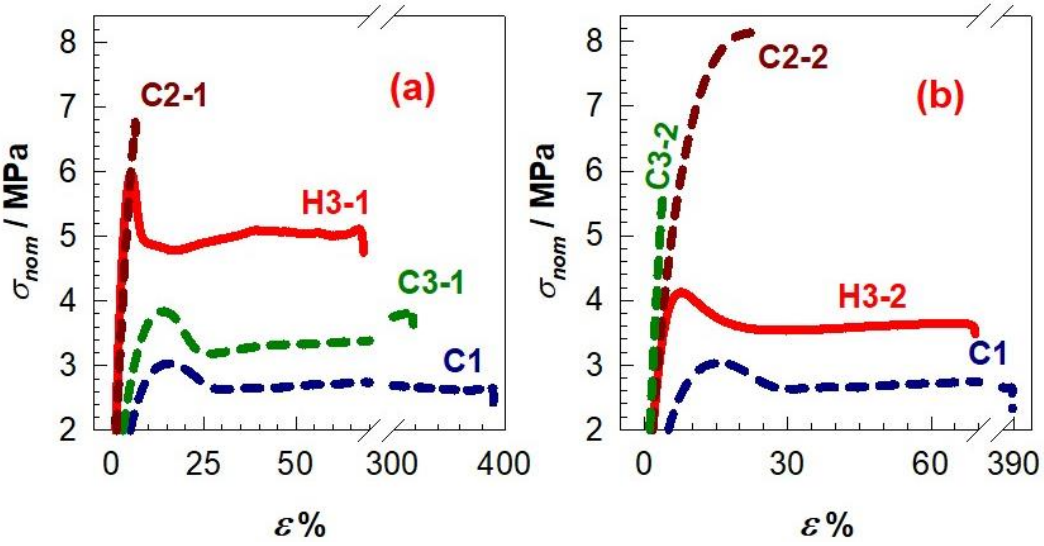

Figure 4.27 : Tensile stress (σ_{nom})(MPa) -strain (%) (ε %) curves of three segmented hybrids (H3-1 and H3-2, solid lines). To compare the three segmented hybrid samples, their own individual components' (dashed lines) elongation results were also added to the graphs. (a) H3-1 and its components C1, C2-1 and C2-1 (b) H3-2 and its components C1, C2-2 and C3-2.

The solid curves in Figures 3 a, b show tensile stress−strain % curves of H3-1 and H3-2 hybrids, respectively, where the nominal stress σ_{nom} is plotted against the strain %, ε %. The dashed curves in the figures are stress− strain curves of hybrids' individual gel components. Here there is two kinds of three segmented hybrids which of both have

the same segment as the weakest and softest component (C1). The difference between these two hybrids is that, one of them has two stretchable and one rigid segment (H3-1, Figure 4.27, (a)) and the other has two rigid and one stretchable segment (H3-2, Figure 4.27, (b)). Hybrid of two rigid parts with a stretchable, low Young's modulus part (H3-2) exhibits a mechanical behavior closer to the stretchable, low Young's modulus segment (C1). However, hybrid of two stretchable, low modulus part with one rigid, high modulus part (H3-1) represents higher modulus and tensile strength but lower stretchability. Since the stress applied on materials to elongate them always concentrate on the weakest part, both of the hybrids deform in the C1 part for the first place. Thus, although hybrid has rigid segments, it represents stretchability; higher tensile strength than that of the weakest part is seen due to the combined mechanical durability effect of all parts up to the total fracture of material. As for the Young's modulus, hence the applied stress concentrates in the weakest part, result is obtained as lower than that of the most rigid segment. In accordance with the case mentioned above about the concentration of applied stress in the weakest part, results revealed that the tensile mechanical properties of hybrids represent the medial mechanical durability of those of their components. H3-1 hybrid, with two stretchable and one rigid segment, has a Young's modulus of 118 ± 2 MPa and tensile strength of 4.6 ± 0.2 MPa while H3-2 hybrid, with two rigid and one stretchable segment, exhibits a lower modulus and tensile strength but relatively higher stretch at break (50% vs 75%). Mechanical measurement results of three-segmented hybrid hydrogels were collected in Table 4.7.

Table 4.7 : Compositions and tensile mechanical properties of gels.

Code	Composition (mol %)				E (MPa)	ε_f (%)	$\sigma_{nom(f)}$ (MPa)
	DMA	AAc	C18A	C17.3M			
C1	70			30	42 (2)	354 (45)	2.5 (0.2)
C2-1	60		40		122 (5)	8 (1)	7.1 (0.5)
C3-1	50			50	74 (9)	287 (35)	4 (0.2)
H1-1	C1/C2-1				55 (2)	319 (13)	4.2 (0.1)
H2-1	C2-1/C3-1				88 (9)	178 (23)	4.3 (0.1)
H3-1	C1/C2-1/C3-1				118 (2)	50 (3)	4.6 (0.2)
C1	70			30	42 (2)	354 (45)	2.5 (0.2)
C2-2	60		15	25	92 (12)	14 (3)	8.2 (1)
C3-2		60	40		144 (14)	4 (0.6)	6 (1)
H1-2	C1/C2-2				60 (1)	300 (45)	3 (0.4)
H2-2	C2-1/C3-2				131 (14)	4 (0.5)	5.6 (1)
H3-2	C1/C2-2/C3-2				89 (4)	75 (10)	3.6 (0.3)

The important point is that the hybrid gel specimens subjected to tensile tests never break at their interface regions. The interface regions remain intact under stress, and

the fracture occurs at C1 segments of hybrid hydrogels. This is due to the higher degree of crystallinity of the interface regions as a mixture of intermeshing individual gel components as compared to the individual gel components separately as well as due to the formation of more ordered crystalline domains in the presence of mixed hydrophobes leading to increased strength of hydrogels [186]. Figure 4.28 shows the comparison of elongation test results of three segmented hybrids (H3-1 and H3-2) with individual components and two segmented hybrids. Two segmented hybrids are denoted as H1-1, H2-1 and H1-2, H2-2, respectively, in Figure 4.28.

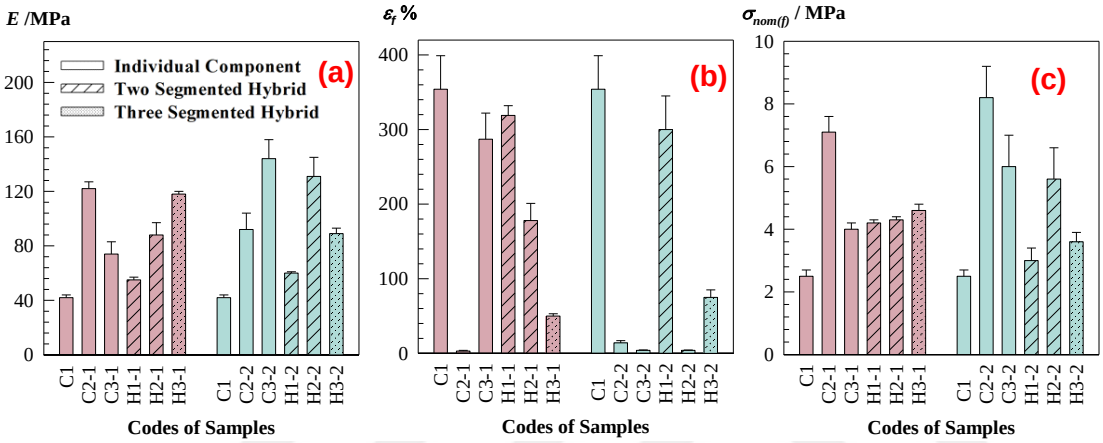

Figure 4.28 : Elongation test results comparison of H3-1 and H3-2 with two segmented hybrids and individual gel segments by their (a) Young's modulus *E* (MPa), (b) percent of strain ε_f % and (c) fracture stress $\sigma_{nom(f)}$ (MPa).

By the consideration of results given together in Figure 4.28, as a general trend, either two or three segmented hybrids were represented Young's modulus *E*, percent of strain ε_f % and fracture stress $\sigma_{nom(f)}$ values in between the highest and lowest mechanical durability values of their individual gel components. Hybrids always break in the weakest segment and never rupture at the interface region.

4.2.2.4 Shape memory

According to the results acquired by DSC measurements, shape memory behavior tests were conducted. Figure 4.29 demonstrates pseudo triple shape-memory capability of H3-1 gel specimen. Although hybrid has three segments with three different T_m, material demonstrates pseudo triple shape-memory behavior due to the close T_m values of C1 and C3-1 segment (37 and 35 °C).

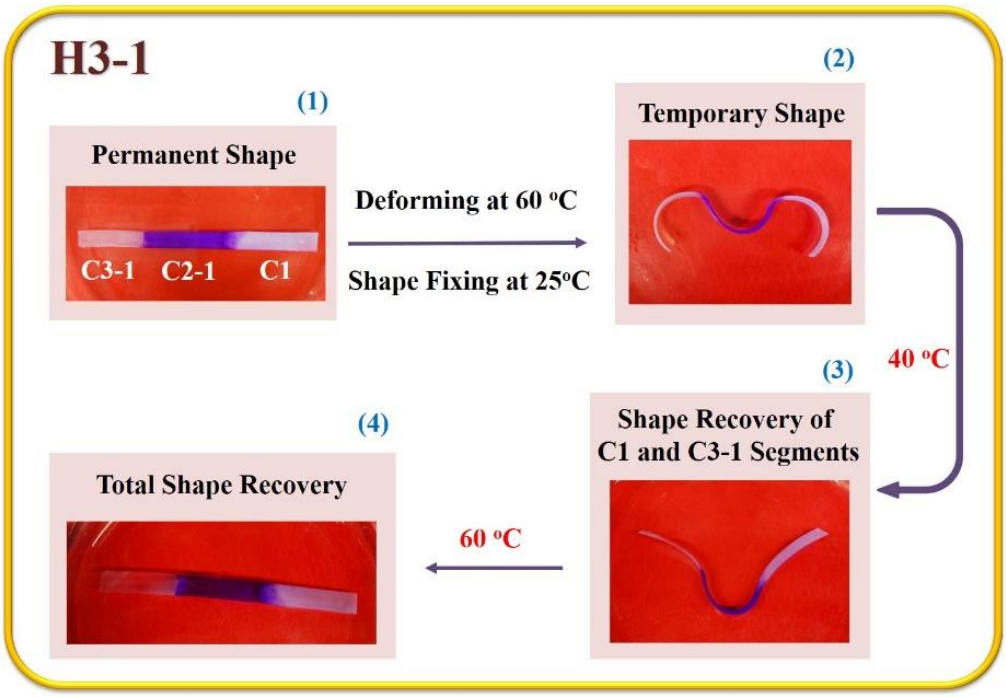

Figure 4.29 : Images demonstrating pseudo-triple shape memory behavior of H3-1 hybrid hydrogel. Permanent shape (1), temporary shape (2), shape recoveries of C1 and C3-1 segments at 40 °C (3), and following shape recovery of C2-1 segment to reach total shape recovery at 60 °C (4).

Figure 4.29 exhibiting the pseudo-triple shape memory behavior of H3-1 hybrid which of its images were labeled as 1, 2, 3 and 4 to follow the procedure. The image labeled by (1) is its permanent shape where the C2-1 zone was blue-violet colored with crystal violet for clarity. The gel is first heated to 60 °C (above the T_m of all segments), and the whole material was deformed to its temporary shape (Figure 4.29, (2)). When the gel is cooled to 25 °C, which is well below the T_m's of all the gel zones, the temporary shape is fixed due to the formation of crystalline domains. For the shape recovery, the gel is first heated to 40 °C to recover the C1 and C3-1 segments to its permanent shape; further heating to 60 °C recovers the total permanent shape (images 3 and 4). For the present supramolecular hydrogels, hydrophobic associations and crystalline domains act as net points and switching segments, respectively, responsible for the shape-memory effect. At temperatures above T_m, hydrophobic associations formed by melting of alkyl crystals determine the permanent shape of the hydrogel. In this state, the hydrogel can easily be deformed under loading to assign temporary shapes to its gel zones. Upon cooling below T_m, side alkyl chains forming crystalline domains fix the temporary shapes of the hydrogel. In typical triple-shape-memory hydrogels, there are two separated crystallizable hydrophobic domains (switching domains) with

different T_m's distributed homogeneously over the whole gel sample [196]. However, in the present hybrid hydrogel, the switching domains are localized in the gel zones, and thus, although each zone has dual shape-memory function, the whole hybrid exhibits triple or multiple shape-memory effect, which may be termed as "pseudo-triple- or multiple- shape memory" behavior. Shape-memory tests conducted on H3-2 hybrids and exhibited in Figure 4.30 revealed the existence of pseudo-multiple shape memory function through the distinct differences in T_m (37, 46 and 56 °C) of hybrid's individual segments.

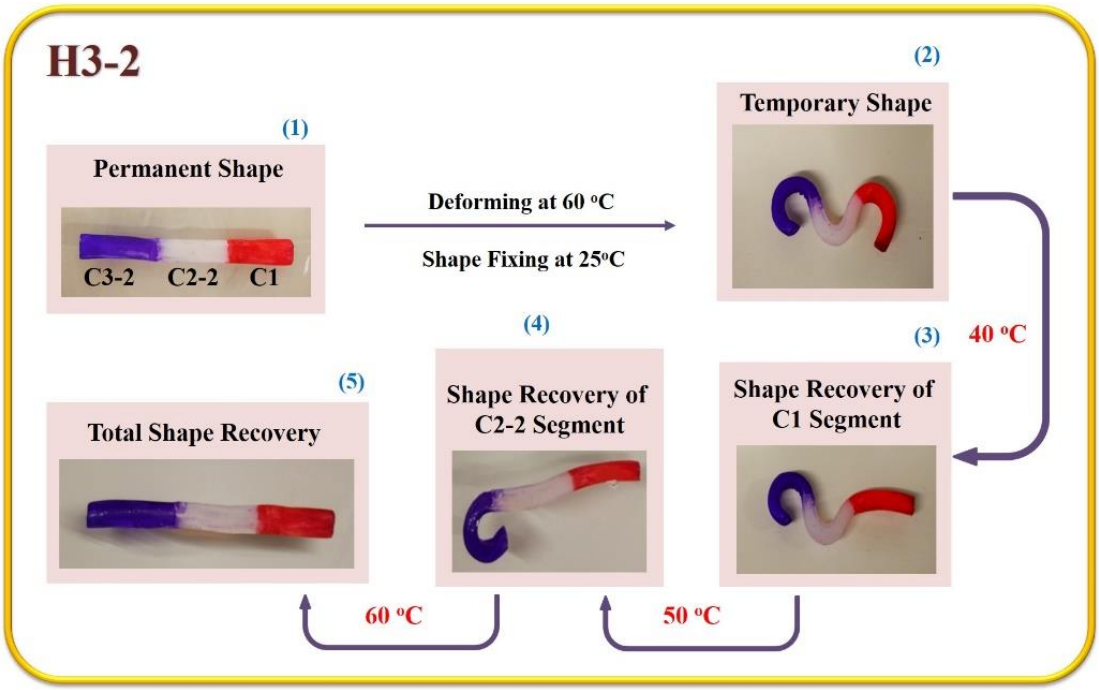

Figure 4.30 : Images demonstrating pseudo multiple-shape-memory behavior of H3-2 hybrid hydrogel. Permanent shape (1), temporary shape (2), successive shape recoveries of C1 (3), C2-2 (4) and C3-2 (5) segments at 40, 50 and 60 °C, respectively.

Figure 4.30 representing the pseudo multiple shape memory behavior of H3-2 hybrid. The image labeled by (1) is its permanent shape where the C1 zone was red and C3-2 zone was blue colored for the clarity. The gel is first heated to 60 °C (above the T_m of all segments), and the whole material was deformed to its temporary shape (Figure 4.30, (2)). When the gel is cooled to 25 °C, which is well below the T_m's of all the gel zones, the temporary shape is fixed due to the formation of crystalline domains. For the shape recovery, the gel is first heated to 40 °C to recover the C1 segment's permanent shape (image 3); further successive heating to 50 and 60 °C recovers the total permanent shape (images 4 and 5). Different from H3-1, H3-2 hybrid gel sample

has three different T_m values which are quite different than each other (37, 46 and 56 °C). Thus, pseudo multiple shape memory behavior can be observed.

5. CONCLUSIONS

Gels, as crosslinked polymer materials, with their capacity of being created in various architectures and chemical compositions to form a versatile and proper in-use material for wide range of applications, attracts much interests. Within this thesis, two different kinds of gels were investigated from two different aspects.

First, single network (SN), double network (DN) and triple network (TN) silk-fibroin based cryogels were investigated in the manner of biocompatibility. Within the second part, multi-segmented hybrid hydrogels were discussed within the framework of their synthesis, creation aspects and mechanical properties.

As a general implication, it was revealed by this thesis that, as well as the critical importance of chemical composition and their reflections on the macro-structure of gel materials, design ideas to reach a new horizon are also crucial. For instance, silk-fibroin SN cryogels are the materials with their known biocompatibilities based on their source as silk-fibroin protein. However, they recently improved by the addition of second generation pores via double-networking concept. The raw-material, silk-fibroin, was the same, but the materials, DN and TN cryogels, have a new architecture. Normally, by increasing silk-fibroin concentration, pore sizes of SN cryogels are getting smaller and corresponding decrease in porosity (%) ratios is seen. In case of DN, TN cryogels, when they compared with their SN silk fibroin concentration equivalents, the porosity ratios, which served as a better environment for cells to have rapid vascularization by means of oxygen and waste exchange without loss in mechanical endurance, were found higher. Therefore, by just altering the design idea, without any change in source and its concentration, more advanced (e.g. biocompatibility) properties can be obtained. Another example of this situation is observed on multi-segmented hybrid hydrogels. Each segment of multi-segmented hybrid hydrogels, by themselves, were outstanding materials with their features such as self healing ability and shape memory behavior. However, when they fused in a single body via a brand new design idea of stratification, they turned into a new

material with an extraordinary hybrid character. With this new hybrid character, these hybrids may serve as a novel material to use in more complex applications.

These means that, rather than an only alteration in the pure chemistry of materials, the design concept variation of materials, by itself, can be a driving force to achieve new improvements on a material, in case of the comparison between two materials in same chemical composition. Detailed, case-spesific implications presented in this thesis are given here under this part.

Silk-based scaffolds are significant group of biomaterials with their various physical characteristics, biocompatibility, and ability to support the attachment, proliferation and differentiation of many types of cells. In order to obtain a scaffold for biomedical applications, proper features such as material clustering, pore size, surface area, wall thickness and homogeneity are crucial.

Within the framework of this thesis, single network (SN), double network (DN) and triple network (TN) silk-fibroin cryogels were investigated in terms of the biocompatibility as pre-made scaffolds. Investigations were carried out on readily-prepared scaffold samples where of their mechanical and morphological properties were already identified by our research group. Pre-identified feature-dependent changes in cell viability was tested quantitatively by MTT assay and qualitative observations were conducted through layer-by-layer images (3D images, composite images collected from different depths of scaffold) from Laser Confocal Scanning Microscopy (LCSM). For all cell-culturing purposes, Normal Human Dermal Fibroblast (NHDF) cell line was used.

Among the scaffolds, there were two kinds of materials available to clarify the relationships between cell viability and pore size, surface area and wall thickness. SN cryogels synthesized by increasing fibroin concentrations represents decreasing pore size and porosity while wall thickness is increasing. The other set of cryogels, named as DN and TN through this thesis, formed by double-networking concept represent increasing fibroin concentrations by the penetration of new networks into the SN. However, DN and TN cryogels exhibit no increase in wall thickness with the help of formed pores inside the bigger pores of single network pores, called as second generation pores. Moreover, decreasing in pore size occasioned by second generation pores and increasing fibroin concentration cases were run with increasing surface area.

Besides all, both of two cryogel type have an advantage for biomedical applications as they have interconnected pores.

MTT assay results represented that cryogels with the porosity (%) ratios between 90 and 75% reveal better cell viability (%) ratios which are in correlation with literature. Additionally, it was revealed that the cell viability results are independent from silk-fibroin concetrations (C_{SF}) of cryogels.

Pore size ranges of scaffolds in dermal fibroblast culturing were reported between 5-15μm. Within the range of scaffolds, SN-4 codded cryogel has the bigger pore sizes as 33μm which decrease to 3.4μm for DN-4/29. For both case, MTT say results show good level of cell viability (far more higher than 50 % for 3rd, 7th and 10th days which are the evidence for the absence of acute toxicity). LCSM images received from the SN-4 (33 μm) and TN4/7/20 (4.3μm) cryogels supported the viability results. This good viability results of TN-4/7/20 is attributed to the extraordinary pore architecture generated by second generation pores.

As a summary of the first part of the thesis results, DN and TN cryogels can increase the cell viability and be protected from any loss on mechanical properties as well. For this reason, these “second generation pores” make DN, TN cryogels a good candidate for load-bearing pre-made scaffolding approaches.

Biological tissues are mainly anisotropic, non-homogenous and multi-phasic natural constructs in an intermeshed architecture of hard and soft components with an extremely tough interface. Such important examples are bone, cartilage, ligament, tendon and intervertebral disc (IVD). Hydrogels are important materials with their similarity to biological tissues as they are matrices with ability to entrap the water or aqueus solutions. However, even their common brittle character was overcome by many techniques improved for decades, these high strength hydrogels reported so far were mostly isotropic.

Within this thesis, two- and three- segmented hybrid hydrogels were synthesized by using UV-initiated bulk copolymerization technique as polymerized density-stratified monomer solutions of hydrophobic (at least one or more hydrophobic monomers of C18A, C17.3M or C12M) and hydrophilic (DMA or AAc) monomer mixtures. Hydrophobic monomers carrying alkyl side chains of different lengths lead to the formation of supramolecular, semicrystalline hybrid hydrogels.

Through this concept, it was possible to adjust the mechanical and thermal properties of segments and interfaces by varying the combinations of monomers. By this means, anisotropic biological tissue inspired hybrid hydrogels were demonstrated, as intermeshed hard and soft components through a strong interface(s), which never rupture at interface region(s).

According to the investigations, two-segmented hybrids exhibit a high modulus (0.46−74 MPa) and tensile strength (0.19−3.9 MPa) and sustain 24−30 MPa stresses at 78−83% compressions which are comparable to the natural IVD. In case of three segmented hybrids, obtained results show also a high modulus (89-118 MPa) and tensile strength (3.6−4.6 MPa) with tensile strain of 50−75%.

Multi-segmented hybrids have the ability to self-heal upon heating above melting temperatures (T_m) once one or both of their gel components are damaged. It was also tested by separate examinations that the interface regions, also, have self healing ability. Besides the self healing ability, they exhibit a pseudo triple- or multiple- shape memory effect as well, arising from T_m belonging to the gel components of hybrids. For instance, two-segmented hybrid H2-2 (two-segmented hybrid) have only one semicristalline segment because the other segment shows an amorphous character. Thus, the H2-2 exhibit only dual shape memory. However, H2-1 (two-segmented hybrid) possesses two semicrystalline segments which reflect to the whole body of two-segmented hybrid as a pseudo-triple- shape memory effect. More over, in case of three- segmented hybrids, H3-1 hydrogel comprises of three semicrystalline segments which of their two have close T_m values than that of the remaining segment. Thus, two different T_m are obtained resulted in a pseudo-triple- shape memory. Another hybrid example, three-segmented H3-2 hydrogel, was observed as it has three semicristalline segments, hence three T_m which of these are in far different temperatures. Stemming from these three different T_m, H3-2 is able to exhibit pseudo-multiple- shape memory effect.

The synthetic strategy presented here, thus enables combination of multiple gel components in a single, intermeshed material, leading to the preparation of multiple-shape memory hydrogels with multi-responsivity. Moreover, it is also possible to decide the place of stretchable and rigid parts in a multi component hybrid structure, according to the requisite, by using the monomers in different densities and chemical properties.

REFERENCES

[1] **Osada, Y. and Gong**, **J.-P.** (1998). Soft and Wet Materials: Polymer Gels, *Adv. Mater., 10* (11), 827-837.

[2] **Osada, Y., Gong**, **J.-P. & Tanaka, Y.** (2004). Polymer Gels, *Journal of Macromolecular Science, Part C: Polymer Reviews, 44* (1), 87-112.

[3] **Kurt B., Gulyuz U., Demir, D. D., Okay, O.** (2016). High-strength semi-crystalline hydrogels with self-healing and shape memory functions *European Polymer Journal 81*, 12–23.

[4] **Buwaldaa, S.J., Boerea, K.W.M., Dijkstrab, P.J., Feijenc, J., Vermondena, T., Henninka, W.E.** (2014). Hydrogels in a historical perspective: from simple networks to smart materials, *J. Control. Release, 190*, 254–273.

[5] **Caló, E. and Khutoryanskiy, V.V.** (2015). Biomedical applications of hydrogels: a review of patents and commercial products. *Eur. Polym J., 65*, 252-267.

[6] **Lozinsky, V.I., Galaev I.Y., Plieva, F.M., Savina, I.N., Jungvid, H. and Bo Mattiasson, B.** (2003). Polymeric cryogels as promising materials of biotechnological interest, *Trends in Biotechnology, 21* (10), 445–451.

[7] **Yetiskin, B., Akinci, C., Okay, O.** (2017). Cryogelation within cryogels: Silk fibroin scaffolds with single-, double- and triple-network structures, *Polymer, 128*, 47-56.

[8] **Kundu S.C.** (2014). *Silk Biomaterials for Tissue Engineering and Regenerative Medicine* Woodhead Publishing Series in Biomaterials, *74*, 1-555.

[9] **Rnjak-Kovacina, J., DesRochers T.M., Burke K.A., Kaplan D.L.** (2015) The effect of sterilization on silk fibroin biomaterial properties, *Macromol Biosci., 15* (6), 861-874.

[10] **Sehgal, N., Fortin, J.D.** (2000). Internal Disc Disruption and Low Back Pain *Pain Physician, 3* (2), 143–157.

[11] ***Intervertebral Disc: What is it? What does it do? And how to keep it healthy.*** *(2016). Retrieved October 1, 2017, from http://www.wieberphysicaltherapy.com/intervertebral-disc-keep-healthy/*

[12] **Nerurkar N. L., Elliot D. M., Mauck R.L.** (2010) Mechanical design criteria for intervertebral disc tissue engineering *Journal of Biomechanics, 43*, 1017–1030.

[13] **Wilke, H.J., Heuer, F., Neidlinger-Wilke, C., Claes, L.** (2006) Is a collagen scaffold for a tissue engineered nucleus replacement capable of restoring disc height and stability in an animal model? *Eur Spine J, 15* (Suppl 3), S433–S438.

[14] **Sakai, D., Mochida, J., Iwashina, T, Watanabe, T., Suyama, K., Ando, K., Hotta, T.** (2006) Atelocollagen for culture of human nucleus pulposus cells forming nucleus pulposus-like tissue in vitro: influence on the proliferation and proteoglycan production of HNPSV-1 cells. *Biomaterials, 27* (3), 346–353.

[15] **Sakai, D., Mochida, J., Yamamoto, Y., Nomura, T., Okuma, M., Nishimura, K., Nakai, T., Ando, K., Hotta, T.** (2003) Transplantation of mesenchymal stem cells embedded in Atelocollagen gel to the intervertebral disc: a potential therapeutic model for disc degeneration. *Biomaterials, 24* (20) 3531–3541.

[16] **Leone, G., Torricelli, P., Chiumiento, A., Facchini, A., Barbucci, R.** (2008) Amidic alginate hydrogel for nucleus pulposus replacement. *J Biomed Mater Res A, 84* (2), 391–401.

[17] **Mizuno, H., Roy, A.K., Vacanti, C.A., Kojima, K., Ueda, M., Bonassar, L.J.** (2004) Tissue-engineered composites of anulus fibrosus and nucleus pulposus for intervertebral disc replacement. *Spine, 29* (12), 1290–1297.

[18] **Wan, Y., Feng, G., Shen, F.H., Laurencin, C.T., Li, X.** (2008) Biphasic scaffold for annulus fibrosus tissue regeneration. *Biomaterials, 29* (6), 643–652.

[19] **Dang, J.M., Sun, D.D., Shin-Ya, Y., Sieber, A.N., Kostuik, J.P., Leong, K.W.** (2006) Temperature-responsive hydroxybutyl chitosan for the culture of mesenchymal stem cells and intervertebral disk cells. *Biomaterials, 27* (3), 406–418.

[20] **Saad, L., Spector, M.** (2004) Effects of collagen type on the behavior of adult canine annulus fibrosus cells in collagen-glycosaminoglycan scaffolds. *J Biomed Mater Res A, 71* (2), 233– 241.

[21] **Alini, M., Li, W., Markovic, P., Aebi, M, Spiro, R.C., Roughley, P.J.** (2003) The potential and limitations of a cell-seeded collagen/ hyaluronan scaffold to engineer an intervertebral disc-like matrix. *Spine, 28* (5), 446–454.

[22] **Richardson, S.M., Curran, J.M., Chen, R., Vaughan-Thomas, A., Hunt, J.A., Freemont, A.J., Hoyland, J.A.** (2006) The differentiation of bone marrow mesenchymal stem cells into chondrocyte-like cells on poly-L-lactic acid (PLLA) scaffolds. *Biomaterials, 27* (22), 4069–4078.

[23] **Chang, G., Kim, H.J., Kaplan, D., Vunjak-Novakovic, G., Kandel, R.A.** (2007) Porous silk scaffolds can be used for tissue engineering annulus fibrosus. *Eur Spine J, 16* (11), 1848–1857.

[24] **Nerurkar N. L., Elliot D. M., Mauck R.L.** (2007) Mechanics of oriented electrospun nanofibrous scaffolds for annulus fibrosus tissue engineering. *J Orthop Res, 25* (8), 1018–1028.

[25] **Wilda, H., Gough, J.E.** (2006) In vitro studies of annulus fibrosus disc cell attachment, differentiation and matrix production on PDLLA/45S5 Bioglass composite films. *Biomaterials, 27* (30), 5220–5229.

[26] **Chan, B.P., Leong, K.W.** (2008) Scaffolding in tissue engineering: general approaches and tissue-specific considerations *Eur Spine J, 17* (Suppl 4), S467–S479.

[27] **Chang, G., Kim, H.J., Vunjak-Novakovic, G., Kaplan, D.L. and Kandel, R.** (2010) Enhancing annulus fi brosus tissue formation in porous silk scaffolds, *J Biomed Mater Res A , 92*, 43–51.

[28] **See, E.Y., Toh, S.L. and Goh, J.C.** (2012) Simulated intervertebral disc-like assembly using bone marrow-derived mesenchymal stem cell sheets and silk scaffolds for annulus fi brosus regeneration, *J Tissue Eng Regen Med, 6*, 528–535.

[29] **Park, S.H., Gil, E.S., Cho, H., Mandal, B.B., Tien, L.W., Min, B.H. and Kaplan, D.L.** (2012) Intervertebral disk tissue engineering using biphasic silk composite scaffolds, *Tissue Eng Part A, 18*, 447–458.

[30] **Park, S.H., Gil, E.S., Mandal, B.B., Cho, H., Kluge, J.A., Min, B.H. and Kaplan, D.L.** (2012) Annulus fibrosus tissue engineering using lamellar silk scaffolds, *J Tissue Eng Regen Med., 6* (3), 24–33.

[31] **Bhattacharjee, M., Miot, S., Gorecka, A., Singha, K., Loparic, M., Dickinson, S., Das, A., Bhavesh, N.S., Ray, A.R., Martin, I. and Ghosh, S.** (2012) Oriented lamellar silk fi brous scaffolds to drive cartilage matrix orientation: towards annulus fibrosus tissue engineering, *Acta Biomater., 8*, 3313–3325.

[32] **Chan, B.P., Leong, K.W.** (2008) Scaffolding in tissue engineering: general approaches and tissue-specific considerations *Eur Spine J, 17* (Suppl 4), S467–S479.

[33] **Karp, J.M., Langer, R.** (2007) Development and therapeutic applications of advanced biomaterials. *Curr Opin Biotechnol., 18* (5), 454–459.

[34] **Langer, R., Tirrell, D.A.** (2004) Designing materials for biology and medicine. *Nature, 428* (6982), 487–492.

[35] **O'Brien, F. J., Harley, B. A., Yannas, I. V., & Gibson, L. J.** (2005) The effect of pore size on cell adhesion in collogen-GAG caffolds, *Biomaterials, 26*, 433-441.

[36] **Engler, A. J., Sen, S., Sweeney, H. L., & Discher, D. E.** (2006) Matrix elasticity directs stem cell lineage specification *Cell, 126* (4), 677-689.

[37] **Peyton, S. R., & Putnam, D.** (2005) Extracellular matrix rigidity governs smooth muscle cell motility in a biphasic fashion *Journal of Cell Phsiology, 204* (1), 198-209.

[38] **Chang, H-I, Wang, Y.** (2011) *Regenerative Medicine and Tissue Engineering - Cells and Biomaterials* (Edited by Prof. Daniel Eberli) ISBN: 978-953-307-663-8 *InTech Chapter, 27*, 569-588.

[39] **Brodie, J.C., Goldie, E., Connel, G., Merry, J., Grant, M.H.** (2005) Osteoblast interactions with calcium phosphate ceramics modified by coating with type I collagen. *J Biomed Mater Res A, 73* (4), 409–421.

[40] **Borschel, G.H., Huang, Y.C., Calve, S., Arruda, E.M., Lynch, J.B., Dow, D.E., … , Brown, D.L.** (2005) Tissue engineering of recellularized small-diameter vascular grafts. *Tissue Eng, 11* (5–6), 778–786.

[41] **Hall, S.** (1997) Axonal regeneration through acellular muscle grafts. *J. Anat. 190* (1), 57–71.

[42] **Ingram, J.H., Korossis, S., Howling, G., Fisher, J., Ingham, E.** (2007) The use of ultrasonication to aid recellularization of acellular natural tissue scaffolds for use in anterior cruciate ligament reconstruction. *Tissue Eng, 13* (7), 1561–1572.

[43] **Badylak, S.F.** (2004) Xenogeneic extracellular matrix as a scaffold for tissue reconstruction. *Transpl Immunol, 12* (3–4), 367–377.

[44] **Zheng, M.H., Chen, J, Kirilak, Y., Willers, C., Xu, J., Wood, D.** (2005) Porcine small intestine submucosa (SIS) is not an acellular collagenous matrix and contains porcine DNA: possible implications in human implantation. *J Biomed Mater Res B Appl Biomater, 73* (1), 61–67.

[45] **Tsuda, Y., Shimizu, T., Yamato, M., Kikuchi, A., Sasagawa, T., Sekiya, S., … , Okano, T.** (2007) Cellular control of tissue architectures using a three-dimensional tissue fabrication technique. *Biomaterials, 28* (33), 4939–4946.

[46] **Yang, J., Yamato, M., Shimizu, T., Sekine, H., Ohashi, K., Kanzaki, M., … , Okano, T.** (2007) Reconstruction of functional tissues with cell sheet engineering. *Biomaterials, 28* (34), 5033–5043.

[47] **Lanza, R.P., Hayes, J.L., Chick, W.L.** (1996) Encapsulated cell technology. *Nat. Biotechno., 14* (9), 1107–1111.

[48] **Orive, G., Herna´ndez, R.M., Gasco´n, A.R., Calafiore, R., Chang, T.M., De Vos, P., … , Pedraz, J.L.** (2003) Cell encapsulation: promise and progress. *Nat. Med., 9* (1), 104–107.

[49] **Orive, G., Herna´ndez, R.M., Rodrı´guez Gasco´n, A., Calafiore, R., Chang, T.M., De Vos, P., … , Pedraz, J.L.** (2004) History, challenges and perspectives of cell microencapsulation. *Trends Biotechnol., 22* (2), 87–92.

[50] **Langer, R., Vacanti, J.P.** (1993) Tissue engineering. *Science, 260* (5110), 920–926.

[51] **Vacanti, J.P., Langer, R.** (1999) Tissue engineering: the design and fabrication of living replacement devices for surgical reconstruction and transplantation. *Lancet, 354* (Suppl 1), SI32–SI34.

[52] **Ak F., Oztoprak Z., Karakutuk I., Okay O.** (2013) Macroporous silk fibroin cryogels. *Biomacromolecules, **14***, 719-727.

[53] **Vepari, C., Kaplan, D.L.** (2007) Silk as a biomaterial, *Prog. Polym. Sci. 32*, 991-1007.

[54] **Vollrath, F., Porter, D.** (2009) Silks as ancient models for modern polymers, *Polymer, 50*, 5623-5632.

[55] **Hardy, J.G., Romer, L.M., Scheibel, T.R.** (2008) Polymeric materials based on silk proteins, *Polymer, 49*, 4309-4327.

[56] **Melke, J., Midha, S., Ghosh, S. Ito, K., Hofmann, S.** (2016) Silk fibroin as biomaterial for bone tissue engineering, *Acta Biomater*., *31*, 1-16.

[57] **Karageorgiou, V., Kaplan, D.L.** (2005) Porosity of 3D biomaterial scaffolds and osteogenesis, *Biomaterials, 26*, 5474-5491.

[58] **Nazarov, R., Jin, H.J., Kaplan, D.L.** (2004) Porous 3-D scaffolds from regenerated silk fibroin, *Biomacromolecules, 5*, 718-726.

[59] **Ki, C.S., Park, S.Y., Kim, H.J., Jung, H.M., Woo, K.M., Lee, J.W., Park, Y.H.** (2008) Development of 3-D nanofibrous fibroin scaffold with high porosity by electrospinning: implications for bone regeneration, *Biotechnol. Lett. 30*, 405-410.

[60] **Hutmacher, D.W.** (2000) Scaffolds in tissue engineering bone and cartilage, *Biomaterials, 21*, 2529-2543.

[61] **Li, M.Z., Lu, S.Z., Wu, Z.Y., Yan, H.J.** (2001) Study on porous silk fibroin materials. I. Fine structure of freeze-dried silk fibroin, *J. Appl. Polym. Sci*., *79*, 2185-2191.

[62] **Cao, Z., Wen, J., Yao, J., Chen, X., Ni, Y., Shao, Z.** (2013) Facile fabrication of the porous three-dimensional regenerated silk fibroin scaffolds, *Mater. Sci. Eng. C, 33*, 3522-3529.

[63] **Lv, Q., Feng, Q.L.** (2006) Preparation of 3-D regenerated fibroin scaffolds with freeze drying method and freeze drying/foaming technique, *J. Mater. Sci. Mater. Med. 17*, 1349-1356.

[64] **Liu, X., Ma, P.X.** (2004) Polymeric scaffolds for bone tissue engineering, *Ann. Biomed. Eng. 32*, 477-486.

[65] **Zhang, Q., Yan, S., Li, M.** (2009) Silk fibroin based porous materials, *Materials, 2*, 2276-2295.

[66] **Kim, U.J., Park, J., Kim, H.J., Wada, M., Kaplan, D.L.** (2005) Three-dimensional aqueous derived biomaterial scaffolds from silk fibroin, *Biomaterials, 26*, 2775-2785.

[67] **Min, S., Gao, X., Liu, L., Tian, L., Zhu, L., Zhang, H., Yao, J.** (2009) Fabrication and characterization of porous tubular silk fibroin scaffolds, *J. Biomater. Sci., 20*, 1961-1974.

[68] **Zhou, C.Z., Confalonieri, F., Medina, N., Zivanovic, Y., Esnault, C., Yang, T., Jacquet, M., Janin, J., Duguet, M., Perasso, R., Li, Z.G.** (2000) Fine organization of *Bombyx mori* fibroin heavy chain gene, *Nucleic Acids Res., 28*, 2413-2419.

[69] **Jin, H.J., Kaplan, D.L.** (2003) Mechanism of silk processing in insects and spiders, *Nature, **424***, 1057-1061.

[70] **Gong, J.P., Katsuyama, Y., Kurokawa, T., Osada, Y.** (2003) Double-network hydrogels with extremely high mechanical strength, *Adv. Mater, 15*, 1155-1158.

[71] **Tanaka, Y., Kuwabara, R., Na, Y.-H., Kurokawa, T., Gong, J.P., Osada, Y.** (2005) Determination of fracture energy of high strength double network hydrogels, *J. Phys. Chem. B, 109*, 11559-11562.

[72] **Gong, J.P., Katsuyama, Y., Kurokawa, T., Osada, Y.** (2003) Double-network hydrogels with extremely high mechanical strength, *Adv. Mater*, *15*, 1155-1158.

[73] **Ahmed, S., Nakajima, T., Kurokawa, T., Haque, M. A., Gong, J.P.** (2014) Brittle-Ductile Transition of Double Network Hydrogels: Mechanical Balance of Two Networks as the Key Factor, *Polymer*, *55*, 914-923.

[74] **Nakajima, T., Fukuda, Y., Kurokawa, T., Sakai, T., Chung, U., Gong, J.P.** (2013) Synthesis and Fracture Process Analysis of Double Network Hydrogels with a Well-Defined First Network, *ACS Macro Lett.*, *2*, 518-521.

[75] **Webber, R.E., Creton, C., Brown, H.R., Gong, J.P.** (2007) Large strain hysteresis and Mullins effect of tough double-network hydrogels, *Macromolecules*, *40*, 2919-2927.

[76] **Es-haghi, S.S., Leonov, A.I.;, Weiss, R.A.** (2013) On The Necking Phenomenon in Pseudo-Semi-Interpenetrating Double-Network Hydrogels, *Macromolecules*, *46*, 6203-6208.

[77] **Nakayama, A., Kakugo, A., Gong, J.P., Osada, Y., Takai, M., Erata, T., Kawano, S.** (2004) High mechanical strength double-network hydrogel with bacterial cellulose, *Adv. Funct. Mater.*, *14*, 1124-1128.

[78] **Xin, H., Saricilar, S.Z., Brown, H. R., Whitten, P.G., Spinks, G.M.**, (2013) Effect of First network topology on the toughness of double network hydrogels, *Macromolecules, 46* (16), 6613-6620.

[79] **Harrass, K., Kruger, R., Müller, M., Albrecht, K., Groll, J.** (2013) Mechanically strong hydrogels with reversible behaviour under cyclic compression with MPa loading. *Soft Matter, 9* (10), 2869-2877.

[80] **Yasuda, K., Gong, J.P., Katsuyama, Y., Nakayama, A., Tanabe, Y., Kondo, E., Ueno, M., Osada, Y.** (2005) Biomechanical properties of high-tougness double network hydrogels, *Biomaterials*, *26*, 4468-4475.

[81] **Hu, J., Kurokawa, T., Nakajima, T., Sun, T. L., Suekama, T., Wu, Z. L., Liang, S.M., Gong, J.P.** (2012) High fracture efficiency and stress concentration phenomenon for microgel-reinforced hydrogels based on double-network principle, *Macromolecules, 45* (23), 9445-9451.

[82] **Fei, R., George, J.T., Park, J., Means, A.K., Grunlan, M.A.** (2013) Ultra strong thermoresponsive hydrogels, *Soft Matter, 9*, 2912-2919.

[83] **Myung, D., Koh, W., Ko, J., Hu, Y., Carrasco, M., Noolandi, J., Ta, C.N., Frank, C.W.** (2007) Biomimetic strain hardening in interpenetrating polymer network hydrogels. *Polymer*, *48*, 5376-5387.

[84] **Waters, D.J., Engberg, K., Parke-Houben, R., Ta, C.N., Jackson, A.J., Toney, M.F., Frank, C.W.** (2011) Structure and Mechanism of Strength Enhancement in Interpenetrating Polymer Network Hydrogels, *Macromolecules*, *44* (14), 5776-5587.

[85] **Argun, A., Can, V. Altun, U., Okay, O.** (2014) Non-ionic double and triple network hydrogels of high mechanical strength, *Macromolecules, 47* (18), 6430-6440.

[86] **Zhao, Q., Sun, J., Wu, X., Lin, Y.** (2011) Macroporous double-network cryogels: formation mechanism, enhanced mechanical strength and temperature/pH dual sensitivity, *Soft Matter, 7*, 4284-4293.

[87] **Lou, T., Wang, X., Song, G., Gu, Z., Yang, Z.** (2014) Fabrication of PLLA/beta-TCP nanocomposite scaffolds with hierarchical porosity for bone tissue engineering, *Int. J. Biol. Macromol,. 69*, 464-470.

[88] **Xiong, G., Luo, H., Zhu, Y., Raman, S., Wan, Y.** (2014) Creation of macropores in threedimensional bacterial cellulose scaffold for potential cancer cell culture, *Carbohydr. Polym., 114*, 553-557.

[89] **Wang, T., Feng, Z.-Q., Leach, M.K., Wu, J., Jiang, Q.** (2013) Nanoporous fibers of type-I collagen coated poly(l-lactic acid) for enhancing primary hepatocyte growth and function, *J. Mater. Chem. B, 1*, 339-346.

[90] **Wang, X., Lou, T., Zhao, W., Song, G., Li, C., Cui, G.** (2016) The effect of fiber size and pore size on cell proliferation and infiltration in PLLA scaffolds on bone tissue engineering, *J. Biomater. Appl., 30*, 1545-1551.

[91] **Buckley, C.T., O'Kelly, K.U.** (2010) Fabrication and characterization of a porous multidomain hydroxyapatite scaffold for bone tissue engineering investigations. *J of Biomed. Mater. Research B: App. Biomater., 93B* (2), 459-467.

[92] **Buckley, C.T., O'Kelly, K.U.** (2010) Maintaining cell depth viability: On the efficacy of a trimodal scaffold pore architecture and dynamic rotational culturing. *J. Mater. Sci.: Matter. Med., 21*, 1731-1738.

[93] **Mechels, F.P., Barradas, A.M., van Blitterswijk, C.A., de Boer, J., Feijen, J., Grijpma D.W.** (2010) Effects of the architecture of tissue engineering scaffolds on cell seeding and culturing. *Acta Biomaterials, 6* (11), 4208-4217.

[94] **Ji, C., Khademhosseini, A., Dehghani F.** (2011) Enhancing cell penetration proliferation in chitosan hydrogels for tissue engineering applications. *Biomaterials, 32*, 9719-9729.

[95] **Zeltinger, J., Sherwood, J.K., Graham, D.A., Müeller, R., Griffith, L.G.** (2001) Effect of pore size and void fraction on cellular adhesion, proliferation, and matrix deposition. *Tissue Engineering, 7* (5), 557-572.

[96] **Wake, M.C., Patrick, C.W., and Mikos, A.G.** (1994) Pore morphology effects on the fibrovascular tissue growth in porous polymer substrates. *Cell Transplant, 3* (4), 339-343.

[97] **Yang, S., Leong, K-F., Du, Z., Chua, C-K.** (2001) The design of scaffolds for use in tissue engineering. Part I. Traditional factors. *Tissue Engineering, 7* (6), 679-689.

[98] **Okay, O.** in **G. Gerlach and K.-F. Arndt,** (2009) *Hydrogel sensors and actuators: (**6**) General properties of hydrogels, Springer Series on Chemical Sensors and Biosensors, Springer.*

[99] **Almdal Riso, K., Dyre, J., Hvidt, S., Kramer O.** (1993) Towards a Phenomenological Definition of the Term 'Gel', *Polymer Gels and Networks, 1,* 5-17.

[100] **Noro, A., Hayashi, M. and Matsushita, Y.** (2001) Design and properties of supramolecular polymer gels, *Tissue Eng., 7* (6), 679-689.

[101] **Abdurrahmanoglu, S., Can, V., Okay, O.** (2009) Design of high-toughness polyacrylamide hydrogels by hydrophobic modification, *Polymer. 50,* 5449-5455.

[102] **Ahagon, A., Gent, A.N.** (1975) Treshold fracture energies for elastomers, *J. Polym. Sci.: Polym. Phys. Ed., 13* (10), 1903-1911.

[103] **Tanaka, Y., Gong, J. P., Osada, Y.** (2005) Novel hdrogels with excellent mechanical performance, *Prog. Polym. Sci., 30,* 1-9.

[104] **Haque, M.A., Kurokawa, T., Gong, J.P.** (2012) Super tough double network hydrogels and their application as biomaterials, *Polymer, 53* (9), 1805-1822.

[105] **Haraguchi, K., Takehisa, T.** (2002) Nanocomposite Hydrogels: A Unique Organic–Inorganic Network Structure with Extraordinary Mechanical, Optical, and Swelling/De-swelling Properties, *Adv. Mater., 14* (16), 1120-1124.

[106] **Tuncaboylu, D.C., Sari, M., Oppermann, W., Okay, O.** (2011) Tough and self-healing hydrogels formed via hydrophobic interactions, *Macromolecules, 44,* 4997-5005.

[107] **Okumura, Y., Ito, K.** (2001) The polyrotaxane gels: a topological gel by figure-of-eight cross-links. *Adv Mater., 13,* 485–487.

[108] **Kopeček, J.** (2007) Hydrogel biomaterials: A smart future?, *Biomaterials, 28,* 5185–5192.

[109] **Haraguchi, K, Li, H.J., Okumura, N.** (2007) Hydrogels with hydrophobic surfaces: abnormally high contact angles for water on PNIPA nanocomposite hydrogels. *Macromolecules, 40,* 2299–2302.

[110] **Angelopoulos, S.A., Tsitsilianis, C.** (2006) Thermo-Reversible Hydrogels Based on Poly (N,N-diethylacrylamide) - block- poly (acrylic acid)-block - poly (N,N-diethylacrylamide) Double Hydrophilic Triblock Copolymer *Macromol. Chem. Phys., 207* (23), 2188-2194.

[111] **Sui, K., Gao, S., Wu, W.W., Xia, Y.** (2010) Injectable supramolecular hybrid hydrogels formed by MWNT-grafted-poly(ethylene glycol) and α-cyclodextrin *J. Polym. Sci., Part A: Polym. Chem., 48,* 3145-3151.

[112] **Miquelard-Garnier, G., Demoures, S., Creton, C., Hourdet, D.** (2006) Synthesis and Rheological Behavior of New Hydrophobically Modified Hydrogels with Tunable Properties, *Macromolecules, 39* (23), 8128-8139.

[113] **Boucard, N., Viton, C., Domard, A.** (2005) New aspects of the formation of physical hydrogels of chitosan in a hydroalcoholic medium. *Biomacromolecules, 6* (6), 3227-3237.

[114] **Stahl, P.J., Romano, N.H., Wirtz, D., Yu, S.M.** (2010) PEG-based hydrogels with collagen mimetic peptide-mediated and tunable physical cross-links. *Biomacromolecules, 11* (9), 2336-2344.

[115] **Pan, Y.S., Xiong, D.S.** (2010) Stress relaxation behavior of nano-hydroxyapatite reinforced poly(vinyl alcohol) gel composites as biomaterial, *J. Mater. Sci., 45* (20), 5495-5501.

[116] **Nowak, A.P., Breedveld, V., Pakstis, L., Ozbas, B., Pine, D.J., Pochan, D., Deming, T.J.** (2002) Rapidly recovering hydrogel scaffolds from self-assembling diblock copolypeptide amphiphiles *Nature, 417* (6887), 424-428.

[117] **Hao, J. and Weiss, R.A.** (2011) Viscoelastic and Mechanical Behavior of Hydrophobically Modified Hydrogels, *Macromolecules, 44*, 9390–9398.

[118] **Candau, F., Selb, J.** (1999) Hydrophobically-modified polyacrylamides prepared by micellar polymerization *Adv. Colloid Interface Sci., 79* (2-3), 149-172.

[119] **Volpert, E., Selb, J., Candau, F.** (1998) Associating behaviour of polyacrylamides hydrophobically modified with dihexylacrylamide *Polymer, 39*, 1025-1033.

[120] **Hill, A., Candau, F., Selb, J.** (1993) Properties of hydrophobically associating polyacrylamides: influence of the method of synthesis *Macromolecules, 26* (17), 4521-4532.

[121] **Regalado, E.J., Selb, J., Candau, F.** (1999) Viscoelastic Behavior of Semidilute Solutions of Multisticker Polymer Chains, *Macromolecules, 32* (25), 8580-8588.

[122] **Candau, F., Regalado, E.J., Selb, J.** (1998) Scaling Behavior of the Zero Shear Viscosity of Hydrophobically Modified Poly(acrylamide)s *Macromolecules, 31* (16), 5550-5552.

[123] **Kujawa, P., Audibert-Hayet, A., Selb, J., Candau, F.J.** (2004) Rheological properties of multisticker associative polyelectrolytes in semidilute aqueous solutions. *Polym. Sci., Part B: Polym. Phys., 42* (9), 1640-1655.

[124] **Kujawa, P., Audibert-Hayet, A., Selb, J., Candau, F.** (2006) Effect of Ionic Strength on the Rheological Properties of Multisticker Associative Polyelectrolytes *Macromolecules, 39* (1), 384-392.

[125] **Gao, B., Guo, H., Wang, J., Zhang, Y.** (2008) Preparation of Hydrophobic Association Polyacrylamide in a New Micellar Copolymerization System and Its Hydrophobically Associative Property *Macromolecules, 41* (8), 2890-2897.

[126] **Chern, C.S., Chen, T.J.** (1998) Effect of Ostwald ripening on styrene miniemulsion stabilized by reactive cosurfactants, *Colloids Surf. A, 138*, 65-74.

[127] **Leyrer, R.J., Machtle, W.** (2000) Emulsion polymerization of hydrophobic monomers like stearyl acrylate with cyclodextrin as a phase transfer agent, *Macromol. Chem. Phys., 201*, 1235-1243.

[128] **Lau, W.** (2002) Emulsion Polymerization of Hydrophobic Monomers *Macromol. Symp., 182*, 283-290.

[129] **Tuncaboylu, D. C., Sahin, M., Argun, A., Oppermann, W., Okay, O.** (2012) Dynamics and large strain behavior of self-healing hydrogels with and without surfactants. *Macromolecules, 45* (4), 1991-2000.

[130] **Tuncaboylu, D.C., Argun, A., Sahin, M., Sari, M., Okay, O.** (2012) Structure optimization of self-healing hydrogels formed via hydrophobic interactions, *Polymer, 53* (24), 5513-5522.

[131] **Akay, G., Hassan-Raeisi, A., Tuncaboylu, D.C., Orakdogen, N., Abdurrahmanoglu, S., Oppermann, W., Okay, O.** (2013) Self-healing hydrogels formed in catanionic surfactant solutions. *Soft Matter, 9*, 2254-2261.

[132] **Okay, O.** (2015) Self-healing hydrogels formed via hydrophobic interactions, *Adv. Polym. Sci., 268*, 101-142.

[133] **Bilici, C., Okay, O.** (2013) Shape memory hydrogels via micellar copolymerization of acrylic acid and n-octadecyl acrylate in aqueous media, *Macromolecules, 46*, 3125-3131.

[134] **Gulyuz, U., Okay, O.** (2014) Self-healing poly(acrylic acid) hydrogels with shape memory behavior of high mechanical strength, *Macromolecules, 47*, 6889-6899.

[135] **Gulyuz, U., Okay, O.** (2013) Self-healing polyacrylic acid hydrogels, *Soft Matter, 9* (43), 10287-10293.

[136] **Kolomiets, E. and Lehn, J.M.** (2005) Double dynamers: molecular and supramolecular double dynamic polymers, *Chem. Commun., 12*, 1519-1521.

[137] **Lehn, J.M.** (2005) Dynamers: Dynamic molecular and supramolecular polymers, *Prog. Polym. Sci., 30*, 814-831.

[138] **Otto, S., Furlan R.L. and Sanders, J.K.** (2002) Dynamic combinatorial chemistry, *Drug Discovery Today, 7* (2), 117-125.

[139] **Lehn, J.M.** (2007) From supramolecular chemistry towards constitutional dynamic chemistry and adaptive chemistry. *Chem. Soc. Rev., 36* (2), 151-160.

[140] **Wei, Z., Yang, J.H., Zhou, J., Xu, F., Zrĭnyi, M., Dussault, P.H., Osada Y. and Chen Y.M.** (2014) Self-healing gels based on constitutional dynamic chemistry and their potential applications, *Chem. Soc. Rev., 43* (23), 8114–8131.

[141] **Wool, R.P.** (2008) Self-healing materials: a review, *Soft Matter, 4* (3), 400-418.

[142] **Rao, Z., Inoue, M., Matsuda M. and Taguchi, T.** (2011) Quick self-healing and thermo-reversible liposome gel. *Colloids Surf. B Biointerfaces, 82* (1), 196-202.

[143] **Sahoo, N.G., Jung, Y.C., Cho, J.W.** (2007) Electroactive Shape Memory Effect of Polyurethane Composites Filled with Carbon Nanotubes and Conducting Polymer. *Mater. Manuf. Processes, 22* (4), 419−423.

[144] **Koerner, H., Price, G., Pearce, N.A., Alexander, M., Vaia, R.A.** (2004) Remotely actuated polymer nanocomposites--stress-recovery of carbon-nanotube-filled thermoplastic elastomers. *Nat. Mater., 3* (2), 115−120.

[145] **Vaia, R.** (2005) Nanocomposites: Remote-controlled actuators. *Nat. Mater., 4* (6), 429−430.

[146] **Luo, X., Mather, P.T.** (2010) Conductive shape memory nanocomposites for high speed electrical actuation. *Soft Matter, 6* (10), 2146−2149.

[147] **Gong, X-L., Xiao, Y-Y., Pan, M., Kang, Y., Li, B-J. and Zhang, S.** (2016) pH- and Thermal-Responsive Multi-Shape Memory Hydrogel, *ACS Appl. Mater. Interfaces, 8* (41), 27432-27437.

[148] **Schmidt, A.M.** (2006) Electromagnetic Activation of Shape Memory Polymer Networks Containing Magnetic Nanoparticles. *Macromol. Rapid Commun., 27* (14), 1168−1172.

[149] **Zrínyi, M.** (2000) Intelligent polymer gels controlled by magnetic fields. *Colloid Polym. Sci., 278* (2), 98−103.

[150] **Szabó, D., Szeghy, G., Zrínyi, M.** (1998) Shape Transition of Magnetic Field Sensitive Polymer Gels. *Macromolecules, 31* (19), 6541− 6548.

[151] **Li, G., Yan, Q., Xia, H. and Zhao Y.** (2015) Therapeutic Ultrasound-Triggered Shape Memory of Melamine-Enhanced Poly(vinyl alcohol) Physical Hydrogel, *ACS Appl Mater Interfaces., 7* (22), 12067-12073.

[152] **Iqbal, D., Samiullah, M.** (2013) Photo-Responsive Shape-Memory and Shape-Changing Liquid-Crystal Polymer Networks. *Materials, 6* (1), 116-142.

[153] **Lendlein, A., Jiang, H., Junger, O., Langer, R.** (2005) Light-induced shape-memory polymers. *Nature, 434* (7035), 879−882.

[154] **Zhang, X., Zhou, Q., Liu, H., Liu, H.** (2014) UV light induced plasticization and light activated shape memory of spiropyran doped ethylene-vinyl acetate copolymers. *Soft Matter, 10* (21), 3748− 3754.

[155] **Liu, C., Qin, H. and Mather, P.T.** (2007) Review of progress in shape-memory polymers, *J. Mater. Chem., 17*, 1543–1558.

[156] **Osada, Y., Okuzaki, H. & Hori, H.** (1992) A polymer gel with electrically driven motility, *Nature, 355*, 242- 244.

[157] **Katchalsky, A., Hargitay, B., & Kuhn, W.** (1950) Reversible Dilation and Contraction by Changing the State of Ionization of High-Polymer Acid Networks *Nature, 165*, 514-516.

[158] **Katchalsky, A., Oplatka, A. & Steirberg, I. Z.** (1966) Mechanochemical Engines, *Nature, 210*, 565-571.

[159] **Chan, B.Q., Low, Z.W., Heng, S.J., Chan, S.Y., Owh, C, Loh, X.J.** (2016) Recent Advances in Shape Memory Soft Materials for Biomedical Applications. *ACS Appl Mater Interfaces, 8* (16), 10070-10087.

[160] **Forterre, Y., Skotheim, J.M., Dumais, J., Mahadevan, L.** (2005) How the Venus flytrap snaps. *Nature, 433* (7024), 421−425.

[161] **Ota, S.** (1977) Current status of irradiated heat-shrinkable tubing in Japan. *Radiation Physics and Chemistry, 1981*: *18* (1−2), 81−87.

[162] **Zhao, Q., Qi, H.J., Xie, T.** (2015) Recent progress in shape memory polymer: New behavior, enabling materials, and mechanistic understanding, *Progress in Polymer Science, 49-50*, 79-120.

[163] **Xie T.** (2011) Recent advances in polymer shape memory. *Polymer, 52,* 4985–5000.

[164] **Lendlein, A., Kelch, S.** (2002) Shape-memory polymers. *Angew Chem Int Ed., 41*, 2034–2057.

[165] **Behl, M., Zotzmann, J., Lendlein, A.** (2010) Shape-memory polymers andshape changing polymers. *Adv Polym Sci, 226*, 1–40.

[166] **Liu, C., Qin, H., Mather, P.T.** (2007) Review of progress in shape-memory poly-mers. *J Mater Chem, 17*, 1543–1558.

[167] **Mather, P.T., Luo, X.F., Rousseau, I.A.** (2009) Shape memory polymer research. *Annu Rev Mater Res, 39*, 445–471.

[168] **Hu, J.L., Zhu, Y., Huang, H.H., Lu, J.** (2012) Recent advances in shape-memorypolymers: structure, mechanism, functionality, modeling andapplications. *Prog Polym Sci, 37*, 1720–1763.

[169] **Osada, Y., Matsuda, A.** (1995) Shape memory in hydrogels. *Nature, 376*, 219.

[170] **Yasin, A., Zhou, W. F., Yang, H. Y., Li, H. Z., Chen, Y., Zhang, X. Y.** (2015) Shape Memory Hydrogel based on a Hydrophobically-Modified Polyacrylamide (HMPAM)/alpha-CD Mixture via a Host-Guest Approach. *Macromol. Rapid Commun., 36*, 845−851.

[171] **Zhang, Y.Y., Li, Y.M., Liu, W.G.** (2015) Dipole-Dipole and H-Bonding Interactions Significantly Enhance the Multifaceted Mechanical Properties of Thermoresponsive Shape Memory Hydrogels. *Adv. Funct. Mater., 25*, 471−480.

[172] **Ren, Z.Q., Zhang, Y.Y., Li, Y.M., Xu, B., Liu, W.G.** (2015) Hydrogen bonded and ionically crosslinked high strength hydrogels exhibiting Ca^{2+}-triggered shape memory properties and volume shrinkage for cell detachment. *J. Mater. Chem. B, 3*, 6347−6354.

[173] **Li, G., Yan, Q., Xia, H., Zhao, Y.** (2015) Therapeutic-Ultrasound- Triggered Shape Memory of a Melamine-Enhanced Poly(vinyl alcohol) Physical Hydrogel. *ACS Appl. Mater. Interfaces, 7*, 12067−12073.

[174] **Löwenberg, C., Balk, M, Wischke, C., Behl, M., Lendlein, A.** (2017) Shape-Memory Hydrogels: Evolution of Structural Principles To Enable Shape Switching of Hydrophilic Polymer Networks. *Acc Chem Res., 50* (4), 723-732.

[175] **Calvert, P.** (2009) Hydrogels for Soft Machines *Adv. Mater., 21* (7), 743−756.

[176] **Seiffert, S.** (2015) *Ed.: Supramolecular Polymer Networks and Gels; Book Series Adv. Polym. Sci.: Springer, Berlin.*

[177] **Amaral, A.J.R., Pasparakis, G.** (2017) Stimuli responsive self-healing polymers: gels, elastomers and membranes *Polym. Chem., 8,* 6464−6484.

[178] **Apostolakos, J., Durant, T.J.S., Dwyer, C.R., Russell, R.P., Weinreb, J. H., Alaee, F., … , Mazzocca, A.D.** (2014) The enthesis: a review of the tendon-to-bone insertion. *Muscles Ligaments Tendons J., 4* (3), 333−342.

[179] **Rossetti, L., Kuntz, L. A., Kunold, E., Schock, J., Müller, K. W., Grabmayr, H., … , Bausch, A. R.** (2017) The microstructure and micromechanics of the tendon-bone insertion. *Nat. Mater., 16,* 664−670.

[180] **Shaw, H.M., Benjamin, M.** (2007) Structure-function relationship of entheses mechanical load and exercise. *Scand J Med Sci Sports, 17,* 303–315.

[181] **Hu, Z., Zhang, X., Li, Y.** (1995) Synthesis and application of modulated polymer gels. *Science, 269* (5223), 525−527.

[182] **Banik, S.J., Fernandes, N.J., Thomas, P.C., Raghavan, S.R.** (2012) A New Approach for Creating Polymer Hydrogels with Regions of Distinct Chemical, Mechanical, and Optical Properties, *Macromolecules, 45* (14), 5712−5717.

[183] **Gargava, A., Arya, C., Raghavan, S.R.** (2016) Smart Hydrogel-Based Valves Inspired by the Stomata in Plants, *ACS Appl. Mater. Interfaces, 8,* 18430−18438.

[184] **Rose, S., Prevoteau, A., Elzière, P., Hourdet, D., Marcellan, A., Leibler, L.** (2014) Nanoparticle solutions as adhesives for gels and biological tissues. *Nature, 505* (7583), 382−385.

[185] **Yong, X., Simakova, A., Averick, S., Gutierrez, J., Kuksenok, O., Balazs, A. C., Matyjaszewski, K.** (2015) Stackable, covalently fused gels: Repair and composite formation, *Macromolecules, 48,* 1169−1178.

[186] **Beziau, A., de Menezes, R. N. L., Biswas, S., Singh, A., Cuthbert, J., Balazs, A. C., Kowalewski, T., Matyjaszewski, K.** (2017) Combining ATRP and FRP Gels: Soft Gluing of Polymeric Materials for the Fabrication of Stackable Gels, *Polymers, 9* (6), 186-196.

[187] **Deng, G., Ma, Q., Yu, H., Zhang, Y., Yan, Z., Liu, F., Liu, C., Jiang, H., Chen, Y.** (2015) Macroscopic Organohydrogel Hybrid from Rapid Adhesion between Dynamic Covalent Hydrogel and Organogel *ACS Macro Lett., 4* (4), 467−471.

[188] **Yuk, H., Zhang, T., Lin, S., Parada, G.A., Zhao, X.** (2016) Tough bonding of hydrogels to diverse non-porous surfaces. *Nat. Mater., 15* (2), 190−196.

[189] **Huang, M., Furukawa, H., Tanaka, Y., Nakajima, T., Osada, Y., Gong, J.P.** (2007) Importance of Entanglement between First and Second Components in High-Strength Double Network Gels, *Macromolecules, 40* (18), 6658-6664.

[190] **Bastide, J., Candau, S.J.** (1996) Structure of Gels as Investigated by Means of Static Scattering Techniques, *In Physical Properties of Polymeric Gels; Cohen Addad, J. P., Ed.; Wiley: New York,* 143.

[191] **Shibayama, M.** (1998) Spatial inhomogeneity and dynamic fluctuations of polymer gels, *Macromol. Chem. Phys. 199* (1), 1-30.

[192] **Shibayama, M., Ikkai, F., Nomura, S.** (1994) Complexation of poly(vinyl alcohol)–congo red aqueous solutions. 3. Dynamic light scattering study, *Macromolecules, 27* (22), 6383-6388.

[193] **Sittampalam S. G., et al.** (2016) *Assay Guidance Manual, Eli Lilly & Company and the National Center for Advancing Translational Sciences*.

[194] **ISO 10993-5:2009**, *Biological evaluation of medical devices Part 5: Tests for in vitro cytotoxicity, Stage: 90.92 (2013-01-05), ISO/TC 194*.

[195] **F.P. Mechels, A.M. Barradas, C.A. van Blitterswijk, J. de Boer, J., Feijen, D.W. Grijpma** (2010) Effects of the architecture of tissue engineering scaffolds on cell seeding and culturing. *Acta Biomaterials, 6* (11), 4208-4217.

[196] **Nöchel, U., Behl, M., Balk, M., Lendlein, A.** (2016) Thermally-induced triple-shape hydrogels: Soft materials enabling complex movements. *ACS Appl. Mater. Interfaces, 8,* 28068−28076.

[197] **Bilici, C., Ide, S., Okay, O.** (2017) Yielding behavior of tough semicrystalline hydrogels. *Macromolecules, 50,* 3647−3654.

[198] **Mogri, Z., Paul, D.R.** (2001) Gas sorption and transport in side-chain crystalline and molten poly(octadecylacrylate). *Polymer, 42,* 2531−2542.

[199] **Bilici, C., Okay, O.** (2013) Shape memory hydrogels via micellar copolymerization of acrylic acid and n-octadecyl acrylate in aqueous media. *Macromolecules, 46,* 3125−3131.

[200] **Mogri, Z., Paul, D.R.** (2001) Gas sorption and transport in side-chain crystalline and molten poly(octadecylacrylate). *Polymer, 42,* 2531−2542.

[201] **Bisht, H.S., Pande, P.P., Chatterjee, A.K.** (2002) Docosyl acrylate modified polyacrylic acid: synthesis and crystallinity. *Eur. Polym. J., 38,* 2355−2358.

[202] **Broadhurst, M.G.** (1962) An analysis of the solid phase behavior of the normal paraffins. *J. Res. Natl. Bur. Stand., Sect. A,* ***66A***, 241−249.

[203] **Jordan, E.F., Feldeisen, D.W., Wrigley, A.N.** (1971) Side-chain crystallinity. I. Heats of fusion and melting transitions on selected homopolymers having long side chains. *J. Polym. Sci., Part A-1: Polym. Chem., 9,* 1835−1851.

CURRICULUM VITAE

Name Surname **: Aslıhan ARĞUN**

Place and Date of Birth **:** Acıpayam, 22.10.1985

E-Mail **:** asliargun@gmail.com

EDUCATION **:**

- **B.Sc.** **:** 2010, Gazi University, Faculty of Science and Literature, Chemistry
- **M.Sc.** **:** 2013, Istanbul Technical University, Graduate School of Science, Engineering And Technology, Chemistry

PROFESSIONAL EXPERIENCE AND REWARDS:

- Research Project Assistant , 114Z312 – *TUBITAK (The Scientific and Technological Research Council of Turkey) Project* – Design of biocompatible hydrogels with regions of different chemical and mechanical properties (2014-2017). (Success Story, 2018- TUBITAK)
- Research Project Assistant , 211T044 – *TUBITAK and RFBR (Russian Foundation for Basic Research) Project* – Biocompatible, functional cryogels with tunable mechanical properties (2013-2014).
- Research Project Assistant , 109T646 - *TUBITAK and BMBF (International Bureau of the Federal Ministry of Education and Research of Germany) Project* – Design of hydrophobically modified hydrogels with improved mechanical properties (2012-2013).

PUBLICATIONS, PRESENTATIONS AND PATENTS ON THE THESIS:

- **Argun A.**, Gulyuz U., Okay O., 2018 (submitted): "Semi-crystalline, three-segmented hybrid gels with multiple shape memory effect" *Macromol. Symp.*
- **Argun A.**, Gulyuz U., Okay O., 2018: "Interfacing Soft and Hard Materials with Triple Shape-Memory and Self-Healing Functions." *Macromolecules* 51 (7), 2437-2446.
- Okay O., **Argun A.,** Gülyüz Ü., 2018: Interfacing Soft and Hard Materials with Triple Shape-Memory and Self-Healing Functions (Oral Presentation) *International Congress – 2nd Biomedical Engineering Congress (IBMEC 2018)*, May 24-27, 2018 Near East University, Nicosia, TRNC.

OTHER PUBLICATIONS, PRESENTATIONS AND PATENTS:

- **Argun A.**, Can V., Altun U., Okay O., 2014: "Nonionic double and triple network hydrogels of high mechanical strength." *Macromolecules* 47, 6430-6440.
- **Argun A.**, Tuncaboylu D.C., Algi M.P., Okay O., 2014: "Surfactant-induced healing of tough hydrogels formed via hydrophobic interactions." *Colloid and Polymer Science* 292, 511-517.
- Tuncaboylu D.C., **Argun A.**, Algi M.P., Okay O., 2013: "Autonomic self-healing in covalently crosslinked hydrogels containing hydrophobic domains." *Polymer* 54 (23), 6381-6388.
- Tuncaboylu D.C., **Argun A.**, Sahin M., Sari M., Okay O., 2012: "Structure optimization of self-healing hydrogels via hydrophobic interactions." *Polymer* 53 (24), 5513-5522.
- Tuncaboylu D.C., Sahin M., **Argun A.**, Oppermann W., Okay O., 2012: "Dynamics and large strain behavior of self-healing hydrogels with and without surfactants." *Macromolecules* 45 (4), 1991-2000.
- **Argun A.,** Okay O., 2016: Nonionic double and triple network hydrogels (Oral Presentation) *International Congress – 23rd Polymer Networks Group Meeting (PNG 2016)*, June 19-23, 2016 KTH Royal Institute of Technology, Stockholm, Sweden.
- **Argun A.,** Okay O., 2014: Self-healing behavior of hydogels formed by hydrophobic associations. (Oral Presentation) *National Congress - IV. Physical Chemistry Congress,* June 05-08, 2014 Pamukkale University, Denizli, Turkey.
- **Argun A.**, Tuncaboylu C. D., Okay O., 2012: Effect of Surfactant concentration on the mechanical properties of hydrophobically modified polyacrylamide hydrogels. (Poster Presentation) *International Congress - IUPAC MACRO 2012, World Polymer Congress,* June 24-29, 2012 Virginia Tech, Blacksburg,VA, USA.
- Tuncaboylu C. D., **Argun A.**, Okay O., 2012: Self-healing hydrogels via hydrophobic associations. (Oral Presentation) *International Congress - IUPAC MACRO 2012 – World Polymer Congress,* June 24-29, 2012 Virginia Tech, Blacksburg,VA, USA.

- **Argun A.**, Tuncaboylu, C. D., Okay O., 2011: Effect of temperature and electrolyte concentration on solubilization of hydrophobic monomers. (Poster Presentation) *International Congress - Polymer for Advances Technologies, October 2-5, 2011 Lodz, Poland.*
- **Argun A.**, Tuncaboylu, C. D., Okay O., 2011: Solubilization of large hydrophobes in worm-like micelles: effects of temperature and electrolyte concentration. (Poster Presentation) *Congress with International Participation - One Day Workshop: Recent Advances in Synthetic and Biological Gels,* September 21, 2011 Istanbul Technical University, Istanbul, Turkey.